BABAR Analysis Document #205
Version 3.0
July 4, 2001

Supporting document for the summer, 2001 sin2β analysis

Contact: David Lange

This document contains detailed descriptions of parts of the sin2β analysis that are not already covered by other *BABAR* Analysis Documents. The CP event selection, fitting method, validation analyses, systematics, and cross checks are documented here. We rely heavily on BAD115, which serves the same purpose for the Run 1 analysis.

Direct contributors to this document: Juerg Beringer, Vuko Brigljević, Bob Cahn, Riccardo Faccini (Technical coordinator), Yury Kolomensky, David Lange, Owen Long, David MacFarlane, Fernando Martinez-Vidal, Sören Prell, Shahram Rahatlou, Patrick Robbe, Vincent Tisserand, Stepháne T'Jampens, Wouter Verkerke, Cecilia Voena, Jim Weatherall, and Julian von Wimmersperg.

Contents

This document serves as a summary of supporting information for the Run 1 sin2β analysis. The majority of the details are found in other *BABAR* Analysis Documents and are referenced here. This document will be uploaded into the BAD system on a regular basis. However, the reader is encouraged to access the very latest version. This is possible by checking out the head from CVS:

```
cvs co BAD/note205
cd BAD
cvs co pubboard
cd note205
ln -sf ../pubboard
latex sin2beta.tex
latex sin2beta.tex
dvips -o sin2beta.ps sin2beta
```

If you are updating an old version of `BAD/note205`, you might have trouble if new subdirectories have appeared. In this case, directories must be checked out from cvs explicitly. For example, `cvs co BAD/note205/psChic`.

1 Changes from previous versions

1.1 Version 3.0

- Final results for the PRL are in. Majority of systematic studies documented.

1.2 Version 2.0

- Version prepared for July 1,2001 meeting - significant additions
- Incorporate changes from BAD reading
- Include $\chi_{c1}K^0_S$ with other *CP* =-1 channels
- First round of numbers and plots for summer publication in. More coming in Version 3.0

1.3 Version 1.0

(Changes are from BAD115)

- Removed Run 1 numbers from tables. Removed eps figures for now.
- Added $\chi_{c1}K^0_S$ and $J/\psi K^{*0}$ modes
- Shorten Equation 19 with suggestion from Bob Cahn.
- Added list of changes from the PRL

2 Analysis changes from Run 1

Beyond adding new data, the following list represents the major changes to the sin2β analysis from that published in PRL (ref..)

- Revert to `BtaSelFit` vertexing algorithm with beam constraints and beam energy constraints
- Added $\chi_{c1} K^0_S$ and $J/\psi\, K^{*0}$ modes
- Bug fix in the gamma conversion selector
- Tightened $p_{\rm t,miss}$ cut in $J/\psi\, K^0_L$ channel.
- Resolution function bias changed to scale with the event by event error.

3 *CP* violation through mixing

(Note: As of June 30, 2001, this section has been copied from the PRD (pub_0103) draft.)

CP violation has been a central concern of particle physics since its discovery in 1964 [1]. Interest was heightened by Sakharov's observation [2] in 1967 that without *CP* violation, a universe that began as matter–anti-matter symmetric could not have evolved into the asymmetric one we now see. An elegant explanation of the *CP*-violating effects in K^0_L decays is provided by the *CP*-violating phase of the three-generation Cabibbo-Kobayashi-Maskawa (CKM) quark-mixing matrix [3]. However, existing studies of *CP* violation in neutral kaon decays and the resulting experimental constraints on the parameters of the CKM matrix [4] do not provide a stringent test of whether the CKM phase describes *CP* violation [5]. Moreover, the Standard Model does not, through the CKM phase, incorporate enough *CP* violation to explain the current matter–anti-matter asymmetry [7]. Understanding *CP* violation thus remains a pressing challenge.

B mesons provide an excellent testing ground for *CP* violation through particle–anti-particle mixing. A particle that is purely B^0 at time $t = 0$ will oscillate between that state and $\overline{B}^0$ with a frequency Δm_d, the difference between the masses of the two neutral B mass eigenstates. If decays to a *CP* eigenstate f (for example, $J/\psi\, K^0_S$) are observed, any difference between the rates when starting with a B^0 and with a $\overline{B}^0$ is a manifestation of *CP* violation. In some circumstances, including those in the experiment described here, the fundamental parameters of *CP* violation in the CKM model can be measured from such time-depdendent rate asymmetries, unobscured by strong interactions.

The unitarity of the three generation CKM matrix can be expressed in geometric form as six triangles of equal area in the complex plane. A nonzero area [8] directly implies the existence of a *CP*-violating CKM phase. The most experimentally accessible of the unitarity relations, involving the two smallest elements of the CKM matrix, $V_{\rm ub}$ and $V_{\rm td}$, has come to be known as the Unitarity Triangle. Because the lengths of the sides of the Unitarity Triangle are of the same order, the angles can be large, leading to potentially large *CP*-violating asymmetries from phases between CKM matrix elements.

A state initially prepared as a B^0 ($\overline{B}^0$) can decay directly to $J/\psi\, K^0_S$ or can oscillate into a $\overline{B}^0$ (B^0) and then decay to $J/\psi\, K^0_S$. With little theoretical uncertainty in the Standard Model, the phase difference between these amplitudes is equal to twice the angle $\beta = \arg\left[-V_{\rm cd}V^*_{\rm cb}/V_{\rm td}V^*_{\rm tb}\right]$ of the Unitarity Triangle. The *CP*-violating asymmetry can thus provide a crucial test of the Standard Model. The interference between the two amplitudes, and hence the *CP* asymmetry, is maximal when the mixing probability is at its highest, *i.e.*, after approximately 2.2 B^0 proper lifetimes.

The phenomenon of particle–anti-particle mixing in the neutral B meson system was first observed almost fifteen years ago [9, 10]. The oscillation frequency in $B^0\overline{B}^0$ mixing has been extensively studied with both time-integrated and time-dependent techniques [14]. In the Standard Model, $B^0\overline{B}^0$ mixing occurs through second-order weak diagrams involving the exchange of charge-2/3 quarks, with the top quark contributing the dominant amplitude. A measurement of Δm_d is therefore sensitive to the value of the CKM matrix element $V_{\rm td}$. At present the sensitivity to $V_{\rm td}$ is not limited by experimental precision on Δm_d, but by theoretical uncertainties in the calculation, in particular the quantity $f_B^2 B_B$, where f_B is the B^0 decay constant, and B_B is the so-called bag factor, representing the strong interaction matrix elements.

In e^+e^- storage rings operating at the $\Upsilon(4S)$ resonance a $B^0\overline{B}^0$ pair produced in $\Upsilon(4S)$ decay evolves in a coherent P-wave until one of the B mesons decays. If one of the B mesons ($B_{\rm tag}$) can be ascertained to decay to a state of known flavor at a certain time $t_{\rm tag}$, the other B ($B_{\rm rec}$) is *at that time* known to be of the opposite flavor. Consequently, the probabilities for observing $B^0\overline{B}^0$, B^0B^0 and $\overline{B}^0\overline{B}^0$ pairs produced in $\Upsilon(4S)$ decays is an oscillatory function of $\Delta t = t_{\rm rec} - t_{\rm tag}$, allowing mixing frequencies and *CP* asymmetries to be determined. The charges of identified leptons and kaons are the primary indicators of the flavor of the tagging $B_{\rm tag}$, but other particles also carry flavor information that can be exploited with a neural network algorithm. The second $B_{\rm rec}$ is found either in a flavor eigenstate ($B_{\rm rec} = B_{\rm flav}$) or *CP* eigenstate ($B_{\rm rec} = B_{CP}$) by full reconstruction using its observed long-lived daughters. At the PEP-II asymmetric e^+e^- collider, resonant production of the $\Upsilon(4S)$ provides a copious source of $B^0\overline{B}^0$ pairs moving along the beam axis (z direction) with an average Lorentz boost of $\langle\beta\gamma\rangle = 0.56$. Therefore, the proper decay-time difference Δt is, to an excellent approximation, proportional to the distance Δz between the two B^0-decay vertices along the axis of the boost, $\Delta t \approx \Delta z/c\,\langle\beta\gamma\rangle$. The average separation between the two B decay vertices is $\Delta z = \langle\beta\gamma\rangle\, c\tau_B = 260\,\mu$m, while the typical Δz resolution for the detector is about xxx μm.

3.1 Measurement of B^0 flavor oscillations

For measurement of Δm_d, one B ($B_{\rm flav}$) is fully reconstructed in a flavor eigenstate[1] with $D^{(*)}\pi/\rho/a_1$ or $J/\psi\, K^*$, while the second is tagged with its decay products. The probability for B^0-$\overline{B}^0$ mixing is a function of Δm_d, the difference between the mass eigenstates B^0_H and B^0_L, and the true time difference $\Delta t_{\rm true}$ between the two B decays:

$$Prob(B^0\overline{B}^0 \to B^0B^0 \;or\; \overline{B}^0\overline{B}^0, B^0\overline{B}^0) \propto {\rm e}^{-\Gamma|\Delta t_{\rm true}|}(1 \pm \cos\Delta m_d \Delta t_{\rm true}). \qquad (1)$$

[1]Throughout this paper, flavor-eigenstate decay modes imply also their charge conjugate.

The observed $B^0\overline{B}^0$ system produced in an $\Upsilon(4S)$ decay can be classified as *mixed* or *unmixed* depending on whether the reconstructed flavor-eigenstate B, referred to as $B_{\rm flav}$, has the same or the opposite flavor as the tagging B, referred to as $B_{\rm tag}$. If the Δz resolution and flavor tagging were perfect, the asymmetry

$$A_{\rm mixing}(\Delta t_{\rm true}) = \frac{N_{\rm unmix}(\Delta t_{\rm true}) - N_{\rm mix}(\Delta t_{\rm true})}{N_{\rm unmix}(\Delta t_{\rm true}) + N_{\rm mix}(\Delta t_{\rm true})} \tag{2}$$

as a function of $\Delta t_{\rm true}$ would describe a cosine function with unit amplitude. However, the tagging algorithm incorrectly identifies the tag with a probability w. This mistag rate reduces the amplitude of the oscillation by a dilution factor $\mathcal{D} = (1-2w)$. When more than one type of flavor tag is employed, each will have its own mistag rate, w_i. A simultaneous fit to the mixing frequency and its amplitude allows the determination of both Δm_d and the mistag rates, w_i.

Neglecting any background contributions, the probability density functions (PDF's) for the mixed ($-$) and unmixed ($+$) events can be expressed as the convolution of the oscillatory component $h_\pm$, with a time resolution function $\mathcal{R}(\delta_{\rm t} = \Delta t - \Delta t_{\rm true}; \hat{a})$

$$\mathcal{H}_\pm(\Delta t; \Gamma, \Delta m_d, w, \hat{a}) = h_\pm(\Delta t; \Gamma, \Delta m_d, w) \otimes \mathcal{R}(\delta_{\rm t}; \hat{a}), \tag{3}$$

where $\hat{a}$ are the parameters of the resolution function and

$$h_\pm(\Delta t; \Gamma, \Delta m_d, w) = \frac{1}{4}\,\Gamma\,{\rm e}^{-\Gamma|\Delta t|}\left[1 \pm (1-2w)\cos\Delta m_d \Delta t\right]. \tag{4}$$

A likelihood function is then constructed from the sum of $\mathcal{H}_\pm$ over all mixed and unmixed events, and over the different tag types, i, each with its own characteristic mistag rate w_i

$$\ln\mathcal{L}_{\rm mix} = \sum_i^{\rm tagging}\left[\sum_{\rm unmixed}\ln\mathcal{H}_+(\Delta t; \Gamma, \Delta m_d, w_i, \hat{a}_i) + \sum_{\rm mixed}\ln\mathcal{H}_-(\Delta t; \Gamma, \Delta m_d, w_i, \hat{a}_i)\right]. \tag{5}$$

This can be maximized to extract the mistag fractions w_i and resolution parameters $\hat{a}_i$ and, simultaneously, the mixing rate Δm_d. The correlation between these parameters is small, because the rate of mixed events at low values of Δt, where the $B^0\overline{B}^0$ mixing probability is small, is principally governed by the mistag rate. Conversely, the sensitivity to Δm_d increases at larger values of Δt; when Δt is approximately twice the B lifetime, half of the neutral Bs will have oscillated.

The mistag rate can also be extracted with a time-integrated analysis, as a cross check. Neglecting possible background contributions and assuming the flavor of $B_{\rm flav}$ is correctly identified, the observed time-integrated fraction of mixed events χ_{obs} can be expressed as a function of the $B^0\overline{B}^0$ mixing probability χ_d:

$$\chi_{obs} = \chi_d + (1-2\chi_d)\,w, \tag{6}$$

where $\chi_d = \frac{1}{2}\,x_d^2/(1+x_d^2)$ and $x_d = \Delta m_d/\Gamma$. The current world average for χ_d is 0.174 ± 0.009 [14]. Taking advantage of the available decay time information, the statistical precision on w can be improved by selecting only events that fall into an optimized time interval, $|\Delta t| < t_0$, where t_0 is chosen so that the integrated number of mixed and unmixed events are equal outside this range. Through the use of this optimized Δt interval the time-integrated method achieves nearly the same statistical precision for the mistag rates as the full time-dependent likelihood fit.

3.2 Measurement of CP asymmetries

For measurement of CP asymmetries, one B (B_{CP}) is fully reconstructed in a CP eigenstate with $\eta_{CP} = -1$ ($J/\psi K_S^0$ or $\psi(2S)K_S^0$) or $+1$ ($J/\psi K_L^0$), while the second is tagged with its decay products. The expected time evolution depends both on B^0-$\overline{B}^0$ mixing and on the decay amplitudes of B^0 and $\overline{B}^0$ to the final state through a single complex parameter λ, assuming CPT conservation. Neglecting the difference between the lifetimes of the two neutral B mass eigenstates (which is expected to be much smaller than the mass difference)

$$\lambda = -\frac{|\langle B^0|\mathcal{H}|\overline{B}^0\rangle|}{\langle B^0|\mathcal{H}|\overline{B}^0\rangle}\frac{\langle f|\mathcal{H}|\overline{B}^0\rangle}{\langle f|\mathcal{H}|B^0\rangle} \tag{7}$$

It is clear that λ is independent of any phase convention for the neutral B states. The decay distributions are

$$\begin{aligned} f_\pm(\Delta t_{\rm true}) &= \frac{\Gamma\, {\rm e}^{-\Gamma|\Delta t_{\rm true}|}}{2(1+|\lambda|^2)}\left\{\frac{1}{2}\left(1+|\lambda|^2\right)\pm\right. \\ &\left.(1-2w)\left[Im(\lambda)\sin\Delta m_d\Delta t_{\rm true} - \frac{1}{2}\left(1-|\lambda|^2\right)\cos\Delta m_d\Delta t_{\rm true}\right]\right\}, \end{aligned} \tag{8}$$

where the $+$ or $-$ sign indicates whether the $B_{\rm tag}$ is tagged as a B^0 or a $\overline{B}^0$, respectively. The dilution factor $\mathcal{D} = 1-2w$ accounts for the probability w that the flavor of the tagging B is identified incorrectly.

The distributions are much simpler when $|\lambda| = 1$ and this is the expectation of the Standard Model for decays like $B^0 \to J/\psi K_S$. If all the mechanisms that contribute to the decay have the same weak phase then the ratio of the weak decay amplitudes in Eq. 7 is just $\eta_{CP}{\rm e}^{2i\phi_{wk}}$, where ϕ_{wk} is the weak phase for $\overline{B}^0 \to f$ and η_{CP} is the CP eigenvalue of the final state. For decays like $B^0 \to J/\psi K_S$ the weak phase is zero in the standard (Wolfenstein) representation where non-zero phases only occur for transitions between the first and third generations. The remaining factor in λ is due to the phase introduced by mixing. Because mixing is dominated by the t quark, it is $(V_{\rm tb}V_{\rm td}^*)^2$ that controls the result and consequently the angle β of the Unitarity Triangle that appears. Altogether, for transitions of the type $b \to c\overline{c}s$

$$\lambda = \eta_{CP}{\rm e}^{-2i\beta} \tag{9}$$

The time-dependent rate of decay of the B_{CP} final state is then given by

$$f_\pm(\Delta t;\Gamma,\Delta m_d,w,\sin 2\beta) = \frac{1}{4}\Gamma{\rm e}^{-\Gamma|\Delta t|}\left[1 \mp \eta_{CP}(1-2w)\sin 2\beta\sin\Delta m_d\Delta t\right], \tag{10}$$

In the limit of perfect determination of the flavor of the fully-reconstructed neutral B, the dilution in the mixed and unmixed amplitudes arises solely from the $B_{\rm tag}$ side, allowing the values of the mistag fractions w_i to be determined by studying the time-dependent rate of $B^0\overline{B}^0$ oscillations.

To account for the finite resolution of the detector, the time-dependent distributions $f_\pm$ for B^0 and $\overline{B}^0$ tagged events (Eq. 10) must be convoluted with a time resolution function $\mathcal{R}(\delta_{\rm t} = \Delta t - \Delta t_{\rm true};\hat{a})$:

$$\mathcal{F}_\pm(\Delta t;\Gamma,\Delta m_d,w,\sin 2\beta,\hat{a}) = f_\pm(\Delta t;\Gamma,\Delta m_d,w,\sin 2\beta)\otimes\mathcal{R}(\delta_{\rm t};\hat{a}), \tag{11}$$

where $\hat{a}$ represents the set of parameters that describe the resolution function. In practice, events are separated into different tagging categories as for mixing, each of which has a different mean mistag fraction, w_i, determined individually for each category.

It is possible to construct a *CP*-violating observable

$$\mathcal{A}_{CP}(\Delta t) = \frac{\mathcal{F}_+(\Delta t) - \mathcal{F}_-(\Delta t)}{\mathcal{F}_+(\Delta t) + \mathcal{F}_-(\Delta t)}, \tag{12}$$

which, neglecting resolution effects, is proportional to sin2β:

$$\mathcal{A}_{CP}(\Delta t) \propto \eta_{CP}(1-2w)\sin 2\beta \times \sin \Delta m_d \Delta t. \tag{13}$$

Since no time-integrated *CP* asymmetry effect is expected, an analysis of the time-dependent asymmetry is necessary.

The value of the free parameter sin2β can be extracted using the tagged B_{CP} sample by maximizing the likelihood function

$$\ln \mathcal{L}_{CP} = \sum_i^{\text{tagging}} \left[\sum_{B^0\text{tag}} \ln \mathcal{F}_+(\Delta t; \Gamma, \Delta m_d, \hat{a}, w_i, \sin 2\beta) + \sum_{\overline{B}^0\text{tag}} \ln \mathcal{F}_-(\Delta t; \Gamma, \Delta m_d, \hat{a}, w_i, \sin 2\beta) \right], \tag{14}$$

where the outer summation is over tagging categories i. In practice, the fit for sin2β is performed on the combined flavor-eigenstate and *CP* samples, in order to determine sin2β, the mistag fractions w_i for each tagging category, and the vertex resolution parameters $\hat{a}_i$. Additional terms are included in the likelihood are also required to account for backgrounds and their time dependence.

4 Event selection and yields

Tables 1 to 4 summarize the event selection for CP and non-CP (validation) charmonium final states. The "B_{flav}" sample [15] consists of the modes $B^0 \to D^{(*)}\pi$, $B^0 \to D^{(*)}\rho$, $B^0 \to D^{(*)}a_1$ and $B^0 \to J/\psi K^{*0}(K^{\pm}\pi^{\mp})$, and is illustrated in Figure 16.

The details of the $B \to \chi_{c1}K$ selection cuts are presented in appendix A. Those selections has been fully revised since the previous version of this note [31].

There are a few notatable differences between the selections for branching fraction measurements the the selections used here. The motivation of these changes from the branching fraction measurement is to gain efficiency, with minimal loss of signal purity. In contrast, the branching fraction measurement must control the systematic uncertainty on the efficiency due to fiducial acceptance.

Table 5 summarizies the event yields on the Run 1 data sample for each of the modes considered above. In each case, the yield and purity (defined as the signal fraction for events with $m_{\text{ES}} > 5.27$ GeV for modes other than $J/\psi K^0_L$ and $|\Delta E| < 10$ MeV for $J/\psi K^0_L$) are given separately for the ee and $\mu\mu$ cases.

Figures 1 to 11 show the fit used to extract the yields and purities on events that pass the vertexing requirements in Table 5. With the exception of the $B^0 \to J/\psi K^0_L$ channel, the fits are performed to the beam-energy substituted mass,

$$m_{\text{ES}} \equiv \sqrt{E^{*2} - p^{*2}} \tag{15}$$

Requirement	$J/\psi\ K^{\pm}$	$J/\psi\ K^0_S\ (\pi^+\ \pi^-)$	$J/\psi\ K^0_S\ (\pi^0\ \pi^0)$	$J/\psi\ K^0_L$
M($J/\psi \to ee$) (GeV/c^2)	2.95-3.14			3.0-3.13
M($J/\psi \to \mu\mu$) (GeV/c^2)	3.06-3.14		3.06-3.14	3.06-3.13
M(K^0_S) (GeV/c^2)		0.489-0.507	0.470-0.550	
M(π^0) (GeV/c^2)			0.100-0.155	
E(π^0) (GeV)			>200	
$\lvert\cos\theta_{hel}\rvert$ (ee)	<0.8		<0.7	<0.9
$\lvert\cos\theta_{hel}\rvert$ ($\mu\mu$)	<0.9		<0.8	<0.9
e PID	1(Tight or noCal)			L and VT
μ PID	minI and Loose		1 Loose	L and T
3D K^0_S flt. len.		> 1mm		

Table 1: Summary of the event selection used in the $B \to J/\psi K$ final states. There are additional cuts, not listed here, for the $J/\psi K^0_L$ mode. The $J/\psi K^0_L$ selection is identical to that documented in BAD 56.

Requirement	$J/\psi\ K^{*\pm}\ (K^0_S\ \pi^{\pm})$	$J/\psi\ K^{*\pm}\ (K^{\pm}\ \pi^0)$	$J/\psi\ K^{*0}\ (K^0_S\ \pi^0)$	$J/\psi\ K^{*0}\ (K^+\ \pi^-)$
M(ee) (GeV/c^2)	2.95-3.14			
M($\mu\mu$) (GeV/c^2)	3.06-3.14			
e PID	Tight and Tight			
μ PID	Loose and Loose			
M(K^0_S) (GeV/c^2)	0.489-0.507		0.489-0.507	
K^0_S flt. len.	> 1mm		> 1mm	
K^0_S flt. θ	< 200mrad		< 200mrad	
M(K^*) (GeV/c^2)	0.792-0.992		0.796-0.996	
$\cos\theta_{K^*}$		< 0.95		
M(π^0) (GeV/c^2)		0.106-0.153		
$K^{\pm}$ PID		notAPion		notAPion
E_γ (MeV)		> 30		
Lat$_\gamma$		< 0.8		

Table 2: Summary of the event selection used in the $B^0 \to J/\psi K^*$ final states.

Requirement	$(\ell\ell)\ K^{\pm}$	$(J/\psi\ \pi^{\pm}\ \pi^{\mp})\ K^{\pm}$	$(\ell\ell)\ K^0_S$	$(J/\psi\ \pi^{\pm}\ \pi^{\mp})\ K^0_S$
M(ee) (GeV/c^2)	3.436-3.736	2.95-3.14	3.436-3.736	2.95-3.14
M($\mu\mu$) (GeV/c^2)	3.636-3.736	3.06-3.14	3.636-3.736	3.06-3.14
e PID	VLoose and Tight			
μ PID	VLoose and Loose			
M($\psi(2S)$)-M(J/ψ) (GeV/c^2)		0.574-0.604		0.574-0.604
M(K^0_S) (GeV/c^2)			0.489-0.507	
K^0_S flt. len.			$>$ 1mm	
$K^{\pm}$ PID	notAPion			
M($\pi^+\ \pi^-$) (GeV/c^2)		0.4-0.6		0.4-0.6
$\lvert\cos\theta_{thrust}\rvert$	< 0.9			
$\lvert\cos\theta_{hel}\rvert$	< 0.8			

Table 3: Summary of the event selection used in the $\psi(2S)$ final states.

Requirement	$\chi_{c1}\ K^{\pm}$	$\chi_{c1}\ K^0_S$
M($J/\psi \to ee$) (GeV/c^2)	2.95-3.14	
M($J/\psi \to \mu\mu$) (GeV/c^2)	3.06-3.14	
M($\gamma J/\psi$)-M(J/ψ)	0.38-0.45	
e PID	Loose and Tight	
μ PID	VLoose and Loose	
E(γ) (GeV)	$>$0.15	
θ_γ	0.41-2.409	
Lat(γ)	< 0.8	
A42(γ)	< 0.15	
π^0 veto (γ_2 is the other π^0 daughter)	$[120, 150]$ MeV/c^2 + E(γ_2)$>$ 70 MeV	
M(K^0_S) (GeV/c^2)	-	0.489-0.507
K^0_S flt. len.	-	$>$ 1mm
$K^{\pm}$ PID	notAPion	-

Table 4: Summary of the event selection used in the $\chi_{c1}K$ final states.

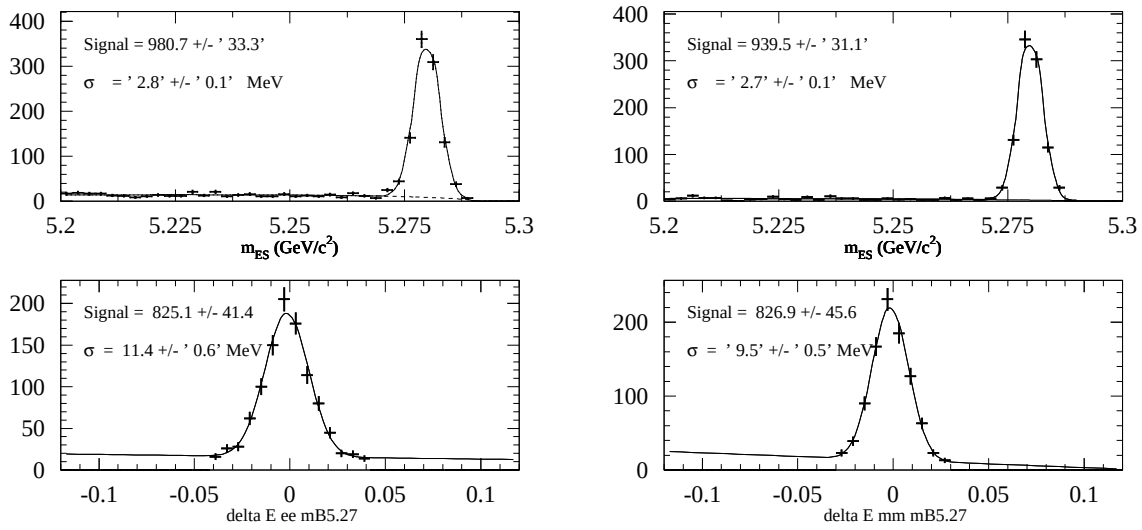

Figure 1: Fits to the $m_{\rm ES}$ and ΔE distributions in the $B \to J/\psi K^{\pm}$ channel for the $J/\psi \to e^+e^-$ (left) and $J/\psi \to \mu^+\mu^-$ (right) modes. Vertexing cuts have not been applied. In Figures **??** to 11, $\sigma(m_{\rm ES})$ is fixed to the average of the $J/\psi \to e^+e^-$ and $J/\psi \to \mu^+\mu^-$ fits tabulated in Table 5. Also, the 3σ ΔE requirement is included in the fits to ΔE, so the sidebands are completely empty (sorry!).

distribution using a Gaussian plus Argus background shape [16]. There is no Gaussian contribution allowed for the background shape.

The $B^0 \to J/\psi K^0_L$ channel handled differently from the other modes, as the K^0_L energy is not measured. It is instead determined using the constraint that $M_B^2 = (p_{J/\psi} + p_{K^0_L})^2$. The remaining degree of freedom is expressed as $\Delta E \equiv E_{J/\psi} + E_{K^0_L} - E_{\rm beam}$. BAD 56 [17] details the $B^0 \to J/\psi K^0_L$ analysis method.

Fig.	Mode		$\sigma\ \Delta E$ (MeV)	ΔE yield	$\sigma\ m_{\rm ES}$ (MeV)	$m_{\rm ES}$ yield	Yield	Purity (%)
??,1	$J/\psi K^{\pm}$	e^+e^-	11.4 ± 0.6	825 ± 41	2.8 ± 0.1	981 ± 33	$\pm$	$\pm$
		$\mu^+\mu^-$	9.5 ± 0.5	830 ± 46	2.7 ± 0.1	940 ± 31	$\pm$	$\pm$
??,2	$J/\psi K^0_S$	e^+e^-	11.8 ± 0.6	222 ± 15	2.8 ± 0.2	215 ± 17	$\pm$	$\pm$
	$(\pi^+\pi^-)$	$\mu^+\mu^-$	10.1 ± 0.4	252 ± 16	2.6 ± 0.1	247 ± 16	$\pm$	$\pm$
??,3	$J/\psi K^0_S$	e^+e^-	—	—	2.7 ± 0.5	54 ± 9	$\pm$	$\pm$
	$(\pi^0\pi^0)$	$\mu^+\mu^-$	—	—	3.5 ± 0.4	57 ± 8	$\pm$	$\pm$
4	$J/\psi K^0_L$	Emc	—	128 ± 17	—	—	127 ± 16	56 ± 5
		Ifr	—	129 ± 17	—	—	124 ± 17	65 ± 6
??,5	$J/\psi K^{*\pm}$	e^+e^-	$\pm$	$\pm$	$\pm$	$\pm$	$\pm$	$\pm$
	$(K^0_S\pi^{\pm})$	$\mu^+\mu^-$	$\pm$	$\pm$	$\pm$	$\pm$	$\pm$	$\pm$
??,??	$J/\psi K^{*\pm}$	e^+e^-	25 ± 1	257 ± 16	3.0 ± 0.4	196 ± 20	$\pm$	$\pm$
	$(K^{\pm}\pi^0)$	$\mu^+\mu^-$	23 ± 1	212 ± 15	3.2 ± 0.2	185 ± 16	$\pm$	$\pm$
??,6	$J/\psi K^{*0}$	e^+e^-	20 ± 2	43 ± 7	4.3 ± 1.0	40 ± 8	$\pm$	$\pm$
	$(K^0_S\pi^0)$	$\mu^+\mu^-$	18 ± 2	40 ± 6	2.9 ± 0.8	31 ± 8	$\pm$	$\pm$
??,7	$J/\psi K^{*0}$	e^+e^-	11.6 ± 0.3	563 ± 24	2.8 ± 0.1	531 ± 24	$\pm$	$\pm$
	$(K^{\pm}\pi^{\mp})$	$\mu^+\mu^-$	10.5 ± 0.3	505 ± 23	2.7 ± 0.1	481 ± 23	$\pm$	$\pm$
??,8	$\psi(2S)K^{\pm}$	e^+e^-	8.3 ± 0.5	157 ± 13	2.7 ± 0.2	151 ± 13	$\pm$	$\pm$
		$\mu^+\mu^-$	9.2 ± 0.5	145 ± 12	2.5 ± 0.4	141 ± 16	$\pm$	$\pm$
??,9	$\psi(2S)K^0_S$	e^+e^-	10.0 ± 1	50 ± 7	3.1 ± 0.4	47 ± 7	$\pm$	$\pm$
		$\mu^+\mu^-$	8.6 ± 1	43 ± 7	2.2 ± 0.3	40 ± 7	$\pm$	$\pm$
??,10	$\chi_{c1}K^{\pm}$	e^+e^-	10.8 ± 0.7	107 ± 10	3.3 ± 0.4	100 ± 11	$\pm$	$\pm$
		$\mu^+\mu^-$	10.0 ± 0.7	103 ± 10	2.6 ± 0.2	97 ± 10	$\pm$	$\pm$
??,11	$\chi_{c1}K^0_S$	e^+e^-	10 ± 2	19 ± 4	2.9 ± 0.7	18 ± 7	$\pm$	$\pm$
		$\mu^+\mu^-$	8 ± 1	27 ± 5	2.6 ± 0.4	26 ± 5	$\pm$	$\pm$

Table 5: Event yields, signal resolutions, and signal purities for the charmonium decay modes. Results are shown separately for the $J/\psi \to e^+e^-$ and $J/\psi \to \mu^+\mu^-$ channels. The ΔE results were determined from a fit to a Gaussian plus flat background contribution using events with $m_{\rm ES} > 5.27$ GeV/c^2. The $m_{\rm ES}$ results were determined from a fit to a Gaussian plus Argus background in a 3σ ΔE window. The final yield and purity are from a Gaussian plus Argus background function fit to the $m_{\rm ES}$ distribution in the same 3σ ΔE window with vertex requirements on the events, as shown in Figures ?? to 11.

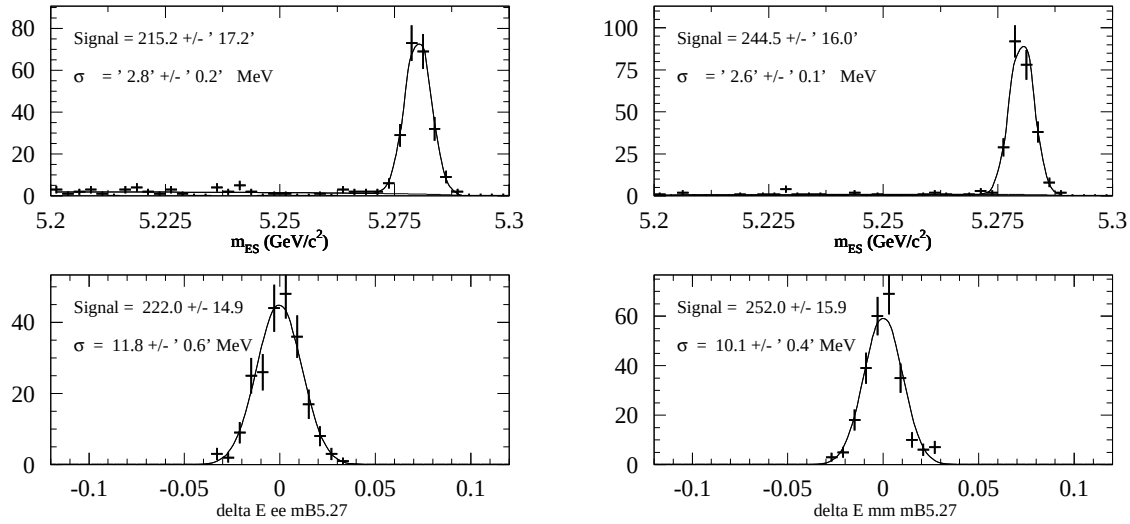

Figure 2: Fits to the $m_{\rm ES}$ and ΔE distributions in the $B \to J/\psi\, K^0_S$ $(\pi^+\pi^-)$ channel for the $J/\psi \to e^+e^-$ (left) and $J/\psi \to \mu^+\mu^-$ (right) modes. Vertexing cuts have not been applied.

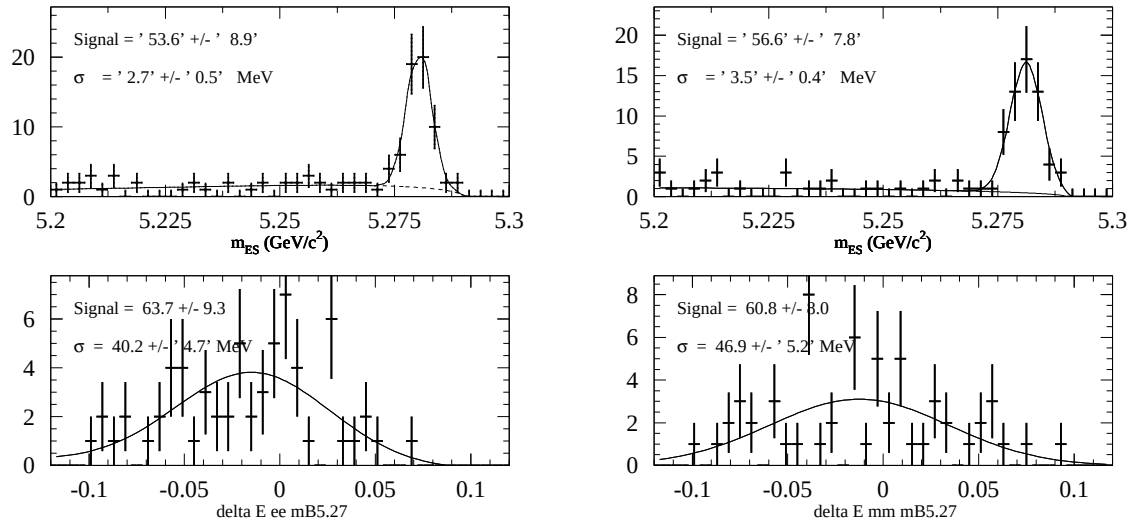

Figure 3: Fits to the $m_{\rm ES}$ and ΔE distributions in the $B \to J/\psi\, K^0_S$ $(\pi^0\pi^0)$ channel for the $J/\psi \to e^+e^-$ (left) and $J/\psi \to \mu^+\mu^-$ (right) modes. Vertexing cuts have not been applied.

Figure 4: Fits to the ΔE distribution in the $B \to J/\psi\, K^0_L$ channel for K^0_L detected in the Emc (left) and Ifr (right) modes. Vertexing cuts have not been applied. The shaded histogram is the fitted background contribution.

Figure 5: ΔE vs. $m_{\rm ES}$ (top) and corresponding 1D distributions in the $B \to J/\psi K^*$ ($K^0_S\pi^\pm$) channel for the $J/\psi \to e^+e^-$ (left) and $J/\psi \to \mu^+\mu^-$ (right) modes. Vertexing cuts have not been applied.

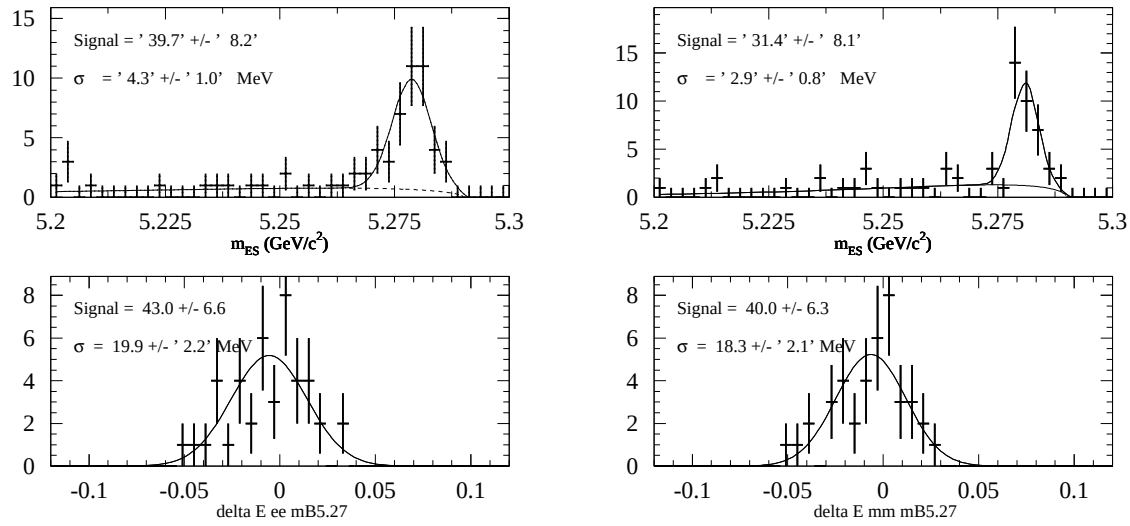

Figure 6: Fits to the $m_{\rm ES}$ and ΔE distributions in the $B \to J/\psi K^{*0}$ ($K^0_S\pi^0$) channel for the $J/\psi \to e^+e^-$ (left) and $J/\psi \to \mu^+\mu^-$ (right) modes. Vertexing cuts have not been applied.

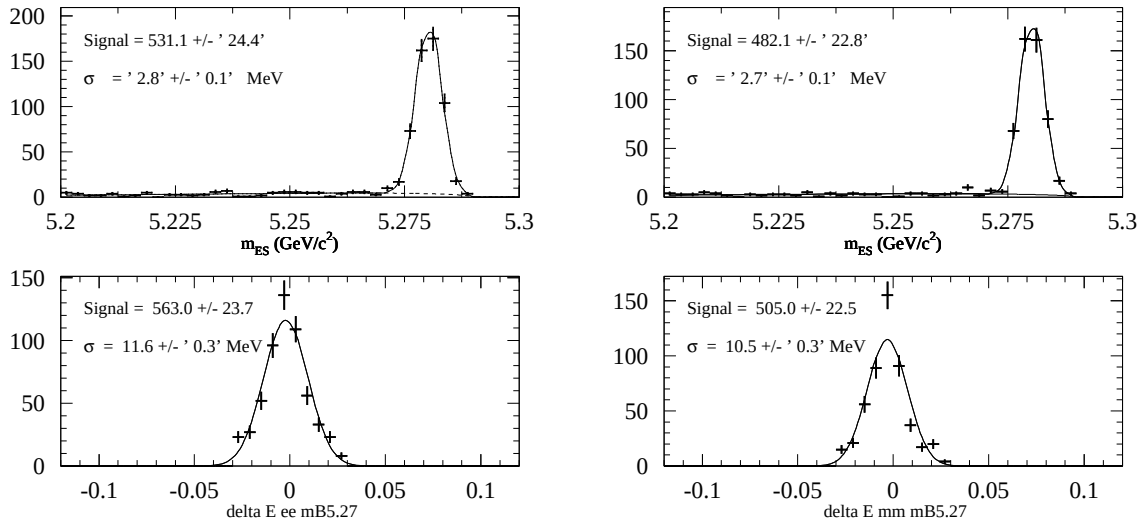

Figure 7: Fits to the $m_{\rm ES}$ and ΔE distributions in the $B \to J/\psi K^*$ ($K^{\pm}\pi^{\mp}$) channel for the $J/\psi \to e^+e^-$ (left) and $J/\psi \to \mu^+\mu^-$ (right) modes. Vertexing cuts have not been applied.

Mode	Fraction of peak	Largest modes
$J/\psi K^0_S$ ($\pi^+\pi^-$)	$0.41 \pm 0.09\%$	$J/\psi K^{*0}$ ($K^+\pi^-$)
$J/\psi K^0_S$ ($\pi^0\pi^0$)	$1.2 \pm 0.2\%$	$J/\psi K^*$ ($K^0_S\pi^0$, $K^0_S\pi^+$)
$\psi(2S)K^0_S$	$2.9 \pm 1.7\%$	$\psi(2S)K^{*0}$
$\chi_{c1}K^0_S$	$1.1 \pm 1.1\%$	$J/\psi K^{*0}$ ($K^0_S\pi^0$)
Average	$0.9 \pm 0.2\%$	

Table 6: The fraction of the Gaussian term in $m_{\rm ES}$ for *CP* modes that comes from background.

4.1 Peaking backgrounds

The inclusive J/ψ Monte Carlo samples have been used to evaluate the level of background that peaks in the $m_{\rm ES}$ distribution. For each channel, the signal events from that mode are removed from the Monte Carlo and a fit is performed to the remaining distribution including a Gaussian term plus an Argus background. Only tagged events are considered. The width of the Gaussian is fixed to an average signal value, 2.75 MeV. Table 6 summarizies the results of these fits for the CP samples. The *CP* fitters use the ratio between the signal contribution and the peaking background as input.

Figure 12 shows the distributions on the largest possible Monte Carlo sample appropiate for each mode. The $J/\psi K^0_S$ modes are evaluated on a sample corresponsing to 219 fb^{-1} while the $\psi(2S)K^0_S$ mode is evaluated on a sample of only 49 fb^{-1} : the majority of the inclusive J/ψ Monte Carlo has in fact been produced with a cut on the momentum of the J/ψ in the lab which at 1.3 GeV. There are some pending questions on whether this

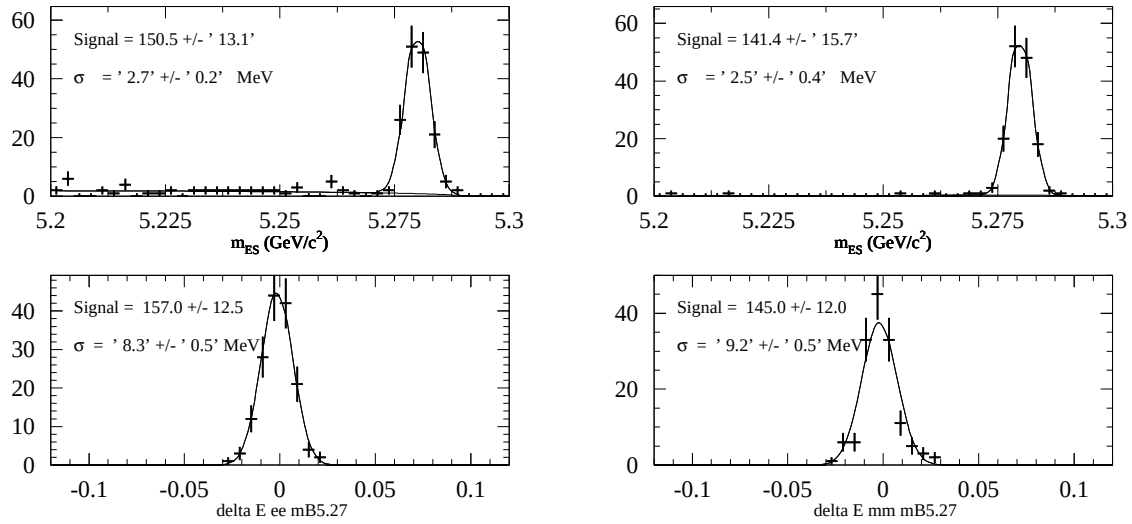

Figure 8: Fits to the $m_{\rm ES}$ and ΔE distributions in the $B \to \psi(2S)K^{\pm}$ channel for the $J/\psi \to e^+e^-$ (left) and $J/\psi \to \mu^+\mu^-$ (right) modes. Vertexing cuts have not been applied.

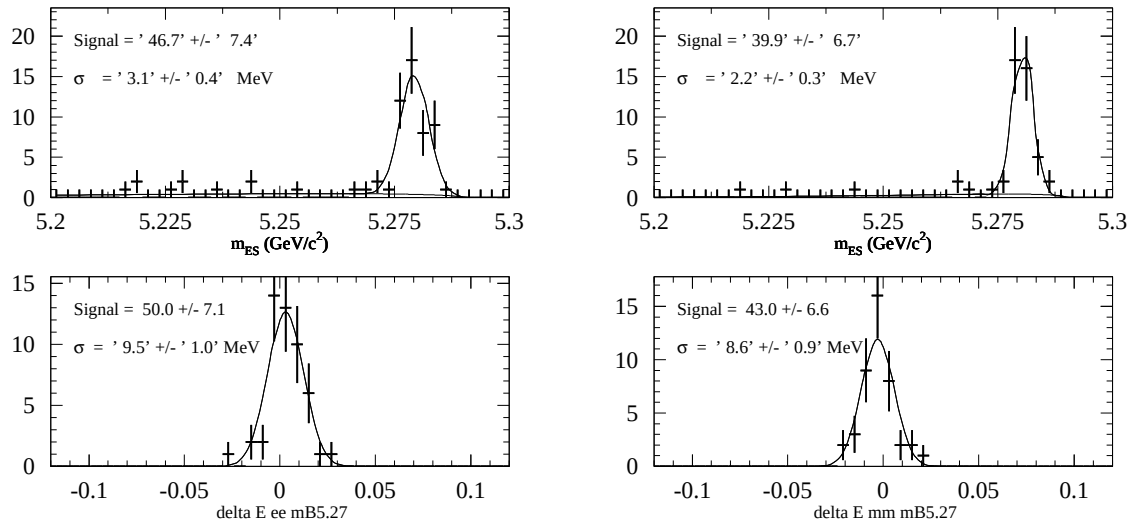

Figure 9: Fits to the $m_{\rm ES}$ and ΔE distributions in the $B \to \psi(2S)K^0_S$ channel for the $J/\psi \to e^+e^-$ (left) and $J/\psi \to \mu^+\mu^-$ (right) modes. Vertexing cuts have not been applied.

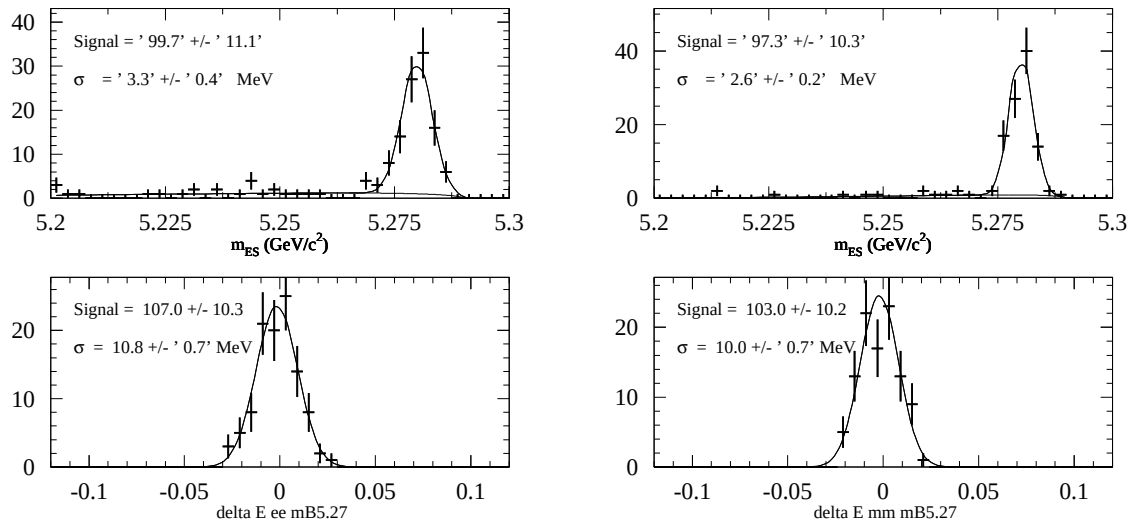

Figure 10: Fits to the $m_{\rm ES}$ and ΔE distributions in the $B \to \chi_{c1} K^{\pm}$ channel for the $J/\psi \to e^+e^-$ (left) and $J/\psi \to \mu^+\mu^-$ (right) modes. Vertexing cuts have not been applied.

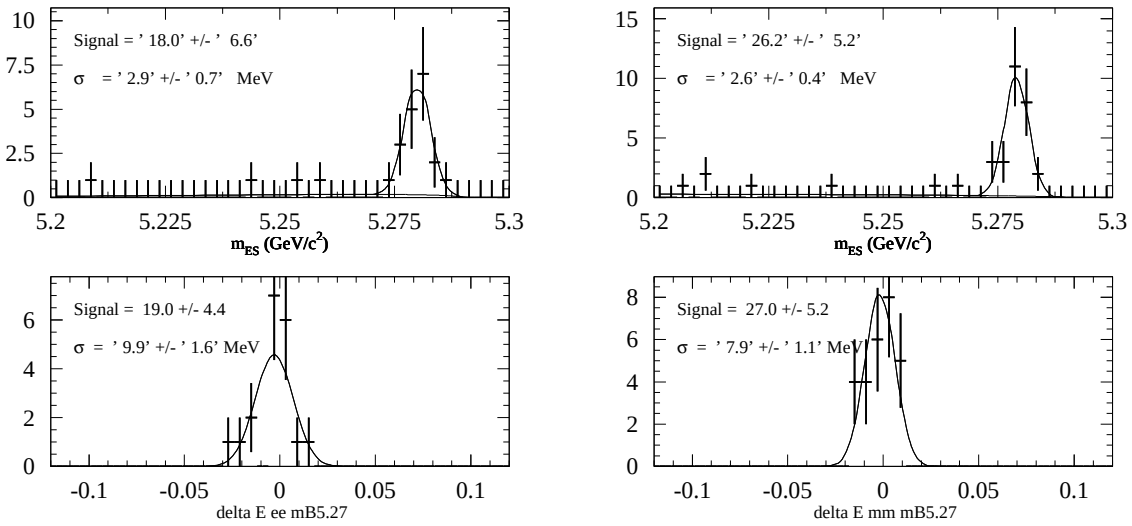

Figure 11: Fits to the $m_{\rm ES}$ and ΔE distributions in the $B \to \chi_{c1} K^0_S$ channel for the $J/\psi \to e^+e^-$ (left) and $J/\psi \to \mu^+\mu^-$ (right) modes. Vertexing cuts have not been applied.

Figure 12: $m_{\rm ES}$ distributions for the *CP* modes on the inclusive-J/ψ MC where the signal contribution has been removed. Fits to the $B^0 \to J/\psi K^0_S$ ($\pi^+\pi^-$) (top, left), and $B^0 \to J/\psi K^0_S$ ($\pi^0\pi^0$) (top, right), and $B^0 \to \psi(2S)K^0_S$ (bottom) channels are shown.

cut distorts the evaluation of the background for the J/ψ modes. In order to account for these uncertainties and for the scarse knowledge on the charmonium branching fractions, a conservative estimate $f = (0.9 \pm 1)\%$ is used.

The $J/\psi K^0_L$ mode is not included in this study as the inclusive-J/ψ background Monte Carlo is used to compute the signal probability as a function of ΔE, thus explicitly accounting for any peaking background.

5 Definition of tagging categories

The complete description and performance of the tagging algorithm is in BAD 119 [18]. The tagging algorithm used is the Elba tagger, with the following groupings:

1. Lepton: Categories 11 ($e + K$), 12 ($\mu + K$), 14 (e), 15 (μ).
2. Kaon: Category 13.
3. NT1: Category 22.
4. NT2: Category 23.

These categories are hierarchical and mutually exclusive. Events with a lepton tag and possibly kaon tags (if the net charge confirms the lepton tag) make up the "Lepton" category. Events with no lepton tag, but with a net kaon charge make up the "Kaon" category. Remaining events, including those with a conflicting lepton and kaon tag are given to the NetTagger algorithm. The neural network output is divided into three categories, ordered in terms of increasing certainty of the tag: "NT1", "NT2", and no flavor tag.

BAD 119 contains Run 1 vs. Run 2 comparisons for the tagging performance. For this measurement, we keep common dilutions and dilution differences for Run 1 and Run 2.

6 Vertexing

The uncertainty in the Δt measurement is dominated by the measurement of the z position of the tagging vertex. The tagging vertex is determined by fitting to a common vertex the tracks not belonging to the B_{CP} or B_{flav} candidate. Reconstructed K^0_S and Λ candidates are used as input to the fit in place of their daughters. Tracks from γ conversions are excluded from the fit. In order to reduce contributions from charm decay, which could bias the vertex estimation, if any track contributes more than 6 to the vertex χ^2, the largest contributor is dropped from the fit and the fit is redone; this process is repeated until no track contributes more than 6 to the χ^2. The time interval Δt between the two B decays is then determined from the Δz measurement, after correcting on an event-by-event basis for the direction of the B with respect to the z direction in $\Upsilon(4S)$ frame. An accepted candidate must have a converged fit for Δz, with an error less than $400\,\mu$m and a measured $|\Delta z| < 3\,$mm.

BADs 254, 102 and 130 describe the vertexing algorithm and systematic studies in detail. We now take advantage of the more refined constraints that `BtaSelFit` applies:

- the beam constraint: from the knowledge of the center of mass four momentum the expected momentum of the tag B can be extracted and a pseudo-trajectory can be defined starting from the beam spot. Requiring the compatibility of the tracks that make the tag side with this pseudo-trajectory helps getting rid of the tracks that do not come directly from the B candidate, hence reducing the "charm" bias.

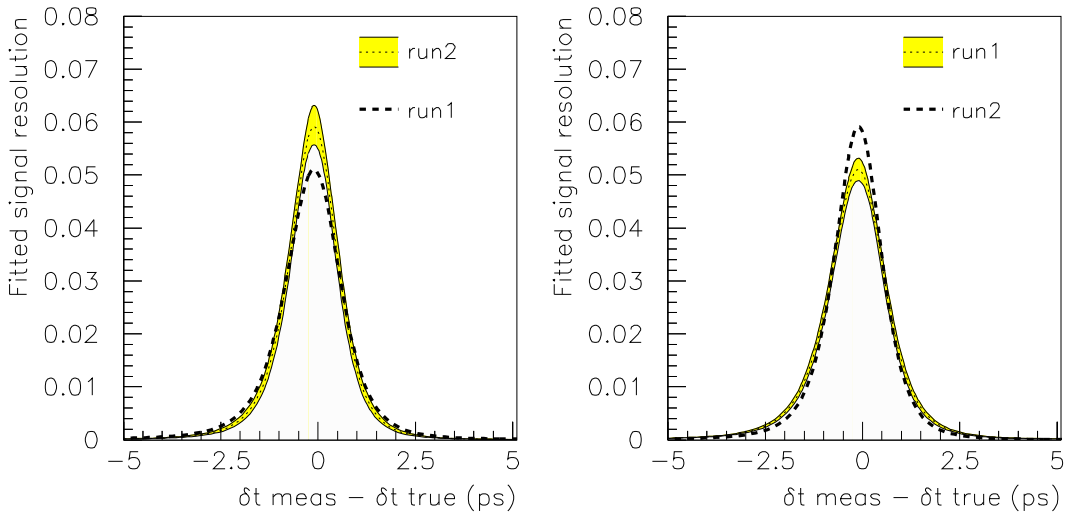

Figure 13: Resolution function determined from the Run 1 and Run 2 $B_{\rm flav}$ data samples. The plot on the left (right) show the run2 (run1) sample with the error envelope from the fit. From these curves, it appears that the run1 and run2 samples are roughly two "sigma" apart from each other.

- the beam spot: in absence of the beam constraint, the B's can be required to be consistent with the beam-spot within errors which take into account the lifetime of the B mesons themselves.

The default resolution function is a triple Gaussian model, where two Gaussians (core and tail) have a width proportional to the event by event error and the third (outlier) has a width fixed to 8 ps. The bias of the outlier Gaussian is fixed to 0, while the core and tail biases scale with the event by event error:

$$\begin{aligned}\mathcal{R}(\delta_{\rm t};\hat{a}) \;=\; & \sum_{k=1}^{2} \frac{f_{\rm core,tail}}{\sigma_{\rm core,tail}\sqrt{2\pi}} \exp\left(-\frac{(\delta_{\rm t}-\delta_{\rm core,tail})^2}{2\sigma_{\rm core,tail}}\right) \;+ \\ & \frac{f_{\rm outlier}}{\sigma_{\rm outlier}\sqrt{2\pi}} \exp\left(-\frac{\delta_{\rm t}^2}{2{\sigma_{\rm outlier}}^2}\right) . \end{aligned} \tag{16}$$

In addition, a different resolution function is used for Run 1 and Run 2, both for the signal and background contributions. The data show significant differences between these data samples, presumably due to the reconstruction code improved used to process the Run 2 data. This is shown for the $B_{\rm flav}$ sample in Figure 13. These differences are accounted for by including a different resolution function for the Run 1 and Run 2 data samples.

Tag	$J/\psi K^0_S$ $(\pi^+\pi^-)$			$J/\psi K^0_S$ $(\pi^0\pi^0)$			$\psi(2S)K^0_S$			$\chi_{c1}K^0_S$			Total		
	B^0	$\overline{B}^0$	Tot	B^0	$\overline{B}^0$	Tot	B^0	$\overline{B}^0$	Tot	B^0	$\overline{B}^0$	Tot	B^0	$\overline{B}^0$	Tot
$e+K$	2	1	3	0	1	1	1	0	1	0	1	1	3	3	6
$\mu+K$	1	3	4	0	1	1	2	0	2	0	2	2	3	6	9
e	9	10	19	2	2	4	3	5	8	1	0	1	15	17	32
μ	8	10	18	1	3	4	2	2	4	0	1	1	11	16	27
Lepton	20	24	44	3	7	10	8	7	15	1	4	5	32	42	74
Kaon	87	95	182	19	18	37	16	16	32	9	11	20	131	140	271
NT1	16	21	37	1	2	3	2	2	4	1	1	2	20	26	46
NT2	29	25	54	10	4	14	8	8	16	4	2	6	51	39	90
Total tag	152	165	317	33	31	64	34	33	67	15	18	33	234	247	481
No tag	137			47			21			10			215		
Tag ε (%)	69.8 ± 2.1			57.7 ± 4.7			76.1 ± 4.5			76.7 ± 6.4			69.1 ± 1.8		

Table 7: *CP* data sample for modes with a $\eta_{CP} = -1$. An $m_{\rm ES} > 5.27$ GeV/c^2 cut is applied for all modes. The lepton category is the sum of the $e+K$, $\mu+K$, e, and μ categories. These numbers include the small number of events that have $|\Delta t| > 20$ ps and $\sigma(\Delta t) > 2.5$ ps. These events are not used in the analysis, and are not included in the PRL numbers. These will be updated in the next version.

Figure 14: $m_{\rm ES}$ and ΔE (for the $J/\psi K^0_L$ channel) distributions for the *CP* modes after tagging requirements. The upper plots show the $B^0 \to J/\psi K^0_S$ $(\pi^+\pi^-)$ and $B^0 \to J/\psi K^0_S$ $(\pi^0\pi^0)$. The lower plots show the $B^0 \to \psi(2S)K^0_S$ and $B^0 \to J/\psi K^0_L$ modes.

7 *CP* data sample

Tables 7 and 8 summarize the *CP* event sample. Events are broken down by flavor tag and tagging category. In addition, Figure 14 shows the tagged data sample for each reconstructed mode.

8 Likelihood fit method

(Note: As of June 30, 2001, this section has been copied from the PRD (pub_0103) draft.)

The value of sin2β is extracted from the *CP* sample using an unbinned maximum likelihood technique using $\ln \mathcal{L}_{CP}$ and the probability density functions $\mathcal{F}_\pm$ of Eq. 11. However, the dilutions factors $\mathcal{D}_i$, Δz resolution parameters $\hat{a}_i$, are also needed for the measurement. Assuming that mistag rates and vertex resolutions do not depend on the particular channel used to reconstruct the B meson, these parameters are best determined using the much larger mixing sample, since they also appear in $\mathcal{L}_{mix}$. In order to properly incorporate the correlations between these parameters and sin2β, the fit is performed by simultaneously maximizing the sum:

$$\ln \mathcal{L}_{CP} + \ln \mathcal{L}_{mix} \tag{17}$$

Tag	CP =-1 modes			$J/\psi K^0_L$			$J/\psi K^{*0}$			Total		
	B^0	$\overline{B}^0$	Tot	B^0	$\overline{B}^0$	Tot	B^0	$\overline{B}^0$	Tot	B^0	$\overline{B}^0$	Tot
$e+K$	3	3	6	2	8	10	0	0	0	5	11	16
$\mu+K$	3	6	9	3	2	5	0	0	0	7	8	15
e	15	17	32	15	6	21	3	1	4	35	25	60
μ	11	16	27	8	4	12	2	2	4	22	23	45
Lepton	32	42	74	28	20	48	5	3	8	69	67	88
Kaon	131	140	271	82	59	141	12	14	26	225	213	4380
NT1	20	26	46	17	10	27	2	4	6	39	40	79
NT2	51	39	90	33	24	57	7	3	10	91	66	157
Total tag	234	247	481	160	113	273	26	24	50	420	384	804
No tag	266			142			19			376		
Tag ε (%)	69.1 ± 1.8			65.8 ± 2.3			72.5 ± 5.4			68.1 ± 1.4		

Table 8: CP data sample. An $m_{\rm ES} > 5.27$ GeV/c^2 cut is applied for all modes except the $J/\psi K^0_L$ channel, where a $|\Delta E| < 10$ MeV cut is used. The lepton category is the sum of the $e+K$, $\mu+K$, e, and μ categories. These numbers include the small number of events that have $|\Delta t| > 20$ ps and $\sigma(\Delta t) > 2.5$ ps. These events are not used in the analysis, and are not included in the PRL numbers. This will be updated in the next version.

using the combined tagged flavor-eigenstate and CP samples. The values of B^0 lifetime and Δm_d are kept fixed in extracting sin2β. The value of Δm_d is obtained with an unbinned maximum likelihood fit using the tagged flavor-eigenstate B^0 sample alone.

8.1 Mistag asymmetries

The probabilites of mistagging a B^0 or $\overline{B}^0$ meson are expected to be very nearly, but not exactly, equal. The response of the detector to positive pions and kaons differs from its response to negative pions and kaons due to differences in total and charge-exchange cross sections. To account for any possible mistag differences, we introduce separate mistag probabilities w for B^0 and $\overline{w}$ for $\overline{B}^0$ with the conventions

$$\begin{array}{rclcrcl} \langle w \rangle & = & \frac{1}{2}(w+\overline{w}); & & \delta w & = & (w-\overline{w}) \\ \mathcal{D} & = & 1-2w; & & \overline{\mathcal{D}} & = & 1-2\overline{w} \\ \langle \mathcal{D} \rangle & = & \frac{1}{2}(\mathcal{D}+\overline{\mathcal{D}}); & & \delta\mathcal{D} & = & (\mathcal{D}-\overline{\mathcal{D}}) \end{array}$$

The time distributions for the mixing and CP samples will thus depend on whether the tag was identified as a B^0 or a $\overline{B}$

$$\begin{array}{rcl} f_{mix,\ tag=B^0} & \propto & [(1+\frac{1}{2}\Delta\mathcal{D}) - \langle\mathcal{D}\rangle \cos\Delta m_d \Delta t] \\ f_{unmix,\ tag=B^0} & \propto & [(1+\frac{1}{2}\Delta\mathcal{D}) + \langle\mathcal{D}\rangle \cos\Delta m_d \Delta t] \\ f_{mix,\ tag=\overline{B}^0} & \propto & [(1-\frac{1}{2}\Delta\mathcal{D}) - \langle\mathcal{D}\rangle \cos\Delta m_d \Delta t] \\ f_{unmix,\ tag=\overline{B}^0} & \propto & [(1-\frac{1}{2}\Delta\mathcal{D}) + \langle\mathcal{D}\rangle \cos\Delta m_d \Delta t] \\ f_{CP,\ tag=B^0} & \propto & [(1+\frac{1}{2}\Delta\mathcal{D}) - \eta_{CP}\langle\mathcal{D}\rangle \sin 2\beta \sin\Delta m_d \Delta t] \\ f_{CP,\ tag=\overline{B}^0} & \propto & [(1-\frac{1}{2}\Delta\mathcal{D}) + \eta_{CP}\langle\mathcal{D}\rangle \sin 2\beta \sin\Delta m_d \Delta t] \end{array} \quad (19)$$

where we have taken $|\lambda| = 1$ and ignored the convolution with the resolution function.

8.2 Background modeling

In the presence of backgrounds, the probability distribution functions $\mathcal{H}_\pm$ of Eq. 3 and $\mathcal{F}_\pm$ of Eq. 11 must be extended to include a term for each significant background source. The backgrounds for the flavor eigenstates and $\eta_{CP} = -1$ modes are quite small and are mostly combinatoric in nature. However, for the $B^0 \to J/\psi K^0_L$ channel the backgrounds are substantial and originate mainly from other $B \to J/\psi X$ modes that have, to a very good approximation, the same flavor tagging and Δt resolution properties as the signal. The background properties of the flavor eigenstates, $\eta_{CP} = -1$ modes, and the non-J/ψ background in the $B^0 \to J/\psi K^0_L$ channel are determined empirically from sideband events in the data.

8.2.1 Background formulation for flavor eigenstates and $\eta_{CP} = -1$ modes

The background parameterizations are allowed to differ for each tagging category. Each event belongs to a particular tagging category, i. In addition, the event is classified as either mixed ($-$) or unmixed ($+$) for a flavor-eigenstate or by whether B_{tag} was a B^0 ($+$) or a $\overline{B}^0$ ($-$) for a *CP*-eigenstate. Thus a distribution must be specified for each possibility $(+/-, i)$

$$\mathcal{H}_{\pm,i} = f^{\rm flav}_{i,\rm sig}\mathcal{H}_\pm(\Delta t;\Gamma,\Delta m_d,w_i,\hat{a}_i) + f^{\rm flav}_{i,\rm peak}\mathcal{B}^{\rm flav}_{\pm,i,\rm peak}(\Delta t;\hat{a}_i) + \sum_{\beta=\rm bkgd} f^{\rm flav}_{i,\beta}\mathcal{B}^{\rm flav}_{\pm,i,\beta}(\Delta t;\hat{b}_i) \quad (20)$$

for flavor-eigenstates, and

$$\mathcal{F}_{\pm,i} = f^{CP}_{i,\rm sig}\mathcal{F}_\pm(\Delta t;\Gamma,\Delta m_d,w_i,\sin 2\beta,\hat{a}_i) + f^{CP}_{i,\rm peak}\mathcal{B}^{CP}_{\pm,i,\rm peak}(\Delta t;\hat{a}_i) + \sum_{\beta=\rm bkgd} f^{CP}_{i,\beta}\mathcal{B}^{CP}_{\pm,i,\beta}(\Delta t;\hat{b}_i) \quad (21)$$

for *CP*-eigenstates. The fraction of background events for each source and tagging category is a function of $m_{\rm ES}$ and is given by $f_{i,\beta}$. The peaking and combinatorial background PDFs, $\mathcal{B}_{\pm,i,\rm peak}$ and $\mathcal{B}_{\pm,i,\beta}$, provide an empirical description the Δt distribution of the background events in the sample, including a resolution function parameterized by $\hat{a}_i$ and $\hat{b}_i$ respectively. These distributions are normalized so that for each i and β

$$\int_{-\infty}^{\infty} d\Delta t(\mathcal{B}_{+,i,\beta} + \mathcal{B}_{-,i,\beta}) = 1. \quad (22)$$

The probability that a B^0 candidate is a signal or a background event is determined from a separate fit to the observed $m_{\rm ES}$ distributions of $B_{\rm flav}$ or B_{CP} candidates. We describe the $m_{\rm ES}$ shape with a single Gaussian distribution $\mathcal{S}(m_{\rm ES})$ for the signal and an ARGUS parameterization $\mathcal{A}(m_{\rm ES})$ for the background. Based on this fit, the event-by-event signal and background probabilities that appear as the relative weights for the

various signal and background terms in Eq. 20 and 21 are given by

$$\begin{aligned} f_{i,\mathrm{sig}}(m_{\mathrm{ES}}) &= \frac{(1-\delta_{\mathrm{peak}})\mathcal{S}(m_{\mathrm{ES}})}{\mathcal{S}(m_{\mathrm{ES}})+\mathcal{A}(m_{\mathrm{ES}})} \\ f_{i,\mathrm{peak}}(m_{\mathrm{ES}}) &= \frac{\delta_{\mathrm{peak}}\mathcal{S}(m_{\mathrm{ES}})}{\mathcal{S}(m_{\mathrm{ES}})+\mathcal{A}(m_{\mathrm{ES}})} \\ \sum_{\beta=\mathrm{bkgd}} f_{i,\beta}(m_{\mathrm{ES}}) &= \frac{\mathcal{A}(m_{\mathrm{ES}})}{\mathcal{S}(m_{\mathrm{ES}})+\mathcal{A}(m_{\mathrm{ES}})} \end{aligned} \tag{23}$$

The fraction δ_{peak} of the signal Gaussian distribution that is due to peaking backgrounds is determined from Monte Carlo simulation.

Backgrounds arise from many different sources. Rather than attempting to determine the various physics contributions we use an empirical description in the likelihood fit, allowing for background components with various time dependences. For the B_{flav} sample, the background time distributions considered, each with its own effective dilution factor $\mathcal{D}_i$ and either a common resolution function $\mathcal{R}(\Delta t;\hat{b}_i)$ or the signal resolution function $\mathcal{R}(\delta_{\mathrm{t}}=\Delta t-\Delta t_{\mathrm{true}};\hat{a}_i)$, are

$$\begin{aligned} \mathcal{B}^{\mathrm{flav}}_{\pm,i,1} &= (1/2)(1\pm\mathcal{D}^{\mathrm{flav}}_{i,1})\ \delta(\Delta t)\otimes\mathcal{R}(\delta_{\mathrm{t}};\hat{b}_i), \\ \mathcal{B}^{\mathrm{flav}}_{\pm,i,2} &= (\Gamma^{\mathrm{flav}}_{i,2}/4)(1\pm\mathcal{D}^{\mathrm{flav}}_{i,2})\ \mathrm{e}^{-\Gamma^{\mathrm{flav}}_{i,2}|\Delta t|}\otimes\mathcal{R}(\delta_{\mathrm{t}};\hat{b}_i), \\ \mathcal{B}^{\mathrm{flav}}_{\pm,i,3} &= (\Gamma^{\mathrm{flav}}_{i,3}/4)(1\pm\mathcal{D}^{\mathrm{flav}}_{i,3}\cos\delta m_{i,3}\Delta t)\ \mathrm{e}^{-\Gamma^{\mathrm{flav}}_{i,3}|\Delta t|}\otimes\mathcal{R}(\delta_{\mathrm{t}};\hat{b}_i), \\ \mathcal{B}^{\mathrm{flav}}_{\pm,i,\mathrm{peak}} &= (\Gamma_{i,\mathrm{peak}}/4)(1\pm\mathcal{D}^{\mathrm{flav}}_{i,\mathrm{peak}}\cos\delta m_{i,\mathrm{peak}}\Delta t)\ \mathrm{e}^{-\Gamma^{\mathrm{flav}}_{i,\mathrm{peak}}|\Delta t|}\otimes\mathcal{R}(\delta_{\mathrm{t}};\hat{a}_i), \end{aligned} \tag{24}$$

corresponding to prompt, non-prompt, and mixing background components, as well as a peaking contribution. For the $\eta_{CP}=-1$ sample, the possible background contributions are

$$\begin{aligned} \mathcal{B}^{CP}_{\pm,i,1} &= (1/2)\delta(\Delta t)\otimes\mathcal{R}(\delta_{\mathrm{t}};\hat{b}_i), \\ \mathcal{B}^{CP}_{\pm,i,2} &= (\Gamma_{i,2}/4)(1\pm\mathcal{D}^{CP}_{i,2}\sin\Delta m_d\Delta t)\ \mathrm{e}^{-\Gamma^{CP}_{i,2}|\Delta t|}\otimes\mathcal{R}(\delta_{\mathrm{t}};\hat{b}_i), \\ \mathcal{B}^{CP}_{\pm,i,\mathrm{peak}} &= (\Gamma_{i,\mathrm{peak}}/4)(1\pm\mathcal{D}^{CP}_{i,\mathrm{peak}}\sin\Delta m_d\Delta t)\ \mathrm{e}^{-\Gamma^{CP}_{\mathrm{peak}}|\Delta t|}\otimes\mathcal{R}(\delta_{\mathrm{t}};\hat{a}_i), \end{aligned} \tag{25}$$

corresponding to prompt and CP background components as well as a peaking contribution. The background resolution function parameters $\hat{b}_i$ are common with the background resolution function of the B_{flav} sample. The likelihood fit includes as free parameters the fraction of each time component, as well as apparent lifetimes, resolutions, mixing frequencies and dilutions that best describe the events with high weights for being background. These parameters, and additional assumptions made are described below, in Section 8.5.

8.2.2 Background formulation for $B^0\to J/\psi K^0_L$

(See BAD206 for further details)
The higher background level in the $B^0\to J/\psi K^0_L$ channel requires a more extensive treatment of the background properties. The data are used to determine the relative amount of signal, background from $B\to J/\psi X$ events, and events with a misreconstructed

Sample	EMC	IFR
Data	228	119
Signal	128 ± 17	129 ± 17
$B \to J/\psi X$	89 ± 11	65 ± 10
Non-J/ψ background	14 ± 2	5 ± 1

Table 9: $B \to J/\psi K^0_L$ ΔE fit results for the EMC and IFR samples. Numbers quoted are in the $\Delta E < 10$ MeV signal region.

$J/\psi \to \ell\ell$ candidate. Along with a Monte Carlo simulation of the channels that contribute to the $B \to J/\psi X$ background, this information is used to formulate the PDF model. In addition, some of the $J/\psi X$ background modes, such as $B^0 \to J/\psi K^{*0}$ and $B^0 \to J/\psi K^0_S$ have a non-zero CP asymmetry (η_{CP}), as given in Table 10. The value of the asymmetry in $B^0 \to J/\psi K^{*0}(K^0_L\pi^0)$ is taken from the measurement of $R_T = 0.16 \pm 0.04 \pm 0.??$ in Ref. [11]. The probability density functions $\mathcal{F}_\pm$ of Eq. 11 are given by

$$\begin{aligned}
\mathcal{F}_{\pm,i} &= f_{i,sig}(\Delta E)\mathcal{F}_\pm(\Delta t;\Gamma,\Delta m_d, w_i, \sin 2\beta, \hat{a}_i) \\
&+ \sum_{\alpha=J/\psi X} f_{i,\alpha}(\Delta E)\ \mathcal{F}_\pm(\Delta t;\Gamma,\Delta m_d, \eta_{f,\alpha}, w_i, \sin 2\beta, \hat{a}_i) \\
&+ f_{i,\mathrm{non}-J/\psi}(\Delta E)\ \mathcal{B}^{KL}_\pm(\Delta t;\hat{b}). \qquad (26)
\end{aligned}$$

Each event is classified according to its flavor tagging category (i), flavor tag value ($\pm$), and the K^0_L reconstruction category (j), which is either EMC or IFR. The signal fraction $f_{i,sig}$ and background fractions $f_{i,\alpha}$ and $f_{i,\mathrm{non}-J/\psi}$ are determined as a function of ΔE and are the same for all tag categories. The shape of the signal and background ΔE functions are determined either from data (non-J/ψ contribution) or from Monte Carlo samples (signal and $J/\psi X$ background). The normalizations $\int_{-10\ \mathrm{MeV}}^{10\ \mathrm{MeV}} d(\Delta E) f$ are determined from Tables 10 and 9 so that

$$f_{i,\mathrm{sig}}(\Delta E) + f_{i,\mathrm{non}-J/\psi}(\Delta E) + \sum_{J/\psi X} f_{i,\alpha}(\Delta E) = 1. \qquad (27)$$

The non-J/ψ background PDF is given by

$$\mathcal{B}^{KL}_\pm = F_{\tau=0}\mathcal{B}^{CP}_{\pm,i,1} + (1 - F_{\tau=0})\mathcal{B}^{CP}_{\pm,i,2} \qquad (28)$$

where $\mathcal{D}^{CP}_{i,2} = 0$ and the parameters $F_{\tau=0}$, $\Gamma_{i,2} \equiv \Gamma_{\mathrm{bg}}$, and $\hat{b}$ are fixed to values obtained from an external fit of the $m(\ell\ell)$ sideband events as given in Table 11. $\mathcal{R}(\Delta t;\hat{b})$ is the resolution function defined in Eq. 16 with $f_3 = 0.005$ and with core bias δ_1 equal for all tagging categories.

The $J/\psi K^0_L$ sample has a significant amount of background, but most of it is from other J/ψ modes. The Monte Carlo was used to check the flavor tagging efficiency of the inclusive J/ψ background relative to the signal for the K^0_L mode. The Monte Carlo

Event type	EMC (%)	IFR (%)	Effective CP
Signal	55.5	64.9	1
$B^0 \to J/\psi K^{*0}(K^0_L\pi^0)$	8.6	8.2	-0.68
$B^+ \to J/\psi K^{*\pm}(K^0_L\pi^\pm)$	10.8	14.2	0
$B^0 \to J/\psi K^0_S$	4.9	1.0	-1
$B^0 \to \chi_{c1} K^0_L$	1.3	1.7	$+1$
$B \to J/\psi K^0_L\pi$	0.8	1.0	0
Other $B^0 \to J/\psi X$	12.3	6.4	0
Non $B \to J/\psi X$	5.8	2.6	0

Table 10: Composition of background channels containing that pass the $B^0 \to J/\psi K^0_L$ selection criteria. Events are required to have $\Delta E < 10\,\mathrm{MeV}$.

Parameter	Fit result
$F_{\tau=0}$	0.84 ± 0.49
Γ_{bg}	$0.53 \pm 0.11\,\mathrm{ps}^{-1}$
S_1	1.25 ± 0.45
δ_1	-0.11 ± 0.20
S_2	3.86 ± 0.83
δ_2	-1.18 ± 1.04
f_2	0.23 ± 0.14
f_3	0.005 (fixed)

Table 11: Parameters of the probability distribution function for the non-J/ψ background contribution in the $B^0 \to J/\psi K^0_L$ channel. The biases scale with the reported event by event error.

inclusive J/ψ background fraction is consistent across the flavor tag categories to within a few percent. The flavor tag efficiency for the fake-J/ψ background, determined from the J/ψ sideband, is also roughly consistent with signal. The composition of the $J/\psi K_L^0$ sample is determined from a fit of the ΔE spectrum before flavor tagging. We assume the inclusive J/ψ and fake-J/ψ background fractions are flavor tag independent in the nominal fit and adjust the fractions as a function of flavor tag category, based on the Monte Carlo and J/ψ sideband, as a systematic error.

Some of the decay modes in the inclusive J/ψ background, such as $J/\psi K^{*0}$ and $J/\psi K_S^0$, have an expected *CP* asymmetry. The flavor tag mistag fractions for all *CP* modes in the inclusive J/ψ background were measured in the Monte Carlo and found to be consistent with the values for the signal. We assume that the signal mistag fractions apply to the *CP* modes in the inclusive J/ψ background.

The Δt resolution for the $B \to J/\psi X$ background should be very similar to the signal resolution. However, extra tracks associated with $B^+ \to J/\psi X^+$ decay, such as the charged π from the K^{*+} decay in $B^+ \to J/\psi K^{*+}$, could bias the measurement of Δt since the extra tracks are not associated with the *CP* B vertex and therefore can be used in the tag B vertex. In the Monte Carlo simulation, we find that extra tracks in the $B \to J/\psi X$ decay modes have a negligible effect on the Δt resolution. Therefore, we assume that all $B \to J/\psi X$ background has the same resolution as the signal.

The Δt resolution of the non-J/ψ background was measured using the J/ψ sideband sample. The non-J/ψ Δt resolution parameters were varied by their statistical uncertainties to estimate the systematic uncertainty.

8.3 Background formulation for $B^0 \to J/\psi K^{*0}(K_S^0\pi 0)$

The $B^0 \to J/\psi K^{*0}(K_S^0\pi^0)$ channel is treated much the same as the $B^0 \to J/\psi K_L^0$ channel. Only events with $5.273 < m_{\rm ES} < 5.288$ GeV/c^2 are considered and all events have the same signal and background fractions. Table 12 shows the breakdown of the signal and background fractions for this channel. The likelihood becomes

$$\begin{aligned} \mathcal{F}_{\pm,i} &= f_{i,sig}\mathcal{F}_{\pm}(\Delta t;\Gamma,\Delta m_d,w_i,\sin 2\beta,\hat{a}_i) \\ &+ \sum_{\alpha=J/\psi X} f_{i,\alpha}\mathcal{F}_{\pm}(\Delta t;\Gamma,\Delta m_d,\eta_{f,\alpha},w_i,\sin 2\beta,\hat{a}_i) \end{aligned} \tag{29}$$

for $B^0 \to J/\psi K^{*0}(K_S^0\pi^0)$, as the non $B \to J/\psi X$ contribution is neglected.

8.4 Extensions for direct *CP* search

While the main likelihood fits are performed with the Standard Model expectation that $|\lambda| = 1$, a search for the effects of direct *CP* violation is also made. Such a measurement is also particularly sensitive to possible differences in the fraction of B^0 or $\overline{B}^0$ meson that are tagged. Defining $\epsilon_{\rm tag}$ and $\overline{\epsilon}_{\rm tag}$ as the tagging efficiencies for B^0 and $\overline{B}^0$, and $\epsilon_{\rm r}$ and $\overline{\epsilon}_{\rm r}$ as

Event type	Fraction (%)	Effective CP
Signal	73.6	0.65
$B^+ \to J/\psi K^{*\pm}(K^0_S\pi^\pm)$	17.4	0
$B^0 \to \chi_{cK^0_S}$	2.4	-1
Higher K^* resonances	2.6	0
Non-resonant $B^0 \to J/\psi K^0_S\pi^0$	1.8	0
Other $B^0 \to J/\psi X$	2.4	0
Non $B \to J/\psi X$	0	0

Table 12: Signal and background parameters used in the $B^0 \to J/\psi K^{*0}(K^0_S\pi^0)$ PDF.

the reconstruction efficiencies for B^0 and $\overline{B}^0$ in the $B_{\rm flav}$ sample, it is useful to construct

$$\mu = \frac{\epsilon_{\rm tag} - \overline{\epsilon}_{\rm tag}}{\epsilon_{\rm tag} + \overline{\epsilon}_{\rm tag}}, \qquad \langle\epsilon_{\rm tag}\rangle = \frac{\epsilon_{\rm tag} + \overline{\epsilon}_{\rm tag}}{2} \tag{30}$$

$$\nu = \frac{\epsilon_{\rm r} - \overline{\epsilon}_{\rm r}}{\epsilon_{\rm r} + \overline{\epsilon}_{\rm r}}, \qquad \langle\epsilon_{\rm r}\rangle = \frac{\epsilon_{\rm r} + \overline{\epsilon}_{\rm r}}{2}. \tag{31}$$

For the B_{CP} sample the time-dependent decay rate (Eg. 10) becomes

$$\begin{aligned} f_\pm(t) &= \left[\frac{2\,(1+|\lambda|^2)}{\Gamma} + \frac{2\mu(|\lambda|^2-1)}{\Gamma(1+x_d^2)}\right]^{-1} \mathrm{e}^{-\Gamma|\Delta t|} \\ &\times \left[\frac{1+|\lambda|^2}{2}(1\pm X) + (\mu \pm X')\left(Im\lambda \sin\Delta m_d\Delta t - \frac{1-|\lambda|^2}{2}\cos\Delta m_d\Delta t\right)\right] \end{aligned} \tag{32}$$

where

$$\begin{aligned} X &= \mu\langle\mathcal{D}\rangle + \frac{\delta\mathcal{D}}{2} \\ X' &= \langle\mathcal{D}\rangle + \frac{\mu\delta\mathcal{D}}{2}. \end{aligned} \tag{33}$$

Likewise, for the $B_{\rm flav}$ sample the time-dependent decay rate (Eq. 4) becomes

$$f(t) = \left[1 - \frac{\mu\nu}{1+x_d^2}\right]^{-1} \frac{\Gamma}{4}\mathrm{e}^{-\Gamma|\Delta t|}(1+s_1\nu)\left[1 + s_3X - s_1(\mu + s_3X')\cos\Delta m_d\Delta t\right] \tag{34}$$

where

$$\begin{aligned} s_1 &= 1(-1) \text{ if the reconstructed } B \text{ is a } B^0(\overline{B}^0) \\ s_2 &= 1(-1) \text{ for a mixed(unmixed) event} \\ s_3 &= 1(-1) \text{ for a } B^0(\overline{B}^0) \text{ tag} \end{aligned}$$

The parameters ν, T and μ can be extracted from time integrated numbers of events in the $B_{\rm flav}$ sample. Defining integrated samples of events by

$$\begin{aligned} N_i^{\rm tag} &= N(\text{tag in } i^{th} \text{ category for } B^0 \text{ or } \overline{B}^0, B_{\rm flav} = B^0) \\ \overline{N}_i^{\rm tag} &= N(\text{tag in } i^{th} \text{ category for } B^0 \text{ or } \overline{B}^0, B_{\rm flav} = \overline{B}^0) \\ N_i^{\text{no tag}} &= N(\text{no tag in } i^{th} \text{ category}, B_{\rm flav} = B^0) \\ \overline{N}_i^{\text{no tag}} &= N(\text{no tag in } i^{th} \text{ category}, B_{\rm flav} = \overline{B}^0) \end{aligned} \tag{35}$$

it can be shown that

$$\begin{aligned} \nu &= \frac{N_i^{\rm tag} - \overline{N}_i^{\rm tag} + N_i^{\text{no tag}} - \overline{N}_i^{\text{no tag}}}{N_i^{\rm tag} + \overline{N}_i^{\rm tag} + N_i^{\text{no tag}} + \overline{N}_i^{\text{no tag}}} \\ \langle \epsilon_{\rm tag} \rangle &= \frac{2N_i^{\rm tag}\overline{N}_i^{\rm tag} + \overline{N}_i N_i^{\rm notag} + N_i \overline{N}_i^{\text{no tag}}}{2(N_i^{\rm tag} + \overline{N}_i^{\rm tag})(N_i^{\text{no tag}} + \overline{N}_i^{\text{no tag}})} \\ \mu &= \frac{(1+x_d^2)(\overline{N}_i^{\rm tag} N_i^{\text{no tag}} - N_i^{\rm tag}\overline{N}_i^{\text{no tag}})}{2N_i^{\rm tag}\overline{N}_i^{\rm tag} + \overline{N}_i^{\rm tag} N_i^{\text{no tag}} + N_i^{\rm tag}\overline{N}_i^{\text{no tag}}} \end{aligned} \tag{36}$$

under the assumption that the assumption that nearly all B decays are to final states that can be reached only from one of B^0 and $\overline{B}^0$, and not both. The results for $\langle \epsilon_{\rm tag} \rangle$ and μ are shown in Table 13. The value of ν, averaged over all four tagging categories is 0.004 ± 0.012. While there is no statistically significant difference in the tagging efficiencies or the reconstruction efficiencies given by μ and ν respectively, we use the central values obtained from the $B_{\rm flav}$ sample in performing the fit for $|\lambda|$.

Tagging category	$\langle \epsilon_{\rm tag} \rangle$	μ
`Lepton`	0.095 ± 0.002	0.069 ± 0.032
`Kaon`	0.358 ± 0.003	-0.005 ± 0.014
`NT1`	0.080 ± 0.002	0.061 ± 0.035
`NT2`	0.139 ± 0.002	0.017 ± 0.026

Table 13: Values of $\langle \epsilon_{\rm tag} \rangle$ and μ for the four tagging categories, as determined by counting numbers of tagged and untagged events in the $B_{\rm flav}$ sample.

8.5 Free parameters for the sin2β and Δm_d fits

The unbinned likelihood fit for sin2β has a total of 35 free parameters:

- **Value of sin2β;**
- **Signal resolution function:** Sixteen parameters $\hat{a}_i$ to describe the resolution function for the signal, being scale factors $S_{\rm core}$ for the event-by-event Δz resolution errors of the core and tail Gaussian components, individual core biases $\delta_{1,i}$ for the four tagging categories and a common tail bias δ_2, and the tail f_2 and outlier f_3

Tag category	Dilution
Lepton	0.918
Kaon	0.764
NT1	0.574
NT2	0.256

Table 14: Charged B dilutions used for the peaking background contribution to the $B_{\rm flav}$ events.

fractions. These eight parameters were duplicated for the Run 1 and Run 2 resolution functions. $S_{\rm tail}$ was fixed from Monte Carlo to 3 and the width of the outlier component is taken to be a fixed 8 ps with zero bias;

- **Signal dilutions:** Eight parameters to describe the measured average dilutions $\langle \mathcal{D}_i \rangle$ and dilution differences $\delta\mathcal{D}_i$ in each tagging category.

- **Background resolution function:** Three parameters are used to describe a common resolution function for all non-peaking backgrounds, which is taken as a single Gaussian distribution with a scale factor S_1 for the event-by-event Δz errors and an common bias δ_1, and an outlier fraction f_3; the width of the outlier component is taken to be a fixed 8 ps with zero bias;

- $B_{\rm flav}$ **background composition parameters:** A total of 13 parameters describe the $B_{\rm flav}$ background composition. We make several assumptions to simplify the parameterization shown in Eq. 24 and assign a corresponding systematic uncertainty. The mixing background contribution is assumed to be absent, $f_{i,3}^{\rm flav} = 0$. The size of the peaking background is determined from Monte Carlo simulation to be $\delta_{\rm peak}^{\rm flav} = 1.5 \pm 0.5\%$ of the signal contribution in each tagging category. This contribution is predominately from B^+ events, so $\Delta m_{i,\rm peak} = 0$, $\Gamma_{i,\rm peak}^{\rm flav} = \Gamma_{B^+}$ and $D_{i,\rm peak}^{\rm flav}$ are taken from the B^+ data sample (Table 14). The effective dilutions for the prompt ($D_{i,1}^{\rm flav}$, 4 parameters) and non-prompt ($D_{i,2}^{\rm flav}$, 4 parameters) contributions are allowed to vary. The relative amount of these two contributions is allowed to vary, independently in each tagging category (4 parameters). For the non-prompt contribution, $\Gamma_{i,2}^{\rm flav}$ is assumed to be same for all tagging categories, giving one free parameter.

- *CP* **background composition paramters:** One parameter, the fraction of prompt relative to non-prompt background, assumed to be the same for each tagging category, is allowed to float to describe the *CP* background properties. The effective dilutions of the non-prompt and peaking contribution are set to zero ($D_{i,2}^{CP} = D_{i,\rm peak}^{CP} = 0$), corresponding to no *CP*-asymmetry in the background. The size and parameters of the peaking background is again determined from Monte Carlo simulation. The fraction of the Gaussian contribution that is "peaking" background is shown in Table 6 of the signal contribution, independent of tagging category. This contribution is assumed to have dilutions and lifetime parameters in common with the signal

contribution. Finally, the lifetime of the non–prompt background is assumed to be τ_{B^0} in all tagging categories.

The unbinnned likelihood fit for Δm_d has 34 free parameters, removing sin2β and the parameter for fraction of prompt background in the *CP* sample and leaving Δm_d to float.

8.6 Blind analysis

A the value of sin2β was hidden until June 29 in order to eliminate possible experimenter's bias. We used a method that hides not only the central value for these parameters from the unbinned maximum likelihood fit, but also the visual *CP* asymmetry in the Δt distribution. The error on the asymmetry is not hidden.

The amplitude of the asymmetry $\mathcal{A}_{CP}(\Delta t)$ from the fit was hidden by a one-time choice of sign flip and arbitrary offset based on a user-specified key word. The sign flip hides whether a change in the analysis increases or decreases the resulting asymmetry. However, the magnitude of the change is not hidden. The visual *CP* asymmetry in the Δt distribution is hidden by multiplying Δt by the sign of the tag and adding an arbitrary offset.

With these techniques, systematic studies can be performed while keeping the numerical value of sin2β hidden. In particular, we can check that the hidden Δt distributions are consistent for B^0 and $\overline{B}^0$ tagged events. The same is true for all the other checks concerning tagging, vertex resolution and the correlations between them.

The two new decay modes, $\chi_{cK^0_S}$ and $J/\psi K^{*0}(K^0_S\pi^0)$, were blinded with a separate blinding string until the decision was made to include them for certain in this result. Given that the Run 1 data sample had been previous analyzed, we were not as completely blind as during the analysis for the PRL result. In this case, based on previous experience one could easily determine which direction was "up" and which was "down" given the result (for example) of the $\chi_{cK^0_S}$ fit relative to the others.

9 Results

9.1 $m_{\rm ES}$ fit results

Table 15 as well as Figures 15 and 16 show the results of the $m_{\rm ES}$ fits used to compute the signal and background probabilities in the likelihood fit.

9.2 *CP* + mixing combined fit results

We perform likelihood fits to each of the *CP* samples combined with the $B_{\rm flav}$ mixing sample. The fitted values (with parabolic errors) for the free fit parameters are listed in Tables 16 to 23. The fit results with asymmetric errors (`MINOS`) including the correlation

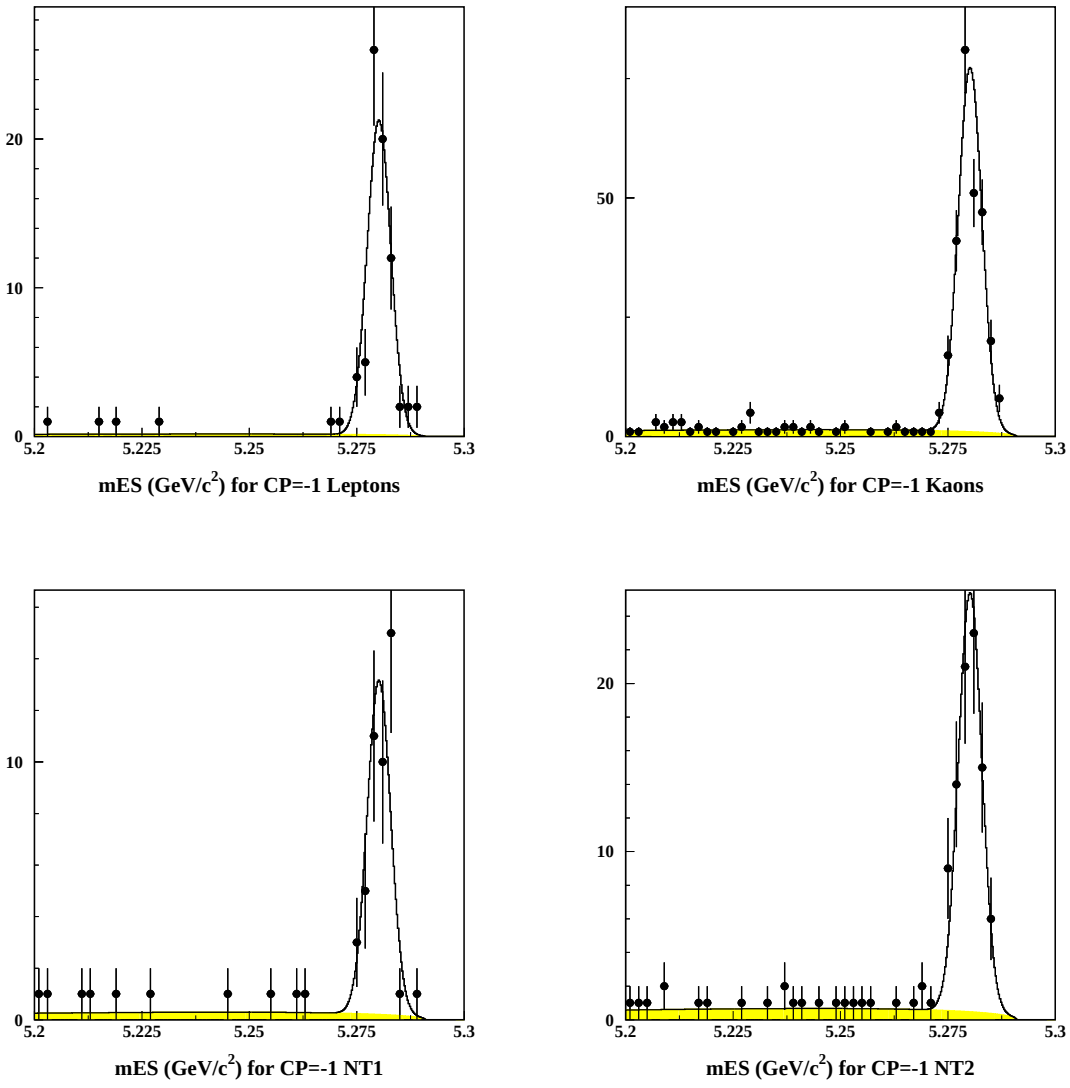

Figure 15: $m_{\rm ES}$ fits to each tagging category for $J/\psi K^0_S$, $\psi(2S)K^0_S$ events. Lepton tags (top, left), kaon tags (top, right), NT1 tags (bottom, left), and NT2 tags (bottom, right) are shown.

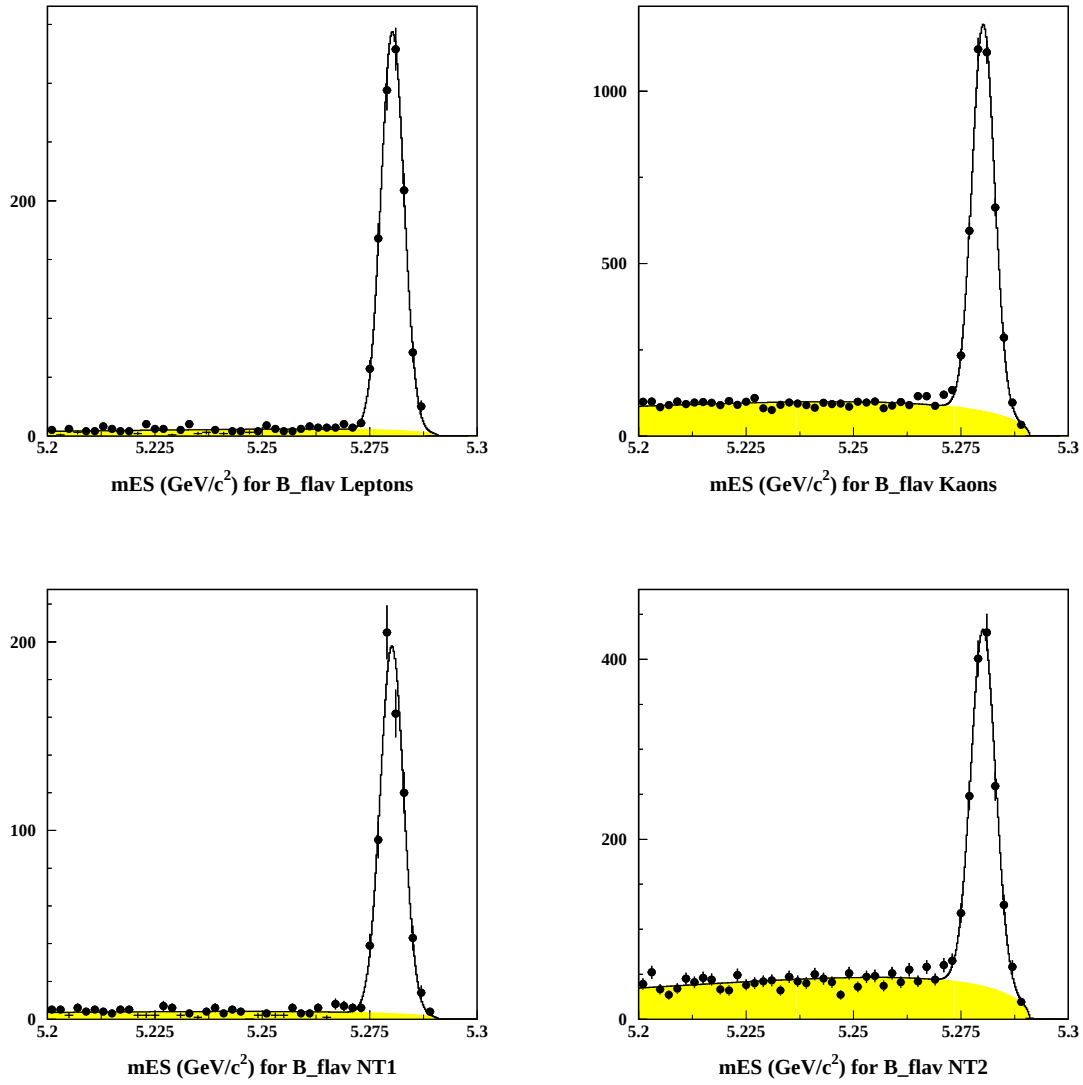

Figure 16: $m_{\rm ES}$ fits to each tagging category for $B_{\rm flav}$ events. Lepton tags (top, left), kaon tags (top, right), NT1 tags (bottom, left), and NT2 tags (bottom, right) are shown.

	Lepton	Kaon	NT1	NT2
	$CP = -1$			
# signal evts	72 ± 9	260 ± 16	44 ± 7	85 ± 9
Mean (MeV/c^2)	5280.2 ± 0.1			
σ (MeV)	2.72 ± 0.09			
# bkg. evts	7 ± 3	58 ± 8	12 ± 3	27 ± 5
Sig. fraction	$91.4 \pm 3.6\%$	$81.9 \pm 2.4\%$	$79.0 \pm 5.9\%$	$76.0 \pm 4.4\%$
κ	-28.1 ± 11.3			
	$B_{\rm flav}$ modes			
# signal evts	1128 ± 34	3687 ± 63	819 ± 30	1428 ± 40
Mean (MeV/c^2)	5280.3 ± 0.1	5280.2 ± 0.1	5280.3 ± 0.1	5280.2 ± 0.1
σ (MeV)	2.65 ± 0.06	2.62 ± 0.04	2.54 ± 0.09	2.87 ± 0.08
# bkg. evts	223 ± 14	3992 ± 65	605 ± 25	1830 ± 45
Sig. fraction	$83.5 \pm 1.2\%$	$48.0 \pm 0.7\%$	$57.5 \pm 1.6\%$	$43.8 \pm 1.2\%$
κ	-41.6 ± 9.4	-28.4 ± 2.2	-34.8 ± 5.6	-36.3 ± 3.3

Table 15: Results of the $m_{\rm ES}$ fits. The Gaussian mean and σ as well as the Argus function κ parameter are fixed using a fit to all tagged events for the $\eta_{CP} = -1$ sample. The normalization of each contribution is allowed to float in a fit to each tagging category. The quoted background s does not refer to the signal region only, but extends down to $m_{\rm ES} > 5.2$ GeV.

matrices are given in Appendix B. We find

$$\begin{aligned} \sin2\beta \text{ (all)} &= 0.59 \pm 0.14, \\ \sin2\beta \ (CP = -1) &= 0.56 \pm 0.15, \\ \sin2\beta \ (J/\psi K^0_L) &= 0.70 \pm 0.34, \\ \sin2\beta \ (J/\psi K^{*0}) &= 0.82 \pm 1.00 \end{aligned} \tag{37}$$

Figure 17 shows the values of $\sin2\beta$ obtained when the fit is performed in bins of Δt. In this case, all parameters except for $\sin2\beta$ are fixed from the nominal fit.

The contribution to the statistical error from free parameters other than $\sin2\beta$ is 0.016, 0.016, or 0.046 for all CP, $\eta_{CP} = -1$, and for $J/\psi K^0_L$ events, respectively. Tables 24 to 27 show the CP results for various subsamples of the data such as tagging category, flavor of the tagging B and J/ψ decay mode. In these fits to the subsamples, both the CP samples and the $B_{\rm flav}$ samples are split. For example, in the fit for $\sin2\beta$ in the with B^0 tagged events also the resolution function parameters are determined from B^0 tagged events only. Events with a $\bar{B}^0$ tag are not considered and therefore do not affect the result. This procedure leads to an interesting feature, if one splits the sample by the flavor of the tagging B. The values of $\sin2\beta$ for the two subsamples are both below the fit value for the combined sample (see eg. Table 25). If one fits only one flavor of the tagging B, the correlation coefficient between $\sin2\beta$ and the resolution function biases is large (eg. 0.3 for the core Gaussian of the lepton category) and has opposite sign for B^0 tagged

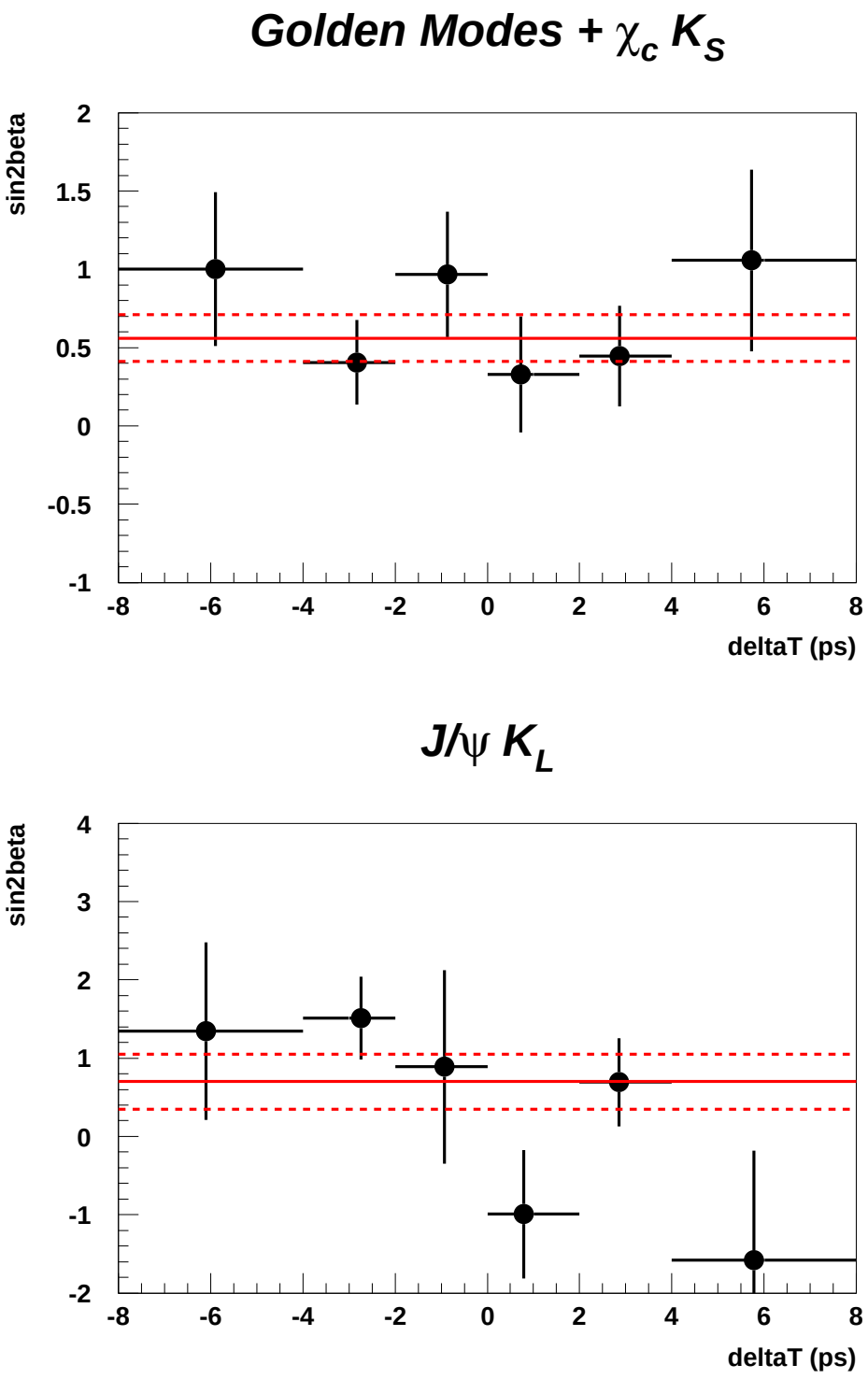

Figure 17: Results when fitting for sin2β in bins of Δt.

Parameter	tFit	CPExtract	DirectCP	Corr.
sin2β	0.563 ± 0.151	0.564 ± 0.151	-	
$\|\lambda\|$	—	—	0.933 ± 0.092	
$\mathcal{I}m\lambda/\|\lambda\|$	—	—	0.561 ± 0.151	
Run 1 Signal Resolution Function				
Scale (core)	1.20 ± 0.11	1.20 ± 0.11	1.20 ± 0.11	
$\delta(\Delta t)$ lepton (core)	0.044 ± 0.126	0.045 ± 0.127	0.044 ± 0.127	
$\delta(\Delta t)$ kaon (core)	-0.246 ± 0.077	-0.246 ± 0.077	-0.2478 ± 0.078	
$\delta(\Delta t)$ NT1 (core)	-0.197 ± 0.150	-0.196 ± 0.150	-0.198 ± 0.150	
$\delta(\Delta t)$ NT2 (core)	-0.317 ± 0.110	-0.323 ± 0.112	-0.323 ± 0.112	
$\delta(\Delta t)$ (tail)	-1.524 ± 1.101	-1.55 ± 1.09	-1.52 ± 1.07	
f(tail)	0.081 ± 0.053	0.081 ± 0.052	0.081 ± 0.052	
f(outlier)	0.005 ± 0.003	0.005 ± 0.003	0.005 ± 0.003	
Run 2 Signal Resolution Function				
Scale (core)	1.15 ± 0.12	1.14 ± 0.11	1.14 ± 0.11	
$\delta(\Delta t)$ lepton (core)	0.018 ± 0.162	0.016 ± 0.160	0.006 ± 0.160	
$\delta(\Delta t)$ kaon (core)	-0.201 ± 0.097	-0.201 ± 0.095	-0.203 ± 0.095	
$\delta(\Delta t)$ NT1 (core)	-0.355 ± 0.208	-0.357 ± 0.208	-0.358 ± 0.209	
$\delta(\Delta t)$ NT2 (core)	-0.147 ± 0.153	-0.142 ± 0.148	-0.144 ± 0.148	
$\delta(\Delta t)$ (tail)	-3.289 ± 3.036	-3.39 ± 3.17	-3.42 ± 3.15	
f(tail)	0.032 ± 0.042	0.031 ± 0.041	0.031 ± 0.040	
f(outlier)	0.000 ± 0.002	0 ± 0.001	0.000 ± 0.001	
Signal dilutions				
$\langle D \rangle$, lepton	0.821 ± 0.027	0.821 ± 0.027	0.820 ± 0.027	
$\langle D \rangle$, kaon	0.649 ± 0.020	0.648 ± 0.020	0.648 ± 0.020	
$\langle D \rangle$, NT1	0.557 ± 0.042	0.558 ± 0.065	0.559 ± 0.042	
$\langle D \rangle$, NT2	0.300 ± 0.037	0.298 ± 0.037	0.297 ± 0.037	
ΔD, lepton	-0.029 ± 0.044	-0.030 ± 0.044	-0.065 ± 0.044	
ΔD, kaon	0.030 ± 0.030	0.031 ± 0.030	0.038 ± 0.030	
ΔD, NT1	-0.126 ± 0.065	-0.125 ± 0.065	-0.153 ± 0.065	
ΔD, NT2	0.103 ± 0.055	0.106 ± 0.055	0.101 ± 0.055	

Table 16: Fitted values for the parameters of the combined *CP* and mixing fit using the $\eta_{CP} = -1$ *CP* modes.

Parameter	tFit	CPExtract	DirectCP	Corr.
Background properties				
τ, mixing bgd [ps]	1.28 ± 0.08	1.28 ± 0.08	1.28 ± 0.08	
$f(\tau = 0)$, *CP* bgd	0.603 ± 0.116	0.605 ± 0.116	0.607 ± 0.116	
$f(\tau = 0)$, mixing bgd, lepton	0.314 ± 0.097	0.313 ± 0.097	0.327 ± 0.096	
$f(\tau = 0)$, mixing bgd, kaon	0.652 ± 0.036	0.650 ± 0.036	0.653 ± 0.036	
$f(\tau = 0)$, mixing bgd, NT1	0.617 ± 0.058	0.616 ± 0.059	0.621 ± 0.058	
$f(\tau = 0)$, mixing bgd, NT2	0.644 ± 0.044	0.645 ± 0.043	0.649 ± 0.043	
Run 1 background resolution function				
Scale (core)	1.500 ± 0.040	1.50 ± 0.040	1.503 ± 0.040	
$\delta(\Delta t)$ core	-0.156 ± 0.032	-0.156 ± 0.032	-0.156 ± 0.032	
f(outlier)	0.016 ± 0.004	0.016 ± 0.004	0.016 ± 0.004	
Run 2 background resolution function				
Scale (core)	1.336 ± 0.044	1.33 ± 0.044	1.335 ± 0.044	
$\delta(\Delta t)$ core	0.018 ± 0.037	0.020 ± 0.037	0.020 ± 0.037	
f(outlier)	0.018 ± 0.005	0.017 ± 0.005	0.017 ± 0.005	
Background dilutions				
$\langle D \rangle$, lepton, $\tau = 0$	0.343 ± 0.276	0.332 ± 0.271	0.311 ± 0.258	
$\langle D \rangle$, kaon, $\tau = 0$	0.450 ± 0.034	0.449 ± 0.035	0.449 ± 0.035	
$\langle D \rangle$, NT1, $\tau = 0$	0.253 ± 0.094	0.253 ± 0.103	0.247 ± 0.010	
$\langle D \rangle$, NT2, $\tau = 0$	0.101 ± 0.054	0.107 ± 0.056	0.106 ± 0.055	
$\langle D \rangle$, lepton, $\tau > 0$	0.323 ± 0.142	0.327 ± 0.144	0.337 ± 0.145	
$\langle D \rangle$, kaon, $\tau > 0$	0.240 ± 0.060	0.244 ± 0.060	0.243 ± 0.061	
$\langle D \rangle$, NT1, $\tau > 0$	0.055 ± 0.141	0.052 ± 0.142	0.058 ± 0.142	
$\langle D \rangle$, NT2, $\tau > 0$	0.098 ± 0.090	0.090 ± 0.093	0.091 ± 0.093	

Table 17: Fitted values for the parameters of the combined *CP* and mixing fit using the $\eta_{CP} = -1$ *CP* modes.

Parameter	tFit	CPExtract	Corr.
sin2β	0.701 ± 0.340	0.699 ± 0.343	
Run 1 signal Resolution Function			
Scale (core)	1.35 ± 0.08	1.35 ± 0.08	
$\delta(\Delta t)$ lepton (core)	0.059 ± 0.124	0.061 ± 0.124	
$\delta(\Delta t)$ kaon (core)	-0.285 ± 0.075	-0.286 ± 0.075	
$\delta(\Delta t)$ NT1 (core)	-0.186 ± 0.144	-0.185 ± 0.144	
$\delta(\Delta t)$ NT2 (core)	-0.340 ± 0.107	-0.346 ± 0.109	
$\delta(\Delta t)$ (tail)	-5.18 ± 2.93	-5.18 ± 2.87	
f(tail)	0.018 ± 0.018	0.019 ± 0.017	
f(outlier)	0.005 ± 0.003	0.005 ± 0.003	
Run 2 signal Resolution Function			
Scale (core)	1.12 ± 0.13	1.11 ± 0.12	
$\delta(\Delta t)$ lepton (core)	-0.015 ± 0.165	-0.019 ± 0.162	
$\delta(\Delta t)$ kaon (core)	-0.187 ± 0.099	-0.188 ± 0.097	
$\delta(\Delta t)$ NT1 (core)	-0.356 ± 0.212	-0.358 ± 0.211	
$\delta(\Delta t)$ NT2 (core)	-0.211 ± 0.156	-0.202 ± 0.150	
$\delta(\Delta t)$ (tail)	-3.199 ± 2.996	-3.31 ± 3.07	
f(tail)	0.039 ± 0.050	0.037 ± 0.046	
f(outlier)	0.000 ± 0.002	0 ± 0.002	
Signal dilutions			
$\langle D \rangle$, lepton	0.822 ± 0.027	0.822 ± 0.027	
$\langle D \rangle$, kaon	0.649 ± 0.020	0.649 ± 0.020	
$\langle D \rangle$, NT1	0.558 ± 0.042	0.558 ± 0.042	
$\langle D \rangle$, NT2	0.305 ± 0.038	0.303 ± 0.037	
ΔD, lepton	-0.010 ± 0.044	-0.011 ± 0.044	
ΔD, kaon	0.045 ± 0.030	0.046 ± 0.030	
ΔD, NT1	-0.104 ± 0.066	-0.104 ± 0.066	
ΔD, NT2	0.100 ± 0.055	0.103 ± 0.055	

Table 18: Fitted values for the parameters of the combined *CP* and mixing fit using the $J/\psi K^0_L$ mode only.

Parameter	tFit	CPExtract	Corr.
Background properties			
τ, mixing bgd [ps]	1.28 ± 0.08	1.27 ± 0.08	
$f(\tau = 0)$, mixing bgd, lepton	0.3111 ± 0.0969	0.309 ± 0.097	
$f(\tau = 0)$, mixing bgd, kaon	0.6459 ± 0.0364	0.644 ± 0.036	
$f(\tau = 0)$, mixing bgd, NT1	0.6122 ± 0.0587	0.611 ± 0.059	
$f(\tau = 0)$, mixing bgd, NT2	0.6383 ± 0.0441	0.639 ± 0.044	
Run 1 background resolution function			
Scale (core)	1.49 ± 0.040	1.49 ± 0.040	
$\delta(\Delta t)$ core	-0.152 ± 0.032	-0.152 ± 0.032	
f(outlier)	0.016 ± 0.004	0.016 ± 0.004	
Run 2 background resolution function			
Scale (core)	1.33 ± 0.04	1.32 ± 0.04	
$\delta(\Delta t)$ core	0.024 ± 0.037	0.026 ± 0.037	
f(outlier)	0.018 ± 0.005	0.017 ± 0.005	
Background dilutions			
$\langle D \rangle$, lepton, $\tau = 0$	0.344 ± 0.282	0.336 ± 0.272	
$\langle D \rangle$, kaon, $\tau = 0$	0.451 ± 0.035	0.450 ± 0.035	
$\langle D \rangle$, NT1, $\tau = 0$	0.256 ± 0.096	0.558 ± 0.042	
$\langle D \rangle$, NT2, $\tau = 0$	0.101 ± 0.055	0.303 ± 0.037	
$\langle D \rangle$, lepton, $\tau > 0$	0.323 ± 0.143	0.325 ± 0.144	
$\langle D \rangle$, kaon, $\tau > 0$	0.242 ± 0.060	0.246 ± 0.060	
$\langle D \rangle$, NT1, $\tau > 0$	0.053 ± 0.140	0.089 ± 0.092	
$\langle D \rangle$, NT2, $\tau > 0$	0.098 ± 0.090	0.089 ± 0.092	

Table 19: Fitted values for the parameters of the combined *CP* and mixing fit using the $J/\psi K^0_L$ mode only.

Parameter	tFit	CPExtract	Corr.
sin2β	0.817 ± 1.00	0.815 ± 1.01	
Run 1 signal Resolution Function			
Scale (core)	1.34 ± 0.09	1.27 ± 0.10	
$\delta(\Delta t)$ lepton (core)	0.014 ± 0.133	0.052 ± 0.129	
$\delta(\Delta t)$ kaon (core)	-0.301 ± 0.085	-0.278 ± 0.080	
$\delta(\Delta t)$ NT1 (core)	-0.163 ± 0.148	-0.145 ± 0.151	
$\delta(\Delta t)$ NT2 (core)	-0.358 ± 0.114	-0.353 ± 0.116	
$\delta(\Delta t)$ (tail)	-5.109 ± 5.120	-1.56 ± 1.23	
f(tail)	0.015 ± 0.026	0.065 ± 0.046	
f(outlier)	0.005 ± 0.004	0.006 ± 0.003	
Run 2 signal Resolution Function			
Scale (core)	1.15 ± 0.13	1.23 ± 0.12	
$\delta(\Delta t)$ lepton (core)	-0.095 ± 0.168	-0.95 ± 0.166	
$\delta(\Delta t)$ kaon (core)	-0.188 ± 0.103	-0.187 ± 0.101	
$\delta(\Delta t)$ NT1 (core)	-0.348 ± 0.215	-0.348 ± 0.214	
$\delta(\Delta t)$ NT2 (core)	-0.184 ± 0.161	-0.182 ± 0.153	
$\delta(\Delta t)$ (tail)	-3.49 ± 3.63	-3.60 ± 3.79	
f(tail)	0.034 ± 0.050	0.033 ± 0.047	
f(outlier)	0.000 ± 0.002	0 ± 0.002	
Signal dilutions			
$\langle D \rangle$, lepton	0.823 ± 0.027	0.822 ± 0.027	
$\langle D \rangle$, kaon	0.648 ± 0.020	0.647 ± 0.020	
$\langle D \rangle$, NT1	0.558 ± 0.042	0.556 ± 0.042	
$\langle D \rangle$, NT2	0.302 ± 0.038	0.297 ± 0.037	
ΔD, lepton	-0.019 ± 0.045	-0.020 ± 0.045	
ΔD, kaon	0.034 ± 0.031	0.035 ± 0.030	
ΔD, NT1	-0.125 ± 0.067	-0.125 ± 0.066	
ΔD, NT2	0.096 ± 0.056	0.099 ± 0.056	

Table 20: Fitted values for the parameters of the combined *CP* and mixing fit using the $J/\psi K^{*0}$ mode only.

Parameter	tFit	CPExtract	Corr.
Background properties			
τ, mixing bgd [ps]	1.28 ± 0.08	1.27 ± 0.08	
$f(\tau = 0)$, mixing bgd, lepton	0.311 ± 0.097	0.305 ± 0.097	
$f(\tau = 0)$, mixing bgd, kaon	0.646 ± 0.037	0.643 ± 0.037	
$f(\tau = 0)$, mixing bgd, NT1	0.612 ± 0.059	0.613 ± 0.059	
$f(\tau = 0)$, mixing bgd, NT2	0.638 ± 0.044	0.647 ± 0.044	
Run 1 background resolution function			
Scale (core)	1.49 ± 0.04	1.49 ± 0.03	
$\delta(\Delta t)$ core	-0.151 ± 0.032	-0.153 ± 0.032	
f(outlier)	0.016 ± 0.004	0.016 ± 0.004	
Run 2 background resolution function			
Scale (core)	1.33 ± 0.04	1.32 ± 0.04	
$\delta(\Delta t)$ core	0.023 ± 0.037	0.025 ± 0.037	
f(outlier)	0.018 ± 0.005	0.018 ± 0.005	
Background dilutions			
$\langle D \rangle$, lepton, $\tau = 0$	0.342 ± 0.278	0.332 ± 0.170	
$\langle D \rangle$, kaon, $\tau = 0$	0.451 ± 0.035	0.449 ± 0.034	
$\langle D \rangle$, NT1, $\tau = 0$	0.256 ± 0.095	0.246 ± 0.083	
$\langle D \rangle$, NT2, $\tau = 0$	0.101 ± 0.054	0.108 ± 0.055	
$\langle D \rangle$, lepton, $\tau > 0$	0.323 ± 0.142	0.327 ± 0.110	
$\langle D \rangle$, kaon, $\tau > 0$	0.243 ± 0.060	0.247 ± 0.058	
$\langle D \rangle$, NT1, $\tau > 0$	0.053 ± 0.140	0.052 ± 0.109	
$\langle D \rangle$, NT2, $\tau > 0$	0.098 ± 0.090	0.084 ± 0.076	

Table 21: Fitted values for the parameters of the combined *CP* and mixing fit using the $J/\psi\, K^{*0}$ mode only.

Parameter	tFit	CPExtract	Corr.
sin2β	0.594 ± 0.137	0.592 ± 0.137	
Run 1 signal Resolution Function			
Scale (core)	1.22 ± 0.12	1.23 ± 0.12	
$\delta(\Delta t)$ lepton (core)	0.074 ± 0.124	0.075 ± 0.125	
$\delta(\Delta t)$ kaon (core)	-0.258 ± 0.076	-0.258 ± 0.076	
$\delta(\Delta t)$ NT1 (core)	-0.210 ± 0.149	-0.208 ± 0.148	
$\delta(\Delta t)$ NT2 (core)	-0.305 ± 0.110	-0.311 ± 0.111	
$\delta(\Delta t)$ (tail)	-1.624 ± 1.425	-1.68 ± 1.46	
f(tail)	0.082 ± 0.064	0.080 ± 0.063	
f(outlier)	0.006 ± 0.003	0.005 ± 0.003	
Run 2 signal Resolution Function			
Scale (core)	1.13 ± 0.12	1.12 ± 0.12	
$\delta(\Delta t)$ lepton (core)	0.050 ± 0.159	0.044 ± 0.158	
$\delta(\Delta t)$ kaon (core)	-0.186 ± 0.095	-0.185 ± 0.094	
$\delta(\Delta t)$ NT1 (core)	-0.332 ± 0.207	-0.333 ± 0.207	
$\delta(\Delta t)$ NT2 (core)	-0.175 ± 0.152	-0.168 ± 0.146	
$\delta(\Delta t)$ (tail)	-3.221 ± 2.748	-3.32 ± 2.84	
f(tail)	0.037 ± 0.044	0.035 ± 0.042	
f(outlier)	0.000 ± 0.001	0 ± 0.014	
Signal dilutions			
$\langle D \rangle$, lepton	0.821 ± 0.027	0.821 ± 0.027	
$\langle D \rangle$, kaon	0.649 ± 0.020	0.648 ± 0.020	
$\langle D \rangle$, NT1	0.560 ± 0.042	0.571 ± 0.042	
$\langle D \rangle$, NT2	0.301 ± 0.037	0.299 ± 0.037	
ΔD, lepton	-0.018 ± 0.044	-0.018 ± 0.044	
ΔD, kaon	0.038 ± 0.029	0.039 ± 0.029	
ΔD, NT1	-0.112 ± 0.064	-0.112 ± 0.064	
ΔD, NT2	0.117 ± 0.054	0.119 ± 0.054	

Table 22: Fitted values for the parameters of the combined *CP* and mixing fit using all *CP* modes.

Parameter	tFit	CPExtract	Corr.
Background properties			
τ, mixing bgd [ps]	1.28 ± 0.08	1.28 ± 0.08	
$f(\tau = 0)$, *CP* bgd	0.602 ± 0.116	0.605 ± 0.116	
$f(\tau = 0)$, mixing bgd, lepton	0.315 ± 0.097	0.313 ± 0.097	
$f(\tau = 0)$, mixing bgd, kaon	0.652 ± 0.036	0.650 ± 0.036	
$f(\tau = 0)$, mixing bgd, NT1	0.617 ± 0.058	0.615 ± 0.059	
$f(\tau = 0)$, mixing bgd, NT2	0.644 ± 0.044	0.644 ± 0.043	
Run 1 background resolution function			
Scale (core)	1.50 ± 0.040	1.50 ± 0.04	
$\delta(\Delta t)$ core	-0.156 ± 0.032	-0.156 ± 0.032	
f(outlier)	0.016 ± 0.004	0.016 ± 0.004	
Run 2 background resolution function			
Scale (core)	1.34 ± 0.04	1.33 ± 0.04	
$\delta(\Delta t)$ core	0.018 ± 0.037	0.020 ± 0.037	
f(outlier)	0.018 ± 0.005	0.017 ± 0.005	
Background dilutions			
$\langle D \rangle$, lepton, $\tau = 0$	0.345 ± 0.276	0.334 ± 0.271	
$\langle D \rangle$, kaon, $\tau = 0$	0.450 ± 0.034	0.449 ± 0.035	
$\langle D \rangle$, NT1, $\tau = 0$	0.252 ± 0.094	0.253 ± 0.103	
$\langle D \rangle$, NT2, $\tau = 0$	0.101 ± 0.054	0.253 ± 0.056	
$\langle D \rangle$, lepton, $\tau > 0$	0.322 ± 0.142	0.326 ± 0.144	
$\langle D \rangle$, kaon, $\tau > 0$	0.240 ± 0.060	0.244 ± 0.060	
$\langle D \rangle$, NT1, $\tau > 0$	0.055 ± 0.141	0.051 ± 0.142	
$\langle D \rangle$, NT2, $\tau > 0$	0.098 ± 0.091	0.090 ± 0.093	

Table 23: Fitted values for the parameters of the combined *CP* and mixing fit using all *CP* modes.

events and $\bar{B}^0$ tagged events. This correlation coefficient is much smaller ($\mathcal{O}(0.01)$) for the combined sample. The Gaussian biases in B^0 and $\bar{B}^0$ tagged sub-samples are consistent, but different at the one sigma level. These shifts in the biases decrease sin2β for both subsamples below sin2β of the combined sample. We have repeated the fit to the B^0 and $\bar{B}^0$ tagged subsamples with the resolution function parameters fixed to their values from the combined fit. The previously observed feature disappears as expected (see eg. Tables 24–27).

Sample	Yields (tagged)	sin2β	
		`tFit`	`CPExtract`
CP sample	$\pm$	$\mathbf{0.594 \pm 0.137}$	$\mathbf{0.592 \pm 0.137}$
$J/\psi K^0_S$ ($K^0_S \to \pi^+\pi^-$)	$\pm$	0.451 ± 0.180	0.451 ± 0.180
$J/\psi K^0_S$ ($K^0_S \to \pi^0\pi^0$)	$\pm$	0.760 ± 0.525	0.702 ± 0.497
$\psi(2S)K^0_S$ ($K^0_S \to \pi^+\pi^-$)	$\pm$	0.474 ± 0.423	0.459 ± 0.436
$B^0 \to \chi_{c1} K^0_S$	$\pm$	2.586 ± 0.612	2.587 ± 0.623
$B^0 \to J/\psi K^0_L$	$\pm$	0.701 ± 0.340	0.699 ± 0.343
$B^0 \to J/\psi K^{*0}$	$\pm$	0.817 ± 1.000	0.815 ± 1.010
`Lepton`	$\pm$	0.537 ± 0.261	0.545 ± 0.259
`Kaon`	$\pm$	0.581 ± 0.182	0.576 ± 0.182
`NT1`	$\pm$	0.892 ± 0.295	0.895 ± 0.392
`NT2`	$\pm$	0.401 ± 0.648	0.392 ± 0.645
B^0-Tag	$\pm$	0.544 ± 0.190	0.547 ± 0.190
$\overline{B}^0$-Tag	$\pm$	0.640 ± 0.200	0.639 ± 0.200
B^0-Tag (reso. fixed)	$\pm$	0.555 ± 0.190	0.556 ± 0.190
$\bar{B}^0$-Tag (reso. fixed)	$\pm$	0.617 ± 0.193	0.617 ± 0.193
$J/\psi \to e^+e^-$	$\pm$	0.488 ± 0.203	0.471 ± 0.201
$J/\psi \to \mu^+\mu^-$	$\pm$	0.698 ± 0.183	0.705 ± 0.185
Run 1	$\pm$	0.449 ± 0.175	0.450 ± 0.176
Run 2	$\pm$	0.824 ± 0.221	0.819 ± 0.041
Control samples			
$B_{\rm flav}$. (no Charmonium)	$\pm$	0.003 ± 0.042	0.003 ± 0.042
B^+-reco. (no Charmonium)	$\pm$	-0.020 ± 0.043	-0.018 ± 0.041
$B^0 \to J/\psi K^{*0}$	$\pm$	0.117 ± 0.123	0.117 ± 0.123
$B^+ \to$ Charmonium X	$\pm$	0.070 ± 0.071	0.070 ± 0.071
$B_{\rm flav}$.	$\pm$	0.015 ± 0.040	0.015 ± 0.039
B^+-reco.	$\pm$	0.003 ± 0.035	0.003 ± 0.035

Table 24: Result of fitting for *CP* asymmetries in the entire *CP* sample and in various subsamples. The yields are for tagged events and are obtained with likelihood fits and are therefore are background subtracted. In the fits to only B^0 or $\overline{B}^0$ tags, the ΔD were fixed to their fitted values in Table 16. In the second set of fits to the B^0 and $\bar{B}^0$ tagged subsamples all parameters except sin2β and $f(\tau = 0)$, *CP* bgd are fixed (see text).

Sample	Yields (tagged)	sin2β tFit	sin2β CPExtract	$\mathcal{I}m\lambda/\|\lambda\|$	$\|\lambda\|$
$\eta_{CP} = -1$	$\pm$	**0.563$\pm$0.151**	**0.564$\pm$0.157**		
Lepton	$\pm$	0.537 ± 0.288	0.549 ± 0.260	0.574 ± 0.014	0.768 ± 0.007
Kaon	$\pm$	0.588 ± 0.200	0.587 ± 0.200	0.587 ± 0.198	0.985 ± 0.121
NT1	$\pm$	0.668 ± 0.452	0.669 ± 0.452	0.573 ± 0.035	0.729 ± 0.022
NT2	$\pm$	0.099 ± 0.742	0.105 ± 0.750	0.278 ± 1.286	2.982 ± 3.961
B^0-Tag	$\pm$	0.499 ± 0.217	0.504 ± 0.218		
$\bar{B}^0$-Tag	$\pm$	0.609 ± 0.220	0.612 ± 0.220		
B^0-Tag (reso. fixed)		0.537 ± 0.214	0.538 ± 0.214		
$\bar{B}^0$-Tag (reso. fixed)		0.579 ± 0.210	0.583 ± 0.210		
$J/\psi \to e^+e^-$		0.541 ± 0.222	0.526 ± 0.219		
$J/\psi \to \mu^+\mu^-$		0.598 ± 0.206	0.606 ± 0.208		
Run 1	$\pm$	0.370 ± 0.196	0.373 ± 0.197		
Run 2	$\pm$	0.859 ± 0.238	0.856 ± 0.237		

Table 25: Result of fitting for *CP* asymmetries in the $\eta_{CP} = -1$ sample and in various subsamples. The yields are for tagged events and are obtained with likelihood fits and are therefore are background subtracted. In the second set of fits to the B^0 and $\bar{B}^0$ tagged subsamples all parameters except sin2β and $f(\tau = 0)$, *CP* bgd are fixed (see text). For NT1 the bias of the tail Gaussian for the signal in Run2 has been fixed to 0.0

9.3 Tagging performance

Table 28 gives the mistag fractions, tagging efficiency, and Q value measured on each sample.

9.4 Is $\sigma(\text{sin2}\beta)$ what we expected?

As described in Section 10.3, the expected error from "*CP*-sized" subsamples of the B^0-reco data is ± 0.132, with a spread (σ) of ± 0.005. Fitting the $\eta_{CP} = -1$ channels, we find an error of ± 0.137 which is 1σ above the expected error.

9.5 Goodness of fit and expected statistical error from Toy MC

Toy Monte Carlo was used to evaluate the goodness of the fit based on the value of the likelihood. The toy samples were made with exactly the same statistics as the real data sample. That is, the same number of events in every flavor-tag-category (lepton, K, NT1, NT2) + flavor-tag-value (B^0 or $\overline{B}^0$) combination. Each toy sample also uses the set of $m_{\rm ES}$ (ΔE) values taken from the non-K^0_L (K^0_L) data sample. Whether each toy event was taken from a pre-generated signal or background sample was determined from the $m_{\rm ES}$ or ΔE value for the event and the results of the $m_{\rm ES}$ or ΔE fit.

Table 29 gives the expected statistical error and log likelihood from the Toy Monte Carlo, the values from the fit of the data, and the fraction of Toy Monte Carlo fits that

Sample	Yields (tagged)	sin2β	
		tFit	CPExtract
$J/\psi K_L^0$	144 ± 19	**0.701±0.340**	**0.699± 0.343**
Lepton	71 ± 14	0.065 ± 0.680	0.057 ± 0.687
Kaon	26 ± 8	0.719 ± 0.451	0.710 ± 0.454
NT1	12 ± 6	1.447 ± 1.099	1.46 ± 1.11
NT2	35 ± 9	2.137 ± 1.371	2.22 ± 1.42
B^0-Tag	91 ± 15	0.470 ± 0.449	0.549 ± 0.453
$\bar{B}^0$-Tag	53 ± 12	1.057 ± 0.548	1.05 ± 0.552
B^0-Tag (reso. fixed)		0.479 ± 0.447	0.479 ± 0.451
$\bar{B}^0$-Tag (reso. fixed)		1.011 ± 0.529	1.005 ± 0.533
$J/\psi \to e^+e^-$	124 ± 16	0.254 ± 0.500	1.129 ± 0.472
$J/\psi \to \mu^+\mu^-$	128 ± 16	1.132 ± 0.469	0.248 ± 0.501
Run 1	175 ± 19	0.707 ± 0.416	0.708 ± 0.420
Run 2	83 ± 13	0.675 ± 0.580	0.669 ± 0.585

Table 26: Result of fitting for *CP* asymmetries in the $J/\psi K_L^0$ *CP* sample and in various subsamples. The yields are for tagged events and are obtained with likelihood fits and are therefore are background subtracted. In the fits to only B^0 or $\overline{B}^0$ tags, the ΔD were fixed to their fitted values in Table 16. In the second set of fits to the B^0 and $\bar{B}^0$ tagged subsamples all parameters except sin2β are fixed (see text). For NT1 the bias of the tail Gaussian for the signal in Run2 has been fixed to 0.0

gave a likelihood less likely than the fit of the data. Figure 18 shows the statistical error and log likelihood distributions from the Toy Monte Carlo fits with the values from the fit of the data indicated with arrows.

The $\chi_{c1}K_s$ sample is the only one that seems unlikely, where only 6 out of 800 (0.8%) toy MC fits had a likelihood less than the fit of the real data sample.

9.6 Raw Asymmetry

One way to visualize the asymmetry measurement is to plot the raw asymmetry as a function of Δt. The raw asymmetry is calculated simply as the asymmetry in the number of B^0 and $\overline{B}^0$ tags, for all tagged events in the signal region. While this quantity ignores the different analyzing power for individual events, from the different flavor tags, the event-by-event Δt resolution, and the amount of background, it still does demonstrate the amount of asymmetry in the data. Also we compare the data to the equivalent raw asymmetry from the maximum likelihood fit, so that at some level the goodness of fit can be examined.

The Δt distributions for B^0 and $\overline{B}^0$ tags as well as the raw asymmetry for $\eta_{CP} = -1$ decays and for $J/\psi K_L^0$ decays are shown in Figure 19. The curves shown are from the maximum likelihood fit. Some comments about how the raw asymmetry plots were made are in order. The raw asymmetry for the curve was made without normalizing the

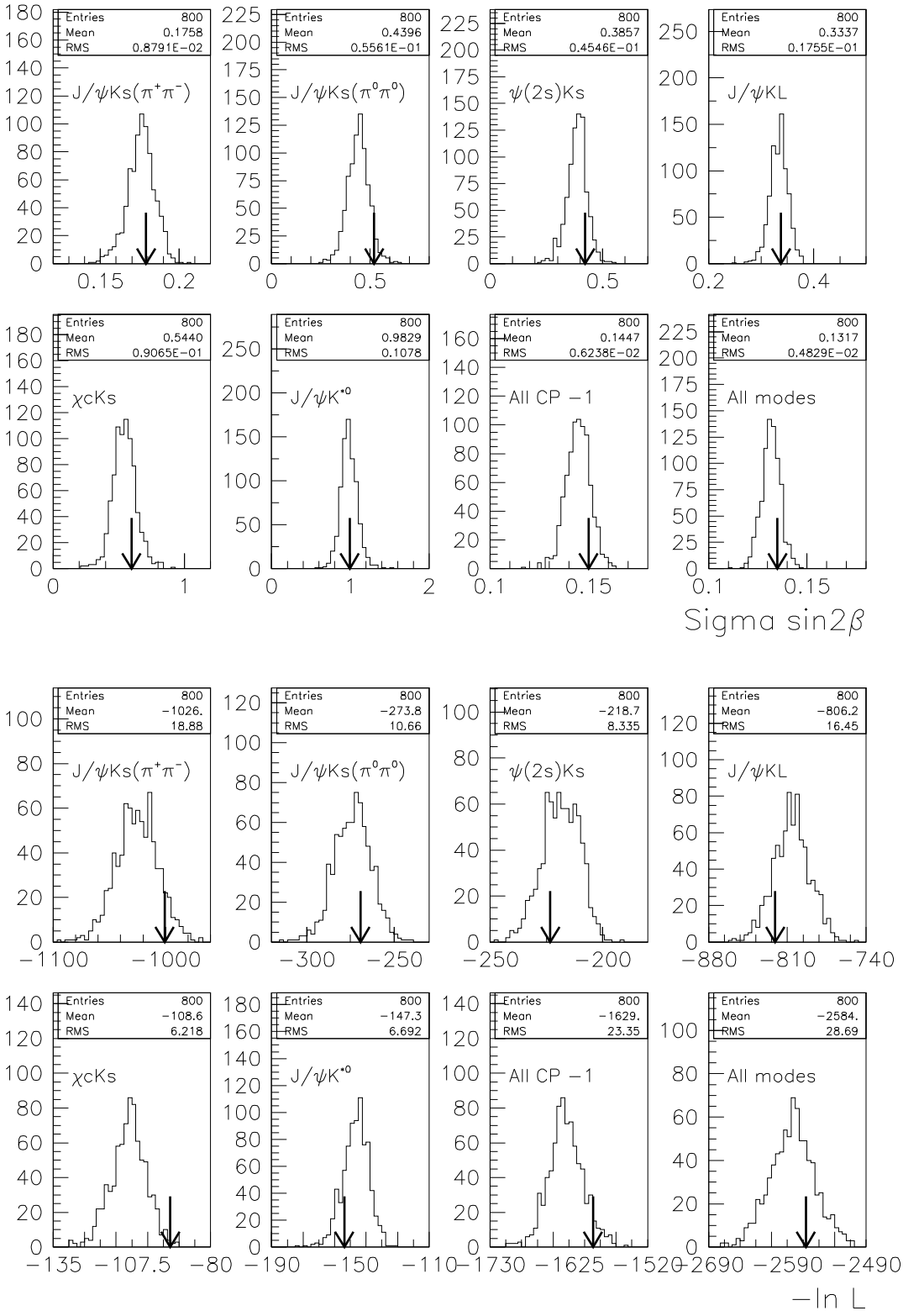

Figure 18: Expected statistical error and log likelihood from Toy Monte Carlo. The arrows indicate the value from the fit of the data.

Sample	Yields (tagged)	sin2β	
		tFit	CPExtract
$J/\psi K^{*0}$	$\pm$	**0.817$\pm$1.000**	**0.815 $\pm$1.010**
Lepton	$\pm$	3.993 ± 1.358	4.00 ± 1.39
Kaon	$\pm$	-1.145 ± 1.308	-1.141 ± 1.322
NT1	$\pm$	At limit	Fail
NT2	$\pm$	At limit	-11.4 ± 6.9
B^0-Tag	$\pm$	2.457 ± 1.356	2.48 ± 1.36
$\bar{B}^0$-Tag	$\pm$	-0.350 ± 1.396	-0.32 ± 1.40
B^0-Tag (reso. fixed)		2.223 ± 1.341	2.234 ± 1.362
$\bar{B}^0$-Tag (reso. fixed)		-0.427 ± 1.345	-0.420 ± 1.362
$J/\psi \to e^+e^-$	$\pm$	-0.062 ± 1.466	-0.03 ± 1.47
$J/\psi \to \mu^+\mu^-$	$\pm$	1.541 ± 1.301	1.55 ± 1.32
Run 1	$\pm$	1.263 ± 1.221	1.254 ± 1.239
Run 2	$\pm$	0.146 ± 1.619	0.154 ± 1.648

Table 27: Result of fitting for *CP* asymmetries in the $J/\psi K^{*0}$ *CP* sample and in various subsamples. The yields are for tagged events and are obtained with likelihood fits and are therefore are background subtracted. In the fits to only B^0 or $\overline{B}^0$ tags, the ΔD were fixed to their fitted values in Table 16. In the second set of fits to the B^0 and $\bar{B}^0$ tagged subsamples all parameters except sin2β are fixed (see text). For NT1 the bias of the tail Gaussian for the signal in Run2 has been fixed to 0.0

likelihood fit; Also very sharp eyed readers may notice that the second oscillation of the curve does not have the same amplitude as the first oscillation (this is much more evident when plotted past 8 ps). This is due to the 8 ps wide outlier gaussian, which washes out the asymmetry at large Δt.

With respect to the data there are also some comments in order. There are ?? events which fall outside the $\pm$8 ps window of these plots. Also some care has been taken in the evaluation of the errors for each data point, due to the low statistics present in some of the bins.

In the case of small statistics, the usual binomial error formula $\sigma_p = \sqrt{p(1-p)/n}$ is a poor error estimate. A better estimate can be found by using the binomial distribution as a function of p, for the case of n events. The errors are taken by integrating the edges of the distribution; the 15.87% point is taken as the 1σ error, as shown in Figure 20 for the case where n=8 and p=1/8 (which are the numbers for the point at $\Delta t = -5$ in the K^0_S raw asymmetry). Of course, the error in p is converted to an error in asymmetry, by $a = 2p - 1$. This procedure, referred to as a Bayesian interval, is discussed in [26]. The confidence interval coverage of this error estimation procedure has been evaluated, and while the coverage does vary as a function of the true value of p, the procedure yields a better approximation of a 1σ confidence interval than either the frequentist approach described in [26] or the naive binomial error formula. The confidence interval coverage for these three cases is shown Figure 20.

Tag	Sample	w	ε (%)	Q (%)
Lepton	$B_{\rm flav}$		11.0 ± 0.3	7.4 ± 0.5
	$CP = -1$		11.0 ± 1.2	7.4 ± 0.9
	$J/\psi\, K_L^0$		10.4 ± 3.0	7.0 ± 2.1
	Total	0.090 ± 0.014	10.9 ± 0.3	7.4 ± 0.5
Kaon	$B_{\rm flav}$		35.8 ± 0.5	15.0 ± 0.9
	$CP = -1$		38.9 ± 1.9	16.3 ± 1.2
	$J/\psi\, K_L^0$		28.3 ± 4.5	11.9 ± 2.0
	Total	0.176 ± 0.010	35.8 ± 0.5	15.0 ± 0.9
NT1	$B_{\rm flav}$		8.0 ± 0.3	2.5 ± 0.4
	$CP = -1$		6.9 ± 0.9	2.2 ± 0.4
	$J/\psi\, K_L^0$		4.8 ± 2.3	1.5 ± 0.8
	Total	0.220 ± 0.021	7.8 ± 0.3	2.5 ± 0.4
NT2	$B_{\rm flav}$		13.9 ± 0.4	1.2 ± 0.3
	$CP = -1$		13.0 ± 1.3	1.2 ± 0.3
	$J/\psi\, K_L^0$		13.9 ± 3.3	1.2 ± 0.4
	Total	0.351 ± 0.019	13.8 ± 0.3	1.2 ± 0.3
All	$B_{\rm flav}$		68.6 ± 0.7	26.2 ± 1.2
	$CP = -1$		69.8 ± 2.7	27.1 ± 1.6
	$J/\psi\, K_L^0$		57.4 ± 6.7	21.6 ± 3.0
	Total	—	68.4 ± 0.7	26.1 ± 1.2

Table 28: Mistag fractions, tagging efficiency, and Q values from the CP+$B_{\rm flav}$ fit.

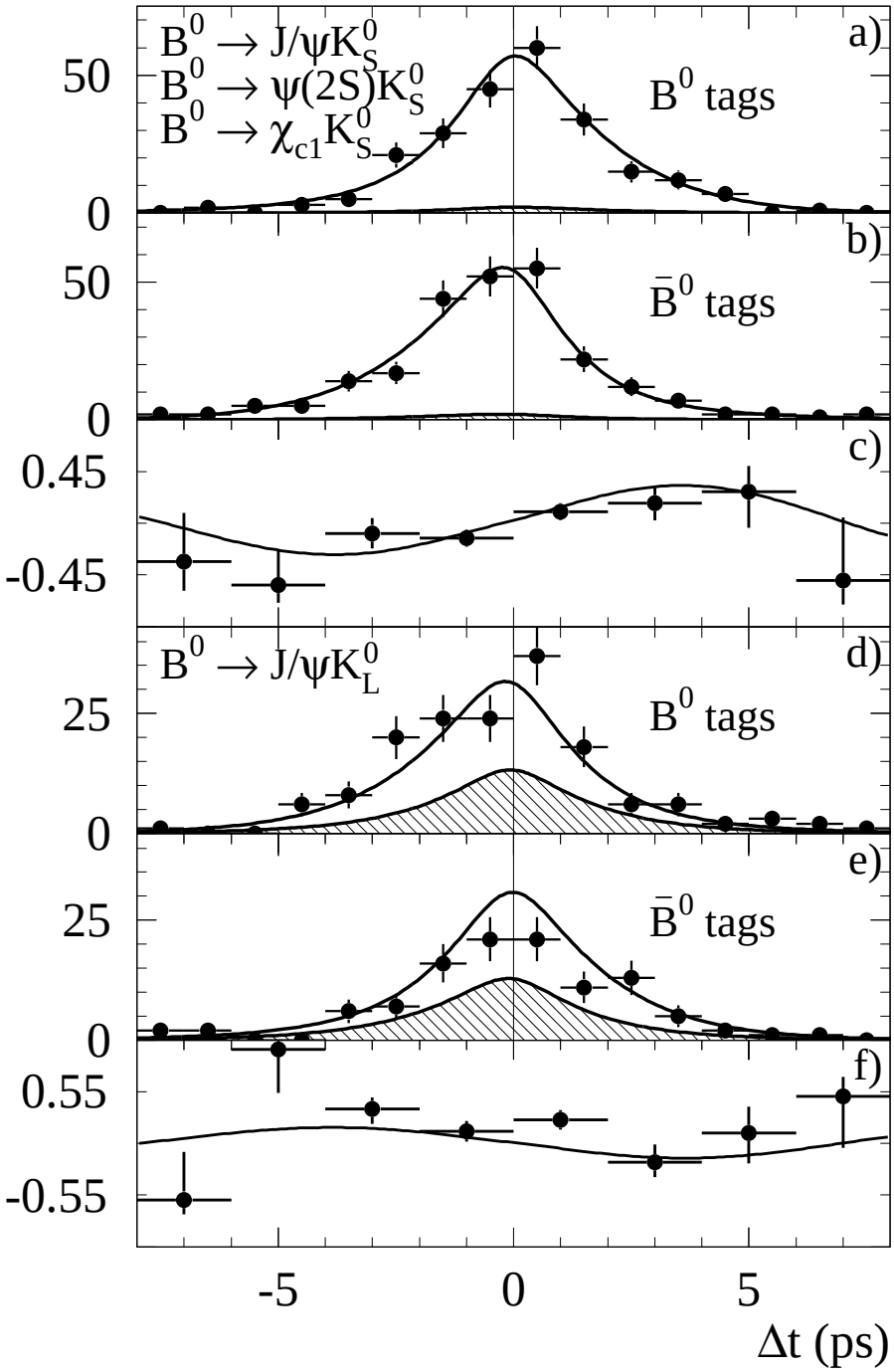

Figure 19: Δt for $B0$ (a,c) and $\overline{B}^0$ (b,e) tags and the raw asymmetry (c,f) for $\eta_{CP} = -1$ modes K^0_S decays and K^0_L decays.

Sample	TMC σ	Data σ	TMC $-\ln\mathcal{L}$	Data $-\ln\mathcal{L}$	Fr TMC > Data
$K_s \to \pi^+\pi^-$	0.176 ± 0.009	0.179	-1026 ± 19	-1000.9	$70/800 = 0.088$
$K_s \to \pi^0\pi^0$	0.440 ± 0.055	0.521	-273.9 ± 11.7	-269.2	$273/800 = 0.341$
$\psi(2s)K_s$	0.386 ± 0.046	0.423	-218.6 ± 8.4	-223.3	$567/800 = 0.709$
Klong	0.333 ± 0.018	0.338	-806.1 ± 16.4	-820.8	$652/800 = 0.815$
$\chi_{c1}K_s$	0.544 ± 0.090	0.597	-108.6 ± 6.2	-94.1	$6/800 = 0.008$
$J/\psi K^{*0}$	0.982 ± 0.106	0.992	-147.3 ± 6.7	-153.1	$646/800 = 0.808$
$\eta_{CP} = -1$	0.145 ± 0.006	0.150	-1629 ± 23	-1592.7	$49/800 = 0.061$
All CP	0.132 ± 0.005	0.135	-2584 ± 29	-2566.6	$214/800 = 0.268$

Table 29: Expected statistical error and negative log likelihood from Toy Monte Carlo compared with the values from the data fits. The last column is the fraction of Toy Monte Carlo experiments that were less likely (larger negative log likelihood) than the data fit.

Figure 20: Details on asymmetric binomial errors a) Binomial distribution for n=8, p=0.125 with the 1σ interval shown. Confidence interval converage for 1σ point as a function of the true p, for b) Bayesian intervals used in raw asymmetry plot, c) Frequentist intervals described in [26], and d) binomial error formula; from a series of monte-carlo trials at various values of p, with n=8. A good confidence interval should include the true value 68% of the time independent of the actual value of p. The Bayesian intervals have an average coverage near 68%, while the frequentist intervals are too large. In all cases the variation of the intervals is due to the discrete nature of the binomial distribution.

The χ^2/dof is xxx for the $\eta_{CP} = -1$ events, and xxx for the $J/\psi K^0_L$ events. Finally, it is worth looking at the raw asymmetry, by tagging category, for the $\eta_{CP} = -1$ events, as shown in Figure 21.

10 Validation Analyses

10.1 Full Monte Carlo studies

10.1.1 Signal only

Fits have been performed to Charmonium and B-reco signal Monte Carlo samples. In each case, dilutions and resolutions measured on the $B_{\rm flav}$ samples were used, and the only free parameter was sin2β. Table 30 summarizes the results of these fits.

In addition, the *CP* signal Monte Carlo events have been broken into subsamples of

Figure 21: Raw asymmetry for $\eta_{CP} = -1$ decays by tagging category, with curves from the combined $\eta_{CP} = -1$ fit.

Mode	Generated sin2β	Fitted sin2β	
		$B_{\rm flav}$	Truth
$J/\psi\, K^0_S\ (\pi^+\pi^-)$	0.1	0.081 ± 0.040	0.087 ± 0.023
$J/\psi\, K^0_S\ (\pi^+\pi^-)$	0.3	0.238 ± 0.040	0.262 ± 0.023
$J/\psi\, K^0_S\ (\pi^+\pi^-)$	0.5	0.506 ± 0.018	0.497 ± 0.010
$J/\psi\, K^0_S\ (\pi^+\pi^-)$	0.7	0.662 ± 0.018	0.714 ± 0.009
$J/\psi\, K^0_S\ (\pi^+\pi^-)$	0.9	0.881 ± 0.035	0.891 ± 0.014
$J/\psi\, K^0_S\ (\pi^0\pi^0)$	0.7	0.709 ± 0.028	0.711 ± 0.014
$\psi(2S)K^0_S\ (\pi^+\pi^-)$	0.7	0.711 ± 0.030	0.707 ± 0.015
$\chi_{c1}K^0_S\ (\pi^+\pi^-)$	-0.7	-0.713 ± 0.030	-0.713 ± 0.015
$J/\psi\, K^{*0}\ (K^0_S\pi^0)$	0.7	0.652 ± 0.057	0.654 ± 0.032
$J/\psi\, K^0_L$	0.7	0.731 ± 0.024	$\pm$
$J/\psi\, K^+$	0.0	-0.002 ± 0.023	0.011 ± 0.014
$\psi(2S)K^+$	0.0	0.080 ± 0.042	0.033 ± 0.025
$\chi_{c1}K^+$	0.0	0.039 ± 0.047	0.045 ± 0.028
$J/\psi\, K^{*0}\ (K^+\pi^-)$	0.0	-0.015 ± 0.030	0.005 ± 0.018
$J/\psi\, K^{*+}\ (K^+\pi^0)$	0.0	0.001 ± 0.036	-0.014 ± 0.021
$J/\psi\, K^{*+}\ (K^0_S\pi^+)$	0.0	-0.044 ± 0.036	-0.034 ± 0.022
$B_{\rm flav}$	0.0	0.000 ± 0.009	-0.001 ± 0.005
$B^\pm$-reco	0.0	$\pm$	$\pm$
$B^\pm$ (Charmonium)	0.0	0.006 ± 0.015	0.005 ± 0.009

Table 30: Results of fits to full Monte Carlo samples. The two columns of fitted sin2β values correspond to fits using dilutions and resolutions either measured from the $B_{\rm flav}$ Monte Carlo sample, or from Monte Carlo truth.

360 events (after vertexing requirements). These subsamples have been used to evaluate the presence of any inherent bias in the measurement of sin2β. Figure 22 shows the pull distribution of sin2β for these subsamples.

10.1.2 Inclusive J/ψ Monte Carlo

In a sample of inclusive J/ψ Monte Carlo corresponding to a luminosity of $219\,\mathrm{fb}^{-1}$ the measurement has been carried on as in data. The results are shown in Table 31 for each of the individual modes. Dilutions and resolution function parameters are fixed to the values measured in the large B_{flav} MC sample.

mode	inclusive J/ψ
	Fitted sin2β
$J/\psi\, K^0_S\ (\pi^+\pi^-)$	0.672 ± 0.057
$J/\psi\, K^0_S\ (\pi^0\pi^0)$	0.714 ± 0.161
$\psi(2S) K^0_S\ (\pi^+\pi^-)$	0.288 ± 0.293
$\chi_{c1} K^0_S\ (\pi^+\pi^-)$	-0.666 ± 0.257
$J/\psi\, K^{*0}\ (K^0_S\pi^0)$	0.822 ± 0.253
$J/\psi\, K^0_L$	0.571 ± 0.092

Table 31: Results of sin2β fits on full Monte Carlo sample with several background assumptions (see text). Generated value: sin2β =0.7 for all modes except for $\chi_{c1}K^0_S$, which was generated with sin2β =-0.7.

10.1.3 *CP* and B_{flav} Monte Carlo

We perform global fits to a sample of signal B_{flav} events and samples of *CP* events. To this end, we split the $J/\psi\, K^0_S\ (\pi^+\pi^-)$ signal MC (sin2β = 0.5) in five samples of which each corresponds in integrated luminosity to the B_{flav} MC sample ($\approx 15\times$ data). These samples are fitted using the full 35 parameter fit. The fit results for sin2β are in good agreement with the input value of 0.5. They are shown in Table 32.

10.1.4 Dilutions in *CP* sample

The Tagmix analysis determines the dilutions at small Δt, while the *CP* fit uses them at $\Delta t\ \Delta m_d = \frac{\pi}{2}$. We have performed a few tests that this does not introduce any bias, in addition to the validations with B_{flav} dilutions, which already validate this aspect.

- fit for dilutions in B_{flav} MC (see table 33)
- fit for w in *CP* events. We fit for mistag rates in the *CP* sample fixing the value of sin2β and compare the measured dilutions with the ones at MC truth level and the fitted values from the B_{flav} sample (see table 33).
- Studies regarding a possible time dependence of the wrong tag fraction on Δt are documented in BAD 119 [18] in Section 6.5.

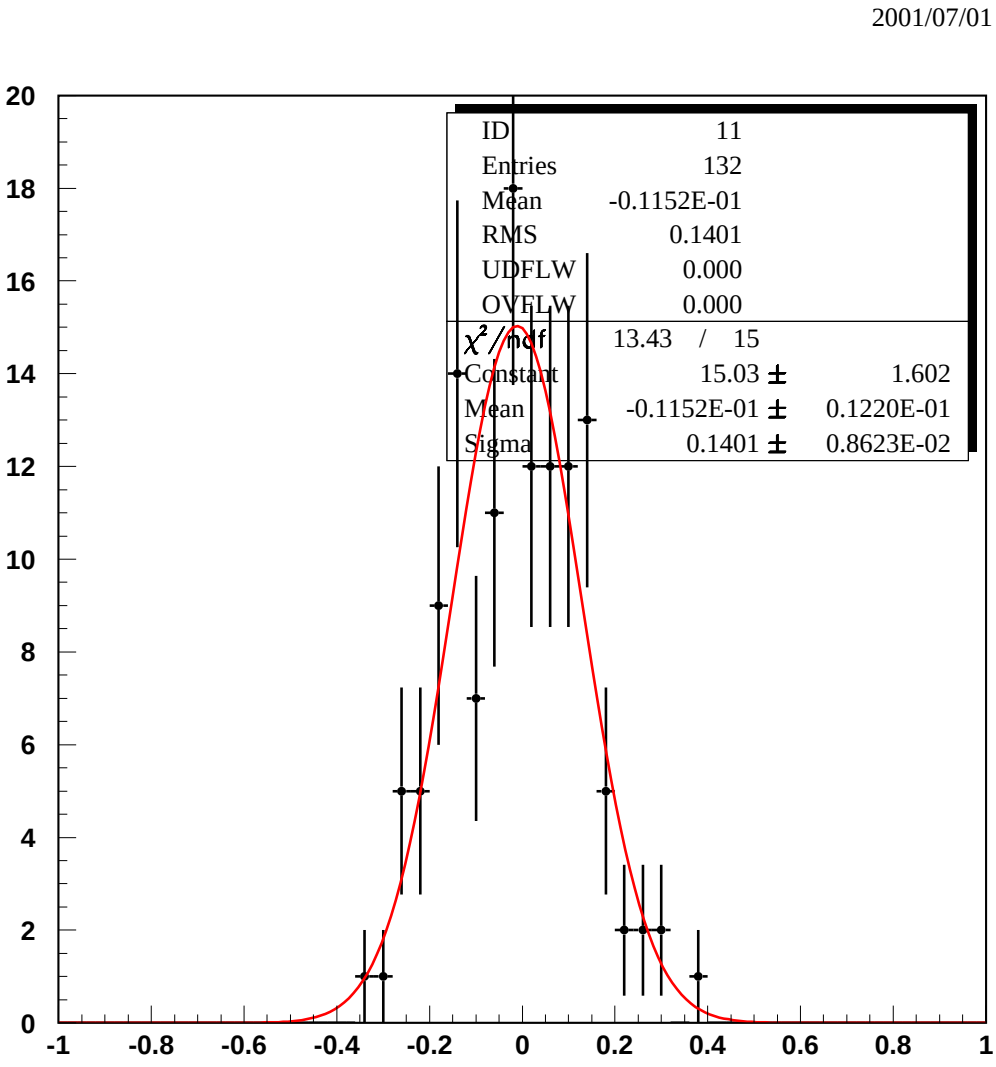

Figure 22: Residual distribution for 560 event subsamples of the *CP* mode signal Monte Carlo. A mean residual of -0.0115 ± 0.0122 is found. As this is consistent with 0, there is no correction applied, and the uncertainty its value is included in the systematic error.

Sample	Fitted sin2β
1	0.680 ± 0.037
2	0.690 ± 0.037
3	0.697 ± 0.037
4	0.675 ± 0.037
5	0.685 ± 0.037
6	0.685 ± 0.037
7	0.690 ± 0.037
8	0.683 ± 0.037
9	0.704 ± 0.036
1–9	0.688 ± 0.001

Table 32: Results of sin2β fits to $B_{\rm flav}$ signal cocktail + $J/\psi\, K^0_S$ ($\pi^+\pi^-$) signal MC samples. All $B_{\rm flav}$ MC ($\approx 15\times$ data) was fitted with 9 different samples of $J/\psi\, K^0_S$ ($\pi^+\pi^-$) signal MC each corresponding to the same luminosity. The combined result is a weighted average of the individual samples. .

Parameter	MC truth	fitted(sin2β =0.7 MC)	$B_{\rm flav}$ (fitted)
w (`Lepton`)	0.092 ± 0.004	0.083 ± 0.016	0.075 ± 0.003
w (`Kaon`)	0.170 ± 0.006	0.180 ± 0.011	0.155 ± 0.003
w (`NT1`)	0.208 ± 0.012	0.147 ± 0.022	0.190 ± 0.005
w (`NT2`)	0.339 ± 0.011	0.356 ± 0.018	0.349 ± 0.005

Table 33: Dilutions as extracted with the *CP* fit in MC with the value of sin2β fixed at the generated one, compared with the MC truth ones.

10.1.5 Lifetime fit

As a consistency check, we let the B lifetime float in fits to the *CP* samples and in the fits to the control samples. The resolution function parameters are fixed to the values obtained from the combined fit to the mixing sample and the $\eta_{CP} = -1$ events. The lifetimes and values for sin2β are listed in Table 34. All measured lifetimes are in good agreement with the PDG values.

10.1.6 Dependence on the J/ψ decay mode

The modes where the J/ψ decays into a pair of electrons or muons are potentially quite different because of the emission of Bremsstrahlung. The fit for sin2β is performed separately on MC events with sin2β =0.5 for the two decay modes. We obtain 0.498± 0.027 for the $J/\psi \to e^+e^-$ and 0.489± 0.027 for the $J/\psi \to \mu^+\mu^-$ mode. The agreement is extremely good.

Sample	τ_B
$\eta_{CP} = -1$	$\pm$
$B^0 \to J/\psi\, K^0_L$	$\pm$
$\eta_{CP} = -1$ + $B^0 \to J/\psi\, K^0_L$	$\pm$
$B_{\rm flav.}$	$\pm$
B^+-reco.	$\pm$
$B^+ \to$ Charmonium X	$\pm$

Table 34: Measured lifetimes and sin2β for *CP* samples and control samples. The PDG average values for the B lifetimes are $\tau_{B^0} = 1.548 \pm 0.032$ ps and $\tau_{B^+} = 1.653 \pm 0.028$ ps.

10.2 Data Periods

10.2.1 Run 1 vs. Run 2

Given the somewhat surpring results on the combined run1 and run2 data, it is mandatory to investigate if the observed changes are consistent with statistics. Table 35 summarizes the results in the two data set for the individual modes. The results in the two runs are compared (their statistical errors are completely uncorrelated). The golden modes have shifted up by 1.4, 1.5 and 0.6 standard deviations respectively, while the other modes have gone down. Overall the result has gone up by 1.3 standard deviations (of the uncorrelated error) if one takes all modes. The modes published in the PRL have moved upwards of 1.8 standard deviations. No evident anomaly is observed.

It is also interesting to understand where does the improvement in the statistical error come from. Two are the effects: the increase in statistics and the improvement in the event per event error and the scale factor (improved alignment). The increase of statistics is studied looking at the value of R_{ev}, the ratio between the observed events per fb^{-1}. Two effects contribute to this ratio: the fact that we were running more on-peak and therefore the number of B pairs produced is higher for a given luminosity and the increased K^0_S efficiency. The overall increase in yield per fb^{-1} of the K^0_S $(\pi^+\pi^-)$ modes is 31%. The B pair production cross-section in run1 was 1.08 nb^{-1} while now it is 1.13 nb^{-1}, thus accounting for 5% of the effect. The tracking efficiency is supposed to be slightly better than the 1960 V run2 data, therefore about 2.5% per track better than the average run1[1]. For the golden modes this justifies an increase of about 10%. The remaining effect can be attributed to increase efficiency specific to K^0_S $(\pi^+\pi^-)$. It has been shown [2] that the K^0_S efficiency increased of about 18%. The total expected improvement is therefore (5+2x2.5+18)%=28% which is pretty much in agreement with the observed 31%.

The last column of table 35 shows the ratio between the expected error, given the number of events, and the actual error. There is an additional 10% improvement in the error. Part of it can be explained due to the change in the central value. Figure 23 shows that changing from sin2β =0.3 to 0.6 the error decreases by 5%. The remaining effect

[1] http://www.slac.stanford.edu/BFROOT/www/Organization/CollabMtgs/2001/detJun2001/Tues3/varnes.ps

[2] http://www.slac.stanford.edu/BFROOT/www/Organization/CollabMtgs/2001/detJun2001/Sun1/smith.pdf page 7

mode	sin2β run1	N$_{ev}$ run1	sin2β run2	N$_{ev}$ run2	R_{ev}	Δ_{12}	R_{exp}
$J/\psi\, K_S^0\ (\pi^+\pi^-)$	0.23 $\pm$ 0.24	305	0.72 $\pm$ 0.27	169	1.37	0.49 $\pm$ 0.36	1.19
$J/\psi\, K_S^0\ (\pi^0\pi^0)$	0.13 $\pm$ 0.65	82	1.62 $\pm$ 0.74	42	1.26	1.49$\pm$0.98	1.23
$\psi(2S)K_S^0\ (\pi^+\pi^-)$	0.31 $\pm$ 0.49	64	1.16 $\pm$ 1.21	28	1.08	0.85 $\pm$1.31	0.61
$\chi_{c1}K_S^0\ (\pi^+\pi^-)$	—	29	1.14 $\pm$ 1.25	17	1.44	—	—
$J/\psi\, K^{*0}\ (K_S^0\pi^0)$	1.26 $\pm$ 1.22	60	0.15 $\pm$ 1.62	23	0.94	-1.11$\pm$2.0	1.20
$J/\psi\, K_L^0$	0.71 $\pm$ 0.42	288	0.68 $\pm$ 0.58	142	1.21	-0.03$\pm$0.72	1.03
$J/\psi\, K_S^0 + \psi(2S)K_S^0$ $+J/\psi\, K_L^0$	0.32 $\pm$ 0.18	739	0.83 $\pm$ 0.23	381	1.27	0.51$\pm$0.29	1.09
all	0.45 $\pm$ 0.18	816	0.82 $\pm$ 0.22	433	1.31	0.37$\pm$ 0.29	1.12

Table 35: comparison between run1 and run2 results. Number of events are also compared.$R_{ev} = \frac{N_2\mathcal{L}_1}{N_1\mathcal{L}_2}$ is the ratio of the number of events per fb^{-1},Δ_{12} is the difference between the two runs while $R_{exp} = \frac{\sigma_1}{\sigma_2}\sqrt{\frac{N_1}{N_2}}$

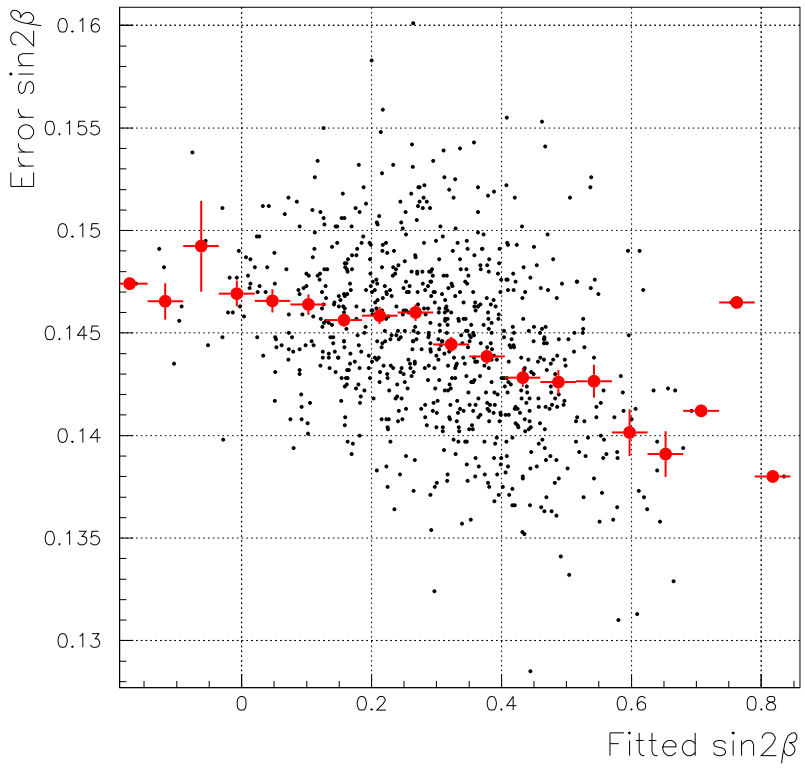

Figure 23: Dependence of the error of sin2β with the central value.

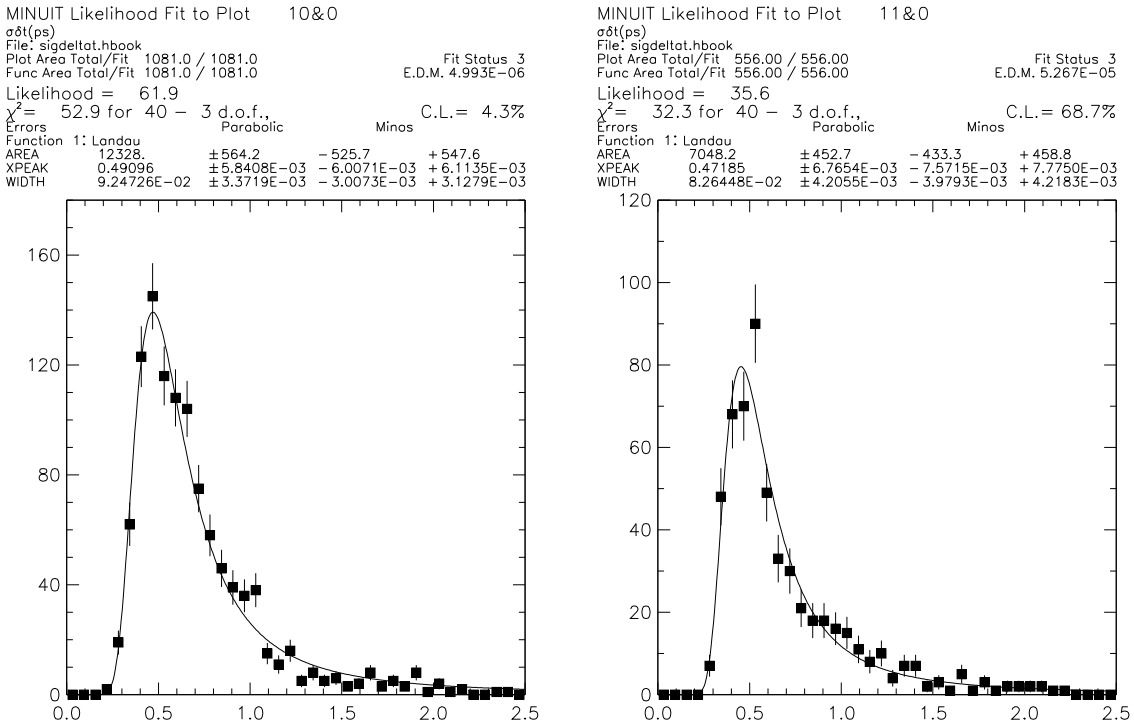

Figure 24: Comparison of the $\sigma\delta t$ distributions in run1 (a) and run2 (b)

can be justified by the improvement in the overall resolution. On one side the event per event error has improved : figure 24 shows that the peak value moves from 0.491± 0.006 (run1) to 0.471 ± 0.007 (run2) while the width goes from 0.092± 0.003 (run1) to 0.083 ± 0.004 (run2) On the other side the scaling factors get smaller thus justifying a decrease in error of 3.4% (see figure 25).

10.3 Data control samples

The $B_{\rm flav}$ and B^+-reco samples as well as the non-*CP* Charmonium modes have been studied as control samples for the data. In these studies, the resolution function parameters and dilutions are fixed to the values obtained from a fit to the $B_{\rm flav}$ sample. Thus, the control sample fits are two parameter fits: the asymmetry and the fraction of prompt background (assumed to be the same for all tagging categories).

Table 24 summarizes the results:

- The measured sin2β in all control samples is compatible with 0. The observed asymmetry in $B^0 \to J/\psi\, K^{*0}$ $(K^+\pi^-)$ is interpreted as a statistical fluctuation. For the Osaka result, fits on this sample measured 0.49 ± 0.26.

- In addition, these samples have been broken up into samples the same size as the current $\eta_{CP} = -1$ sample. These subsamples have been used to show that the measured *CP* asymmetry is compatible with 0 and that the reported values give a

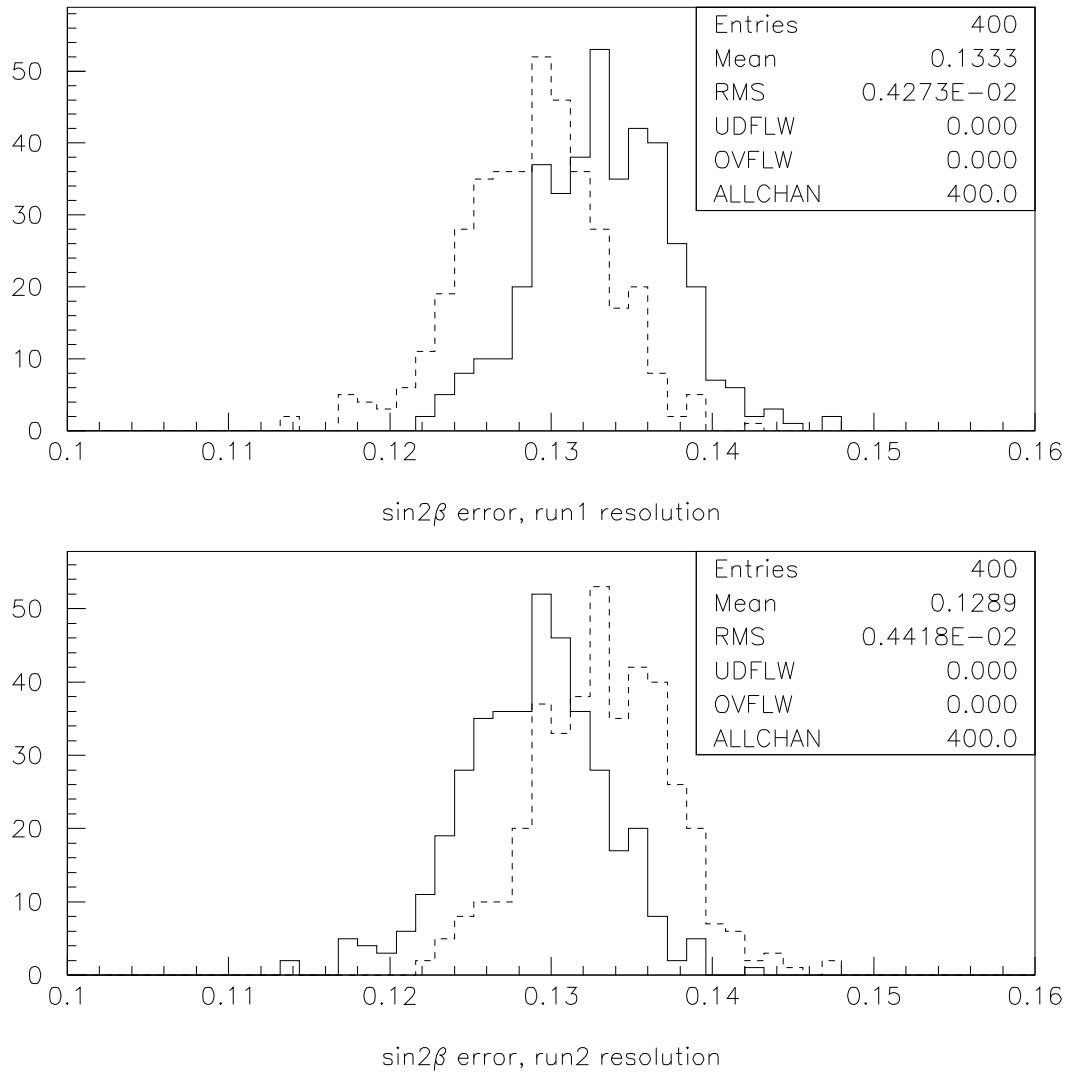

Figure 25: Comparison of the expected error on sin2β in the case of a resolution like the one observed in run1 (top full line or bottom dashed) and the one observed in run2 (top dashed line or bottom full)

reasonable pull distribution. The expected error for the $\eta_{CP} = -1$ event sample is also derived from these subsample fits, and is 0.206 with a spread of ± 0.009.

10.4 Alternative vertexing, tagging, and reconstruction configurations

Table 36 shows results for sin2β for the following alternative vertexing configurations:

- J/ψ mass constraint imposed for the *CP* vertex.
- Using the charmonium (J/ψ or $\psi(2S)$) vertex for the *CP* vertex.
- Do not use the constraints from the beam.
- Removing the K^0_S mass constraint.
- Remove photons from the *CP* vertex.
- Removing the $V0$ veto for the tag vertex.
- Using the "average boost" approximation, computing Δt as $\Delta z / < \beta\gamma >$.
- Using FvtCluster, which includes the beam spot constraint.
- Use only the constraint from the beam spot.

For each fit, the resolution function and dilution parameters are fixed to the nominal values found in Tables 16 to 23, except for FvtClusterer and beam spot only. Moreover, only common events are taking into account. All $\sin 2\beta$ values are blinded, except if precised.

10.4.1 `NOT` and `NetTagger` tagging

As a final cross check of tagging, the $\sin 2\beta$ fit was done for the $\eta_{CP} = -1$ modes using N.O.T. or NetTagger instead of the Elba tagger. For N.O.T., except for merging the categories into 4 final categories (Lepton+Kaon I, Kaon II, Kaon III, SlowPion+Other), the extended version discussed at the sin2beta workshop last November [25] was used. For NetTagger the binned version with 3 categories (NT1a, NT1b, NT2) was used. The results from the fit are shown in table 37.

Between release 10.0.2b and 10.0.3a the packing of the subdetector likelihoods in the micro was changed. In order to check that this does not introduce any problems through the KNet kaon selector – which was trained using SP3 8.8.0 MC with the previous packing and which directly uses the micro likelihoods – the analysis was redone using the SMS kaon selector for tagging. This test was done by producing the ASCII files from tagging ntuples produced using the final sequences, and thus also serves as a validation of the final sequences and a to some extent independent cross check of the analysis. The results are documented in the following tables:

Algorithm	BLIND sin2β (unless otherwise noted)			
	$\eta_{CP} = -1$	$J/\psi\, K^0_L$	$J/\psi\, K^{*0}(K^0_S\pi^0)$	All
Default	0.0304±0.1497	0.1630±0.3382	0.2230±1.1001	0.0520±0.1351
J/ψ mass constraint	0.0270±0.1499	0.1630±0.3382	0.1716±1.1014	0.0484±0.1353
Default (common evts)	0.0294±0.1495	0.1630±0.3382	0.2230±1.1001	0.0511±0.1349
Vtx w/only Charmonium	0.0233±0.1526	0.1630±0.3382	0.0355±1.1112	0.0436±0.1373
Default (common evts)	0.0306±0.1497	0.1630±0.3382	0.2230±1.1001	0.0522±0.1351
No beam constraints	0.0429±0.1590	0.1135±0.3487	-0.6398±1.3558	0.0429±0.1437
Default (common evts)	0.0483±0.1547	0.2265±0.3454	0.3112±1.1245	0.0776±0.1389
no K^0_S mass constraint	0.0290±0.1496	0.1630±0.3382	0.5226±1.0955	0.0514±.1349
Default (common evts)	0.0299±0.1496	0.1630±0.3382	0.2230±1.1001	0.0516±0.1350
Remove photons	0.0571±0.1521	0.1630±0.3382	1.0905±1.1442	0.0879±0.1366
Default (common evts)	0.0264±0.1503	0.1630±0.3382	0.2139±1.0946	0.0487±0.1354
No $V0$ veto	0.0587±0.1496	0.1245±0.3386	0.1671±1.1124	0.0683±0.1353
Default (common evts)	0.0364±0.1496	0.1630±0.3382	0.2230±1.1001	0.0568±0.1350
Boost approx.(UNBLIND)	0.5678±0.1492	0.7466±0.3437	0.7340±1.0767	0.5955±0.1348
Default (common evts)	0.5605±0.1497	0.6933±0.3382	0.7530±1.0999	0.5821±0.1351
Beam Spot only	0.0536±0.1522	0.0862±0.3469	-0.1537±1.1278	0.0554±0.1386
Default (common evts)	0.0132±0.1504	0.1419±0.3372	0.2090±1.0874	0.0396±0.1364
FvtClusterer	0.0631±0.1474	0.2054±0.3354	-0.1525±1.1244	0.0835±0.1344
Default (common evts)	0.0159±0.1510	0.1606±0.3369	0.2934±1.1130	0.0449±0.1365

Table 36: Summary of fits using alternative vertexing configurations.

Tagging algorithm	Effective Q (%)	$\sin 2\beta$	Difference
Elba tagger	26.2 ± 1.2	0.596 ± 0.138	-
N.O.T.	25.4 ± 1.2	0.595 ± 0.137	-0.0006 ± 0.0139
NetTagger	27.0 ± 1.1	0.598 ± 0.134	0.0018 ± 0.0317

Table 37: Results from $\sin 2\beta$ fit done on the run1 plus run2 dataset with different tagging algorithms for all CP modes combined.

Mode	ElbaTagger	N.O.T.		NetTagger	
	sin2β	sin2β	difference	sin2β	difference
$J/\psi\, K_S^0$ $(\pi^+\pi^-)$	0.45 ± 0.18	0.47 ± 0.18	0.02 ±0.03	0.42 ± 0.18	-0.03 ±0.04
$J/\psi\, K_S^0$ $(\pi^0\pi^0)$	0.76 ± 0.53	0.67 ± 0.49	-0.09 ±0.19	0.78 ± 0.50	0.02 ±0.18
$\psi(2S)K_S^0$ $(\pi^+\pi^-)$	0.55 ± 0.42	0.60 ± 0.45	0.05 ±0.17	0.60 ± 0.43	0.05 ±0.23
$\chi_{c1}K_S^0$ $(\pi^+\pi^-)$	2.42 ± 0.67	1.96 ± 0.73	-0.47 ±0.27	2.70 ± 0.64	0.28 ±0.22
$J/\psi\, K^{*0}$ $(K_S^0\pi^0)$	1.20 ± 1.02	0.40 ± 1.10	-0.79 ±0.41	0.46 ± 1.00	-0.73 ±0.21
$J/\psi\, K_L^0$	0.70 ± 0.35	0.82 ± 0.34	0.12 ±0.04	0.85 ± 0.33	0.15 ±0.12
$J/\psi\, K_S^0 + \psi(2S)K_S^0$ $+J/\psi\, K_L^0$	0.53 ± 0.14	0.55 ± 0.14	0.03 ±0.02	0.54 ± 0.14	0.01 ±0.03

Table 38: Results of $\sin 2\beta$ fits with different tagging algorithms on run 1 plus run 2 data set for various CP modes.

10.4.2 Signal probablity determination

When the parameters of the m_{ES} Gaussian plus Argus fit functions are fitted simultaneously with the 35 parameters (increasing the number of free parameters to 58), instead of fixing them to pre-fitted values, sin2β measured on the $\eta_{CP} = -1$ sample increases by 0.00012.

10.4.3 PDF normalization

By default, the fitting algorithms do not account for the cut on on Δt of ± 20 ps. If we normalize the resolution model PDF analytically between -20 and +20 ps, instead of taking the total integral, sin2β increases by 0.00039.

11 Systematics

Table 41 summarizes our estimate of the total systematic error on sin2β. This section describes each contribution to the systematic error as well as other cross checks performed. Refer to supporting BAD documentation for further details on the contributions not unique to the sin2β analysis. There are additional contributions to the systematic error accounted for by fitting for the dilutions and resolutions. These are described in Section 9.

Systematic studies for the $B^0 \to J/\psi\, K_L^0$ mode are further documented in BAD 206 [21].

Tagging Algorithm	$\sin 2\beta$	Difference
Elba tagger, official ASCII files	0.5959 ± 0.1376	—
Elba tagger, ASCII files from tagging ntuples	0.5863 ± 0.1381	-0.0096 ± 0.0117
Elba tagger with SMS kaon selector	0.5430 ± 0.1428	-0.0529 ± 0.0382

Table 39: Results of $\sin 2\beta$ fits with different tagging algorithms on run 1 plus run 2 data set using all CP modes.

Tagging Algorithm	$\sin 2\beta$	Difference
Elba tagger, official ASCII files	0.4537 ± 0.1806	—
Elba tagger, ASCII files from tagging ntuples	0.4399 ± 0.1818	-0.0138 ± 0.0209
Elba tagger with SMS kaon selector	0.3969 ± 0.1874	-0.0568 ± 0.0500

Table 40: Results of $\sin 2\beta$ fits with different tagging algorithms on run 1 plus run 2 data set using only $B^0 \to J/\psi\ K^0_S$ CP events.

11.1 Signal Parameters

The underlying assumption in this analysis is that the resolution function and the dilutions are the same in the B flavour eigenstates and in the CP ones. Deviations from this assumptions are accounted for in the systematic error.

11.1.1 Dilutions

Running on large samples of $B_{\rm flav}$ and CP Monte Carlo, dilutions are extracted and compared[18]. The results are shown in Table 44. The observed shift in sin2β using the two sets of dilutions is assigned as the systematic error.

11.1.2 Resolution function parameters

Running on large samples of $B_{\rm flav}$ and CP Monte Carlo, the resolution function parameters are extracted and compared. The results are shown in Table 45. The observed shift in sin2β using the two sets of resolution function parameters is assigned as the systematic error, 0.003.

In order to test that the fitting procedure is capable of returning an appropriate resolution function a fit on copious signal MC has been performed both floating the resolution function parameters and fixing them to the values extracted making use of the MC truth information. The results are in Table 42. The difference between the two is 0.xxx$\pm$0.xxx. No systematic error is quoted, given that the statistical error on this is already included in the MC statistics test.

In order to evaluate that the difference between the Charmonium and Breco resolution function parameters is actually the same in data and MC, the parameters are extracted from the data from a fit with fixed lifetime to neutral and charged Charmonium events,

Source	*CP* Sample					
	$J/\psi K^0_S$	$J/\psi K^0_L$	$J/\psi K^{*0}$	Full	DirectCP	
					$\mathcal{I}m\lambda$	$\lvert\lambda\rvert$
Signal parameters						
Δt signal resolution	±0.003					±0.009
Δt signal resolution outliers	±0.002	±0.018	±0.03	±0.002	±0.003	±0.002
Δt Art Effect	±0.012				±0.011	±0.003
signal dilutions	±0.027					±0.011
Δt signal resolution model	±0.009	±0.01	±0.07	±0.009	±0.003	±0.003
Background parameters						
Signal probability: *CP* sample	±0.006	—	—	±0.005	±0.006	±0.004
Signal probability: $B_{\rm flav}$ sample	±0.001	$\pm$	$\pm$	±0.002	±0.002	±0.001
M_{ES} endpoint	±0.001	—	—	±0.001	±0.001	±0.001
CP background peaking component	±0.004	—	—	±0.003	±0.005	±0.001
CP background *CP* content (Argus)	±0.015	—	—	±0.015	±0.015	±0.001
CP background *CP* content (Peak)	±0.004	—	—	±0.004	±0.004	±0.001
CP background τ	0	—	—	0	0	0
CP background resolution	±0.002	—	—	±0.002	±0.002	±0.001
$B_{\rm flav}$ background mixing contrib.	±0.001	±0.002	±0.001	±0.002	±0.001	0
$B_{\rm flav}$ background peaking component	0	±0.001	±0.001	0	0	0
external parameters						
B^0 lifetime	±0.001	±0.015	±0.028	±0.002	±0	±0.002
Δm_d	±0.015	±0.012	±0.082	±0.013	±0.015	±0.001
$J/\psi K^0_L$						
Total from BAD 206	—	±0.093	—	±0.011	—	—
$J/\psi K^{*0}(K^0_S\pi^0)$						
Total from Table 48	—	—	±0.11	±0.001	—	—
Direct *CP*						
μ	0.003				0.004	0.012
detector effects						
z scale + boost	±0.003					±0.001
Beam spot	±0.002					±0.006
SVT alignment	±0.027					±0.012
Monte Carlo correction	±0.012					$\pm$
Total systematic error	±0.049	±0.104	±0.162	±0.049	±0.046	±0.024
Statistical error	±0.151	±0.340	±1.01	±0.137	±0.151	±0.092

Table 41: Summary of contributions to the systematic error on sin2β. For the $J/\psi K^0_L$ specific systematic error, the quoted value is from BAD 206.

compared to the corresponding sample in the flavour eigenstates. This is shown in Ta-

Parameter	MC truth	Fitted	right tag	wrong tag
Scale (core)	$\pm$ 0	1.14 ± 0.05	1.10 ± 0.08	1.12 ± 0.15
Scale (tail)	$\pm$	3.0	3.0	3.0
δ Lepton (core)	$\pm$	-0.059 ± 0.055	-0.035 ± 0.055	-0.012 ± 0.293
δ Kaon (core)	$\pm$	-0.253 ± 0.036	-0.268 ± 0.036	-0.557 ± 0.127
δ NT1 (core)	$\pm$	-0.119 ± 0.063	-0.089 ± 0.067	0.160 ± 0.224
δ NT2 (core)	$\pm$	-0.164 ± 0.046	-0.146 ± 0.052	-0.110 ± 0.130
δ (tail)	$\pm$	-3.39 ± 1.45	-1.90 ± 1.53	-1.36 ± 0.89
f(tail) (%)	$\pm$	0.039 ± 0.024	0.068 ± 0.051	0.107 ± 0.061
f(outlier) (%)	$\pm$	0.002 ± 0.001	0.002 ± 0.001	0 ± 0.002

Table 42: Resolution function on *CP* MC as extracted from the fit to the MC truth , in a global fit on the reconstructed Δt and in "right" and "wrong tag" events

ble 45.

In order to evaluate the effect of a different resolution function between the events where the tag is correct and those where the tag is incorrect (so called Art effect) , we have splitted a sample of MC events into "wrong tags" and "right tags". A fit to sin2β and the resolution function parameters has been performed on the two samples and on the original one, sum of the two. In the "wrong tags" and " right tags" samples the dilutions are fixed to -1 and 1 respectively, while they are fixed to the MC truth ones in the original file. The weighted average of the "wrong tags" and " right tags" samples is compared to the result on the global file. The difference is 0.012 and this is considered as systematic error.

Finally, the outlier contribution to the resolution function is varied. We vary the width of the outlier Gaussian between 4 and 12 ps and its bias between –2 ps and +2 ps around the nominal values of 8 ps and zero, respectively. Table 43 shows the variations in sin2β when different parameters for the outlier Gaussian are used. A systematic error for sin2β of 0.002 (0.018,0.03) is assigned for the golden ($J/\psi\, K^0_L$, $J/\psi\, K^{*0}$) events and 0.002 for all events.

11.1.3 Parameterization of the signal resolution function

11.2 Backgrounds parameters

A set of parameters are fixed for the background either because they were extracted from an independent fit (argus + gaussian) or because they were evaluated from an external source (typically MC). Here are the variations that are considered and the corresponding change in measured sin2β.

11.2.1 Signal probability distribution

The effect of the uncertainty on the $m_{\rm ES}$ fit results on sin2β is estimated from fits in which the event-by-event signal probabilities are varied. To this end, we measure a global signal probability for the events in the signal region ($m_{\rm ES} > 5.270$ GeV). This signal probability

Width/Bias	$\delta\sin2\beta$ $\eta_{CP}=-1$	$J/\psi K^0_L$	$J/\psi K^{*0}$	All CP	$\mathcal{I}m\lambda$	$\lvert\lambda\rvert$
Gaussian model						
8/0	–	–	–	–	–	–
4/0	+0.002	−0.017	+0.02	+0.001	+0.002	−0.001
12/0	+0.001	−0.011	+0.02	0	+0.002	0
8/–2	−0.001	−0.005	−0.006	−0.001	0	0
8/+2	0	+0.001	+0.02	0	+0.001	−0.001
Syst. Error	±0.009	±0.01	±0.07	±0.009	±0.003	±0.003

Table 43: Systematic uncertainties in $\sin2\beta$ due to fixed width and bias of the Δt outliers estimated from data by varying the width and bias and replacing the Gaussian outlier model with a flat PDF model. $\delta\sin2\beta$ is the difference of $\sin2\beta$ for the specified fit and the reference fit with a Gaussian outlier with a width of 8 ps and zero bias.

Parameter	$CP=-1$ MC	$B_{\rm flav}$ MC
w (Lepton)	0.092 ± 0.004	0.075 ± 0.003
w (Kaon)	0.170 ± 0.006	0.155 ± 0.003
w (NT1)	0.208 ± 0.012	0.190 ± 0.005
w (NT2)	0.339 ± 0.011	0.349 ± 0.005
$\Delta\ w$ (Lepton)		-0.003 ± 0.005
$\Delta\ w$ (Kaon)	0.012 ± 0.012	-0.020 ± 0.004
$\Delta\ w$ (NT1)	0.030 ± 0.025	0.024 ± 0.008
$\Delta\ w$ (NT2)	-0.055 ± 0.023	-0.032 ± 0.007
$\delta\sin2\beta$	0.027	—

Table 44: Dilutions used for evaluating the effect of the different tagging performances in Charmonium and $B_{\rm flav}$ events and corresponding relative change in $\sin2\beta$. $\Delta w\equiv w-\bar{w}$

is assigned to all events in the signal region and all events with $m_{\rm ES}<5.270$ GeV are assigned zero signal probability. We compare $\sin2\beta$ from a fit with these signal probabilities (*default*) to $\sin2\beta$ from fits for which the signal probabilities are varied by one sigma. We vary the signal probabilites for the golden *CP* sample and for the $B_{\rm flav}$ sample independently and perform the variations conservatively for all tagging categories simultanously. The results are listed in Table 47.

We account for an error in $m_{\rm ES}$ fit results due to the uncertainty in the beam energy by varying the end point of the Argus background shape by ± 2 MeV around the nominal value of 5.291 GeV. We estimate the systematic uncertainty due to the $m_{\rm ES}$ endpoint to be ±0.003 (±0.001), which is the shift corresponding to this variation in the Argus background end point on the $CP=-1$ (full *CP* sample) fits.

Parameter	$B_{\rm flav}$	$CP = -1$ MC
Scale (core)	1.124 ± 0.023	1.070 ± 0.044
Scale (tail)	3.000	3.000
δ core(`Lepton`) (ps)	-0.043 ± 0.024	-0.079 ± 0.029
δ core(`Kaon`) (ps)	-0.224 ± 0.015	-0.166 ± 0.021
δ core(`NT1`) (ps)	-0.124 ± 0.029	-0.038 ± 0.036
δ core(`NT2`) (ps)	-0.175 ± 0.021	-0.102 ± 0.031
δ tail (ps)	-1.596 ± 0.311	-0.615 ± 0.209
f(tail)	0.067 ± 0.012	0.098 ± 0.019
f(outlier)	0.003 ± 0.001	0.003 ± 0.001
$\delta \sin 2\beta$	—	0.003

Table 45: Resolution function parameters used for evaluating the effect of the different vertexing performances in Charmonium and $B_{\rm flav}$ events and corresponding relative change in $\sin 2\beta$.

Parameter	B^0-Reco	B^+-Charmonium
Scale (core)	$\pm$	$\pm$
Scale (tail)	$\pm$	$\pm$
δ(Lepton) (core) [ps]	$\pm$	$\pm$
δ(Kaon) (core) [ps]	$\pm$	$\pm$
δ(NT1) (core) [ps]	$\pm$	$\pm$
δ(NT2) (core) [ps]	$\pm$	$\pm$
δ(tail) [ps]	$\pm$	$\pm$
$f_{\rm tail}$	$\pm$	
$f_{\rm outlier}$	$\pm$	$\pm$

Table 46: Resolution function parameters in B^+-Charmonium and $B_{\rm flav}$ data samples. Due to limited statistics in the B^+-charmonium sample, the fit with all nominal resolution function parameters floated does not converge. Therefore the fraction of events in the tail Gaussian is fixed.

11.2.2 *CP* background peaking component

For non-$J/\psi K^0_L$ modes, background contributions that peak in $m_{\rm ES}$ are estimated by running on the inclusive J/ψ Monte Carlo. A systematic error on $\sin 2\beta$ is assigned using the change in $\sin 2\beta$ results when this background is varied by 100% around the central values described in Section 4.1 to take into account the uncertainty on the branching fractions as well as Monte Carlo statistics and the effect of the $p^*_{J/\psi}$ >1.3 GeV cut on the vast majority of the available MC.

Variation	$\delta\sin2\beta$		
	$B_{\rm flav} + \eta_{CP} = -1$	$B_{\rm flav} + J/\psi K^0_L$	$B_{\rm flav} + \eta_{CP} = -1 + J/\psi K^0_L$
Δ(up-down) $p_{\rm Sig,\ CP,run1}$		—	-0.005
Δ(up-down) $p_{\rm Sig,\ CP,run2}$		—	-0.001
Δ(up-down) $p_{\rm Sig,\ Mix,run1}$			-0.002
Δ(up-down) $p_{\rm Sig,\ Mix,run2}$			-0.001
Syst. Error	$\pm$ 0.003	$\pm$ 0.002	$\pm$ 0.006

Table 47: Systematic errors due to statistical uncertainties in the event-by-event signal probabilities.

11.2.3 *CP* content of background

The *CP* content of the background has two different treatments in the case of the $J/\psi K^0_L$ mode and the other ones.

- for non-$J/\psi K^0_L$ modes, the assumed *CP* of the Argus background contribution is changed from 0 to ±1. This yields a systematic error of $\sin2\beta$ ±0.015. The *CP* of the peaking component is treated in the same fashion, giving an error of ±0.004.

11.2.4 Lifetime and resolution function for *CP* background

The lifetime of the *CP* background has been varied from 0.7 to 2.5 ps, giving no significant systematic uncertainty on $\sin2\beta$.

11.2.5 $J/\psi K^{*0}(K^0_S\pi^0)$ sample composition

As the $J/\psi K^{*0}(K^0_S\pi^0)$ sample composition is derived from Monte Carlo, it must be varied as part of the total systematic error. We have used measured *BABAR* Charmonium branching fractions where possible. Table 48 shows the sample composition variations and the resulting systematic error. The final error is derived by adding each contribution in quadrature.

11.2.6 Mixing contribution to the $B_{\rm flav}$ background

In the nominal fit, the $\tau > 0$ background in the $B_{\rm flav}$ sample is assumed to not mix. As a systematic check we have performed a fit where it is instead assumed to mix. We assign the shift in $\sin2\beta$ as the systematic error, giving ±0.001 to ±0.002, depending on the fitted *CP* sample.

11.2.7 Peaking background in the $B_{\rm flav}$ background

The peaking background in the $B_{\rm flav}$ sample is $1.5 \pm 1.0\%$ [15]. This uncertainty gives a systematic error on $\sin2\beta$ of 0 to ±0.001, depending on the fitted *CP* sample.

Source	Variation	$J/\psi K^{*0}$ fit	Full CP sample fit
Signal $R_\perp$	± 0.06	± 0.08	± 0.0007
CP of non-itemized back.	± 1	± 0.05	± 0.0005
CP of heavy K^* back.	± 1	± 0.04	± 0.0005
CP of non-resonant back.	± 1	± 0.03	± 0.0003
Signal BR	$\pm 10\%$	± 0.01	± 0.0001
$\chi_{cK^0_S}$ BR	$\pm 30\%$	± 0.02	± 0.0002
Non-itemized BR	$\pm 50\%$	± 0.01	± 0.0001
Non-resonant BR	$\pm 50\%$	± 0.01	± 0.0001
Total		± 0.11	± 0.001

Table 48: $J/\psi K^{*0}(K^0_S\pi^0)$ systematic errors.

11.3 External parameters

Table 49 summarizes the results obtained when Δm_d and (or) τ_{B^0} are allowed to float in the fit.

11.4 Detector effects

The possibility of forms of misreconstruction of the data that might not be properly accounted by the measurement technique has been explored. The possible effects we have considered are:

11.4.1 Uncertainty on Boost and the z scale

In order to evaluate a possible effect from the uncertainty on the boost and z scale, the measurement of Δt has been rescaled by 0.6% upwards and downwards in full MC. The effect on the measured sin2β is estimated to be 0.003

11.4.2 SVT misalignment

To study systematic uncertainties from SVT alignments, MC $J/\psi K^0_S$ signal samples with different were produced. As explained in a posting by S. Wagner [3], the SVT alignment is now know with a much better accuracy. This better knowledge of the SVT alignment is however not included in the Run 1 data, which were processed with older alignments. To estimate the systmeatic, samples were generated with a misalignment describing the difference between the alignment used for the analysis and the newer, much better, one. These samples (sets `diffEL` and `diffDL`) were compared with MC samples with a perfect alignment (`Zero` sets). The bias needs to be rescaled to account for the fact, that this misalignment affects only Run 1 data. For each misalignment, we performed the fit in two ways:

[3] `http://babar-hn.slac.stanford.edu:5090/HyperNews/get/sin2beta/287.html`

Fit	sin2β	Δm_d (ps^{-1})	τ_{B^0} (ps)
All CP modes			
Nominal fit	0.592 ± 0.137		
Float Δm_d	0.550 ± 0.130	0.533 ± 0.015	
Float Δm_d and τ_{B^0}	0.560 ± 0.132	0.541 ± 0.016	1.50 ± 0.03
$CP = -1$ modes			
Nominal fit	0.565 ± 0.151		
Float Δm_d	0.512 ± 0.145	0.531 ± 0.015	
Float Δm_d and τ_{B^0}	0.520 ± 0.147	0.540 ± 0.016	1.50 ± 0.03
$J/\psi K^0_L$			
Nominal fit	0.701 ± 0.347		
Float Δm_d	0.753 ± 0.325	0.539 ± 0.015	
Float Δm_d and τ_{B^0}	0.768 ± 0.329	0.546 ± 0.016	1.50 ± 0.03
$J/\psi K^{*0}$			
Nominal fit	0.817 ± 1.01		
Float Δm_d	0.530 ± 0.941	0.534 ± 0.015	
Float Δm_d and τ_{B^0}	0.525 ± 0.954	0.541 ± 0.016	1.51 ± 0.03

Table 49: Results when Δm_d and (or) τ_{B^0} are floated in the sin2β fit.

1. Fitting the resolution function from MC truth and plugging them in a one parameter fit to sin2β.

2. Fitting the resolution function together with sin2β.

The results are summarized in Table 50. The same study is done for the direct CP fit and the results are shown in Table 51.

11.5 Monte Carlo correction

A set of high statistics full MC studies on CP signal events has been performed in order to evaluate possible biases in the measurement. The pull distribution from these studies is shown in Figure 22. The mean pull is consistent with 0, and we make no correction and assign a systematic error, based on the statistics of the Monte Carlo, of ± 0.012.

12 Results of the fit for $|\lambda|$

The result of this fit is:

$$\begin{aligned} \mathcal{I}m\lambda/|\lambda| &= 0.561 \pm 0.151 \\ |\lambda| &= 0.933 \pm 0.092 \end{aligned}$$

Tables 16 and 17 give the results for all free parameters in the fit. Table 25 shows the results of fits to the various subsamples.

Fitting sin2beta and resolution function			
alignment	sin2β	sin2β variation	sin2β variation (rescaled run1)
Zero	0.713 ± 0.058	-	-
ExpandZ001	0.701 ± 0.058	$-.012 \pm 0.005$	-0.007
diffDL	0.670 ± 0.059	$-.043 \pm 0.007$	-0.026
diffEL	0.694 ± 0.059	$-.019 \pm 0.011$	-0.012
Fitting sin2beta only (resolution function from MC truth)			
alignment	sin2β	sin2β variation	sin2β variation (rescaled run1)
Zero	0.728 ± 0.057	-	-
ExpandZ001	0.724 ± 0.058	$-.004 \pm 0.011$	-0.002
diffDL	0.702 ± 0.060	$-.025 \pm 0.017$	-0.015
diffEL	0.713 ± 0.059	$-.015 \pm 0.015$	-0.009

Table 50: Change in the value of sin2β for different alignment sets.

Fitting $\mathcal{I}m\lambda/\lvert\lambda\rvert$, $\lvert\lambda\rvert$ and resolution function					
alignment	$\mathcal{I}m\lambda/\lvert\lambda\rvert$	$\lvert\lambda\rvert$	$\delta(\mathcal{I}m\lambda/\lvert\lambda\rvert)$	$\delta(\mathcal{I}m\lambda/\lvert\lambda\rvert)$ (rescaled run1)	$\delta(\lvert\lambda\rvert)$
Zero	0.732 ± 0.057	1.067 +/- 0.04229	-	-	-
ExpandZ001	0.728 ± 0.058	1.07 ± 0.042	$-.004 \pm 0.011$	-0.003	.003 +/- 0.004
diffDL	0.707 ± 0.060	1.076 ± 0.043	$-.025 \pm 0.017$	-0.015	.009 +/- 0.008
diffEL	0.718 ± 0.059	1.079 ± 0.043	$-.014 \pm 0.015$	-0.008	.012 +/- 0.008
Fitting $\mathcal{I}m\lambda/\lvert\lambda\rvert$ and $\lvert\lambda\rvert$ (resolution function from MC truth)					
alignment	$\mathcal{I}m\lambda/\lvert\lambda\rvert$	$\lvert\lambda\rvert$	$\delta(\mathcal{I}m\lambda/\lvert\lambda\rvert)$	$\delta(\mathcal{I}m\lambda/\lvert\lambda\rvert)$ (rescaled run1)	$\delta(\lvert\lambda\rvert)$
Zero	0.715 ± 0.058	1.048 +/- 0.04308	-	-	-
ExpandZ001	0.703 ± 0.058	1.055 ± 0.043	$-.0121 \pm 0.005$	-0.007	.007 +/- 0.005
diffDL	0.671 ± 0.059	1.056 ± 0.043	$-.0434 \pm 0.007$	-0.026	.008 +/- 0.004
diffEL	0.695 ± 0.059	1.054 ± 0.043	$-.0198 \pm 0.011$	-0.012	.006 +/- 0.005

Table 51: Change in the value of $\mathcal{I}m\lambda/\lvert\lambda\rvert$ and $\lvert\lambda\rvert$ for different alignment sets.

13 Validation of fit for $|\lambda|$

The validation studies for the measurement of $|\lambda|$ can be found in BAD115.

14 Systematics of the fit for $|\lambda|$

Table 41 summarizes our estimate of the total systematic uncertainty on $\mathcal{I}m\lambda/|\lambda|$ and $|\lambda|$. We can split the systematic uncertainties in two categories: those common to the sin2β only fit and the specific systematic uncertainties for the direct CP analysis. For the first ones, the systematic uncertainties have been determined as described in section 11 and will not be described here again.

14.1 Specific systematic uncertainties to the direct CP fit: tagging efficiencies

The only additional we have to add comes from the unertainties on the tagging efficiency differences for B^0 and $\overline{B}^0$, contained in the μ parameter. The systematic uncertainty is determined by varying μ by ± 1 σ according to the errors on μ listed in table 13. Since μ is determined independently for each tagging category, we consider the systematic uncertainties coming for the uncertainty on μ for each tagging category as four uncorrelated uncertainties and add them in quadrature. The resulting systematic uncertainties are 0.014 on $\mathcal{I}m\lambda/|\lambda|$ and 0.028 on $|\lambda|$.

To determine the systematic uncertainties coming from different tagging efficiencies for B^0 and $\overline{B}^0$, we proceed as following:

1. The value of μ for every tag category can be determined from data by counting the number of tagged und untagged events of reconstructed B^0 and $\overline{B}^0$ in the mixing sample[4]. The results are listed in Table 13

2. The likelihood function for the CP signal is modified according to equ. (32).

3. We perform a two parameters fit to $\mathcal{I}m\lambda/|\lambda|$ and $|\lambda|$, by varying μ by $\pm 1\sigma$ of the measured values. The difference with the fit where μ is set to 0 is regarded as systematics uncertainty. The results are showed in Table 14.1.

4. The four categories are treated as uncorrelated. An error is determined for each and they are added in quadrature.

The total systematic error from uncertainties on tagging efficiencies estimated in this way is 0.004 on $\mathcal{I}m\lambda/|\lambda|$ and 0.012 on $|\lambda|$, which is the dominant systematic uncertainty for the latter.

[4]see `http://babar-hn.slac.stanford.edu:5090/HyperNews/get/sin2beta/183.html`

	$\mu - 1\sigma$		$\mu + 1\sigma$	
	$\delta(\mathcal{I}m\lambda/\|\lambda\|)$	$\delta(\|\lambda\|)$	$\delta(\mathcal{I}m\lambda/\|\lambda\|)$	$\delta(\|\lambda\|)$
Lepton	-0.0001	0.0068	0.0002	-0.0067
Kaon	-0.0001	0.0082	-0.0001	-0.0081
NT1	0.003	0.0044	-0.0032	-0.0043
NT2	-0.0032	0.0021	0.0031	-0.0021

Table 52: Systematic uncertainties in $\mathcal{I}m\lambda/|\lambda|$ and $|\lambda|$ due to uncertainties on the difference in tagging efficiencies for B^0 and $\overline{B}^0$, taken from a 2 parameter fit to $\mathcal{I}m\lambda/|\lambda|$ and $|\lambda|$ on the golden CP events only.

A Details of $B \to \chi_{c1} K$ selection cuts

In this appendix we describe the changes in the $B \to \chi_{c1} K$ selection cuts with respect to the previous "CP" selection presented in reference [31].

The previous "CP" selection was mainly based on the branching fractions selections ("BF" selection) detailled in reference [32]. The cuts in the "BF" selection were choosen and adjusted in order to minimize as much as possible the systematic and statistical errors contributions to the BF measurements.

The new "CP" selection cuts are listed in table 4. These cuts were defined to obtain the best compromize in between the highest purity for data sample used for the sin2β fit and to reduce the impact on the signal selection efficiency. These changes apply both to the χ_{c1} $K^{\pm}$ and χ_{c1} K^0_S exclusive B decay modes.

The BF studies [32] have shown that the continuum background is negligible with respect to the dominant inclusive J/ψ background, therefore the $|\cos\theta_{thrust}| < 0.9$ cut, which was previously applied, was removed in order to increase the signal selection efficiency by 10%.

Using a sample of 245000 inclusive J/ψ for B decays SP3 8.8.0 Monte-Carlo (without P^* cut), equivalent to an integrated luminosity of 89.8 fb^{-1}, a study has been performed to demonstrate that with the previous "CP" selection 70% (respectively 10%) of the fake χ_{c1} used to form a B candidate in the grand side band (GSB), have a γ daughter which was in fact produced in the decay of a π^0 (respectively in η decays). This Monte-Carlo sample contains also the $B \to \chi_{c1} K$ signals (the BF assumed from B decays are 6.10^{-4}, this value is consistent with our BF measurements [32]), so it was used to define a veto criteria against π^0. The statiscal significance of the signal and its selection efficiency were both taken into account in the optimization of this π^0 veto. In addition to the other selection cuts, we reject any χ_{c1} with a γ daughter that could be combined with a GoodPhotonLoose Beta candidate, with an energy > 70 MeV, to form a π^0 candidate in the mass window [120,150] MeV/c^2. The preselection cut E(γ_2)$>$ 70 MeV (where γ_2 is the other π^0 daughter) allows to reduce the impact of the combinatoric low energy γ background on the signal selection efficiency. The conclusions of this optimisation are in good agreement with the χ_{c1} selection used by CLEO for its inclusive charmonium from B decays analysis [33]. The relative loss of the signal efficiency, due the π^0 veto, is about 13% and is almost all compensated by the removal of the $|\cos\theta_{thrust}| < 0.9$ cut. The background relative reduction, in the B signal box, is about 45% as estimated from the inclusive J/ψ Monte-Carlo sample.

The M($\gamma J/\psi$)-M(J/ψ) mass difference window cut, used to select χ_{c1} candidates, has also been tighten from [350,450] MeV/c^2 to [380,450] MeV/c^2. The window size is now equivalent to ± 2.5 σ around the χ_{c1} PDG mass [14], where the experimental resolution with the *BABAR* detector is $\sigma = (14 \pm 1)$ MeV/c^2. The relative effect on the signal efficiency is a loss of about 8%, this is slightly higher than expected from a perfect Gaussian distribution. This is due the tail in the lower part of mass difference distribution which is related to reconstruction quality effects for the γ with the electromagnetic calorimeter and also to interactions in the material of the tracking and DIRC parts of the detector (see [32] and [34]). For this new selection, the window size is 30% smaller. With the inclusive J/ψ Monte-Carlo, the background relative reduction in the B signal box has been estimated to

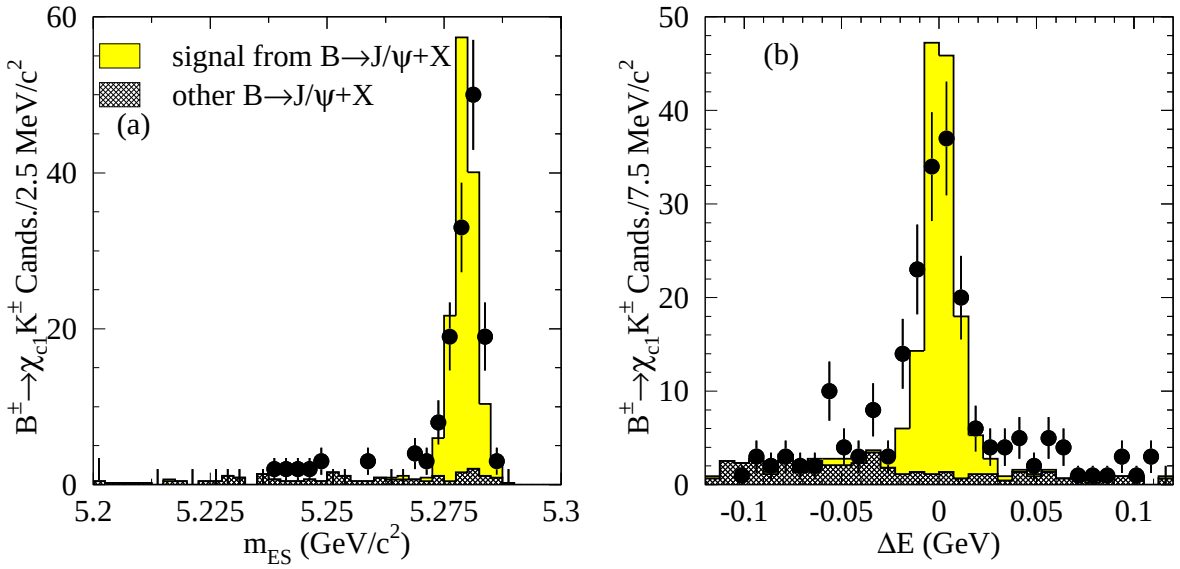

Figure 26: Distribution for the χ_{c1} $K^{\pm}$ decay mode in (a) $m_{\rm ES}$ and (b) ΔE for the new "CP" selection. The points are the Run 1 data, the shaded histograms are Monte-Carlo simulated inclusive J/ψ decays, broken down into the signal and background distributions.

be 35%, indicating a flat distribution of the background for the M($\gamma J/\psi$)-M(J/ψ) variable.

The background distribution in the $|\Delta E| < 120$ MeV vs. $m_{\rm ES} > 5.27$ GeV/c^2 band is also flat. We have reduced the signal band in the size down to $|\Delta E| = \pm 2.5\ \sigma$, where σ are the resolutions measured with the BF data sample presented in reference [32] and written in table 53. A different signal band size is applied to the J/ψ to e^+e^- and $\mu^+\mu^-$ data sub-samples. This is another 15% gain on background reduction and the effect on the signal yield is hardly visible in the inclusive J/ψ Monte-Carlo. In the $m_{\rm ES}$ axis of the ΔE vs. $m_{\rm ES}$ plane, the signal box size is defined as [5.27,5.29] GeV/c^2.

The new "CP" selection is in total 88% as efficient as the one of reference [31]. The background in the signal box has been reduced by 75%. Figures 26 and 27 show the Run 1 $m_{\rm ES}$ and ΔE distributions for this new "CP"selection, both for the χ_{c1} $K^{\pm}$ and χ_{c1} K^0_S exclusive B decay modes and superimposed on the SP3 inclusive J/ψ Monte-Carlo.

Using the inclusive J/ψ SP3 Monte-Carlo we have been able to determine the peaking background contribution in the signal box both for the χ_{c1} $K^{\pm}$ and χ_{c1} K^0_S exclusive B decay modes. We use the method described in reference [32].

Before to apply this method, as we have found a small fraction of $B \to \chi_{c2}K$ events in the GSB (mostly centered at $\Delta E = -46$ MeV), we have removed them from the background sample, as no clear evidence of χ_{c2} signal was seen both in the inclusive [34] and a very preliminary exclusive analysis. Figures 28 and 29 show the Run 1 $m_{\rm ES}$ and ΔE distributions for this new "CP"selection, both for the χ_{c2} $K^{\pm}$ and χ_{c2} K^0_S exclusive B decay modes and superimposed on the SP3 inclusive J/ψ Monte-Carlo. The $B \to \chi_{c2}K$ are the same as for the corresponding $B \to \chi_{c1}K$ exclusive modes, except for the mass difference window cut which is [430,550] MeV/c^2. The BF assumed in the SP3 Monte-Carlo for the $B \to \chi_{c2}K$ modes considered here are 4.10^{-4}. Although no clear signal is

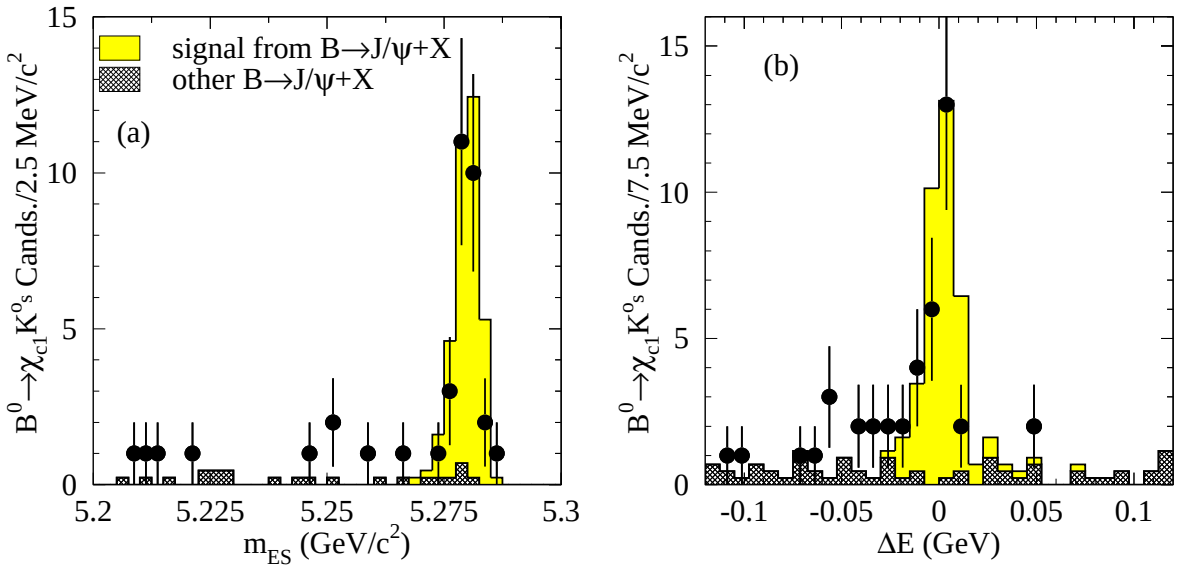

Figure 27: Distribution for the χ_{c1} K^0_S decay mode in (a) $m_{\rm ES}$ and (b) ΔE for the new "CP" selection. The points are the Run 1 data, the shaded histograms are Monte-Carlo simulated inclusive J/ψ decays, broken down into the signal and background distributions.

observed this study deserves more work in order to be able to set a limit on the BF.

The remaining inclusive J/ψ background in the signal box is dominated $(70-80\%)$ by the $J/\psi K^*$ decays. For the χ_{c1} K^0_S mode 60%(40%) of the K^* decay to $K^0_S\pi^\pm(K^0_S\pi^0)$. For the χ_{c1} $K^\pm$ mode 55%(45%) of the K^* decay to $K^\pm\pi^\pm(K^\pm\pi^0)$.

Table 53 shows, for the new "CP" selection, the signal resolutions, number of candidate, Argus and inclusive J/ψ Gaussian peaking backgrounds, event yields and signal purities in the signal box for the $\chi_{c1}K$ decay modes with the Run 1 data (20.7 fb^{-1}) and a Monte Carlo sample of 245000 inclusive J/ψ from B$\bar{\rm B}$ decays (89.8 fb^{-1}). Results are shown separately for the $J/\psi \to l^+l^-$, e^+e^- and $\mu^+\mu^-$ channels. The signal resolution are those of BF analysis [32]. The number of candidates are from an event counting in the signal box as previously defined. The Argus background is from an unbinned likelihood fit to a Gaussian plus Argus background performed on the data sample in the signal band (see figures 30, 31 and 32) and a number of events in the signal box is extracted from the fit. The Gaussian peaking background is determined from an unbinned likelihood fit to a Gaussian plus Argus background performed on the J/ψ inclusive Monte-Carlo in the signal band (as an example see figure 33) and a number of events in the signal box is extracted from the fit. The last value is then normalized according to the equivalent luminosity of the data sample. The 2 last columns of table 53 show the event yield after background subtraction for the Run1 data sample and the corresponding signal purity in the signal box. For the Run 1 data and for this new "CP" selection, the χ_{c1} K^0_S events yield was 1.4 events per fb^{-1} with a purity of $(90.8 \pm 19.6)\%$, the χ_{c1} $K^\pm$ events yield was 6.5 events per fb^{-1} with a purity of $(86.4 \pm 9.5)\%$.

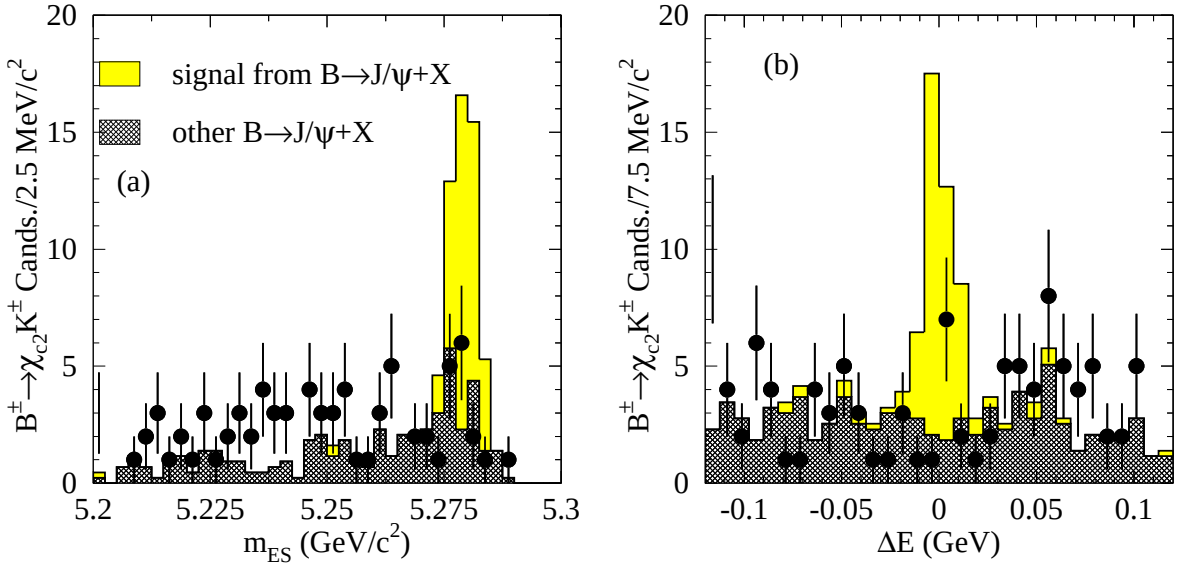

Figure 28: Distribution for the χ_{c2} $K^{\pm}$ decay mode in (a) $m_{\rm ES}$ and (b) ΔE for the new "CP" selection. The points are the Run 1 data, the shaded histograms are Monte-Carlo simulated inclusive J/ψ decays, broken down into the signal and background distributions. The accumulation of events at $\Delta E = 46$ MeV is due to the χ_{c1} $K^{\pm}$ contamination.

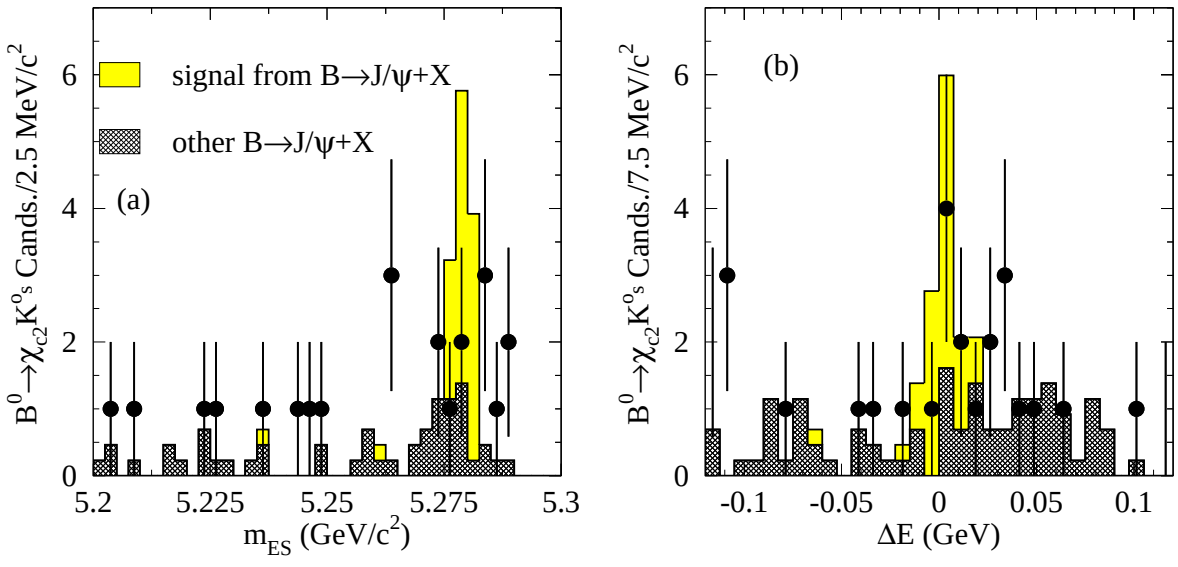

Figure 29: Distribution for the χ_{c2} K^0_s decay mode in (a) $m_{\rm ES}$ and (b) ΔE for the new "CP" selection. The points are the Run 1 data, the shaded histograms are Monte-Carlo simulated inclusive J/ψ decays, broken down into the signal and background distributions.

Mode	J/ψ mode	$\sigma\ \Delta E$ (MeV)	$\sigma\ m_{\rm ES}$ (GeV/c^2)	Cands. sig. box	Argus bckgd.	Gaussian peak. bckgd.	event yield	Purity (%)
$\chi_{c1}K^{\pm}$	l^+l^-	10.3±1.4	2.8±0.3	135	15.3±5.3	3.0±1.4	116.7±12.8	86.4±9.5
	e^+e^-	11.3±2.2	3.9±0.5	64	4.6±2.6	2.6±1.2	56.8±8.5	88.8±13.3
	$\mu^+\mu^-$	9.3±2.2	2.2±0.3	71	7.9±3.5	0.0±0.1	63.1±9.1	88.9±12.9
$\chi_{c1}K^0_S$	l^+l^-	8.2±1.4	2.0±0.4	28	1.7±1.3	0.9±0.6	25.4±5.5	90.8±19.6
	e^+e^-	10.3±2.9	2.3±0.7	13	1.0±1.0	0.5±0.4	11.5±3.8	88.8±29.0
	$\mu^+\mu^-$	7.2±1.4	2.3±0.7	15	1.2±0.9	0.7±0.4	13.1±4.0	87.5±26.6

Table 53: Signal resolutions, number of candidate, Argus and inclusive J/ψ Gaussian peaking backgrounds, event yields and signal purities in the signal box for the $\chi_{c1}K$ decay modes with the Run 1 data (20.7 fb^{-1}) and a Monte Carlo sample of 245000 inclusive J/ψ from B$\bar{\rm B}$ decays (89.8 fb^{-1}). All the errors are statistical only.

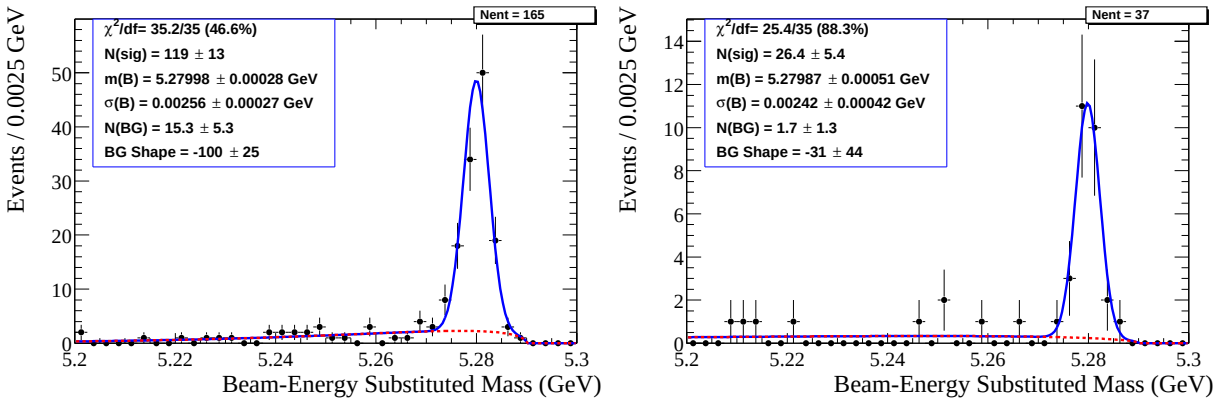

Figure 30: Argus + Gaussian fit to extract the Argus background in the χ_{c1} $K^{\pm}$ (left) and χ_{c1} K^0_S (right) decay modes for the Run1 data sample for $J/\psi \to l^+l^-$ decays.

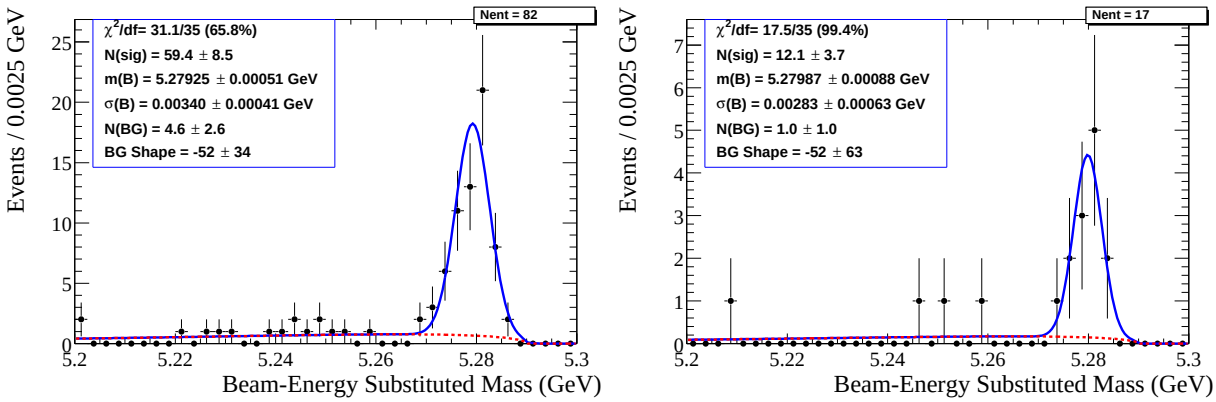

Figure 31: Argus + Gaussian fit to extract the Argus background in the χ_{c1} $K^{\pm}$ (left) and χ_{c1} K^0_S (right) decay modes for the Run1 data sample for $J/\psi \to e^+e^-$ decays.

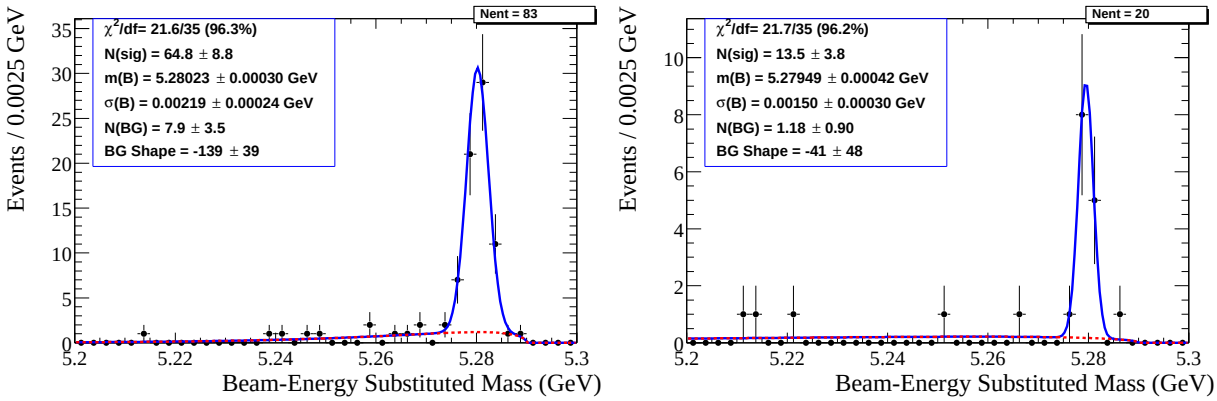

Figure 32: Argus + Gaussian fit to extract the Argus background in the χ_{c1} $K^{\pm}$ (left) and χ_{c1} K^0_S (right) decay modes for the Run1 data sample for $J/\psi \to \mu^+\mu^-$ decays.

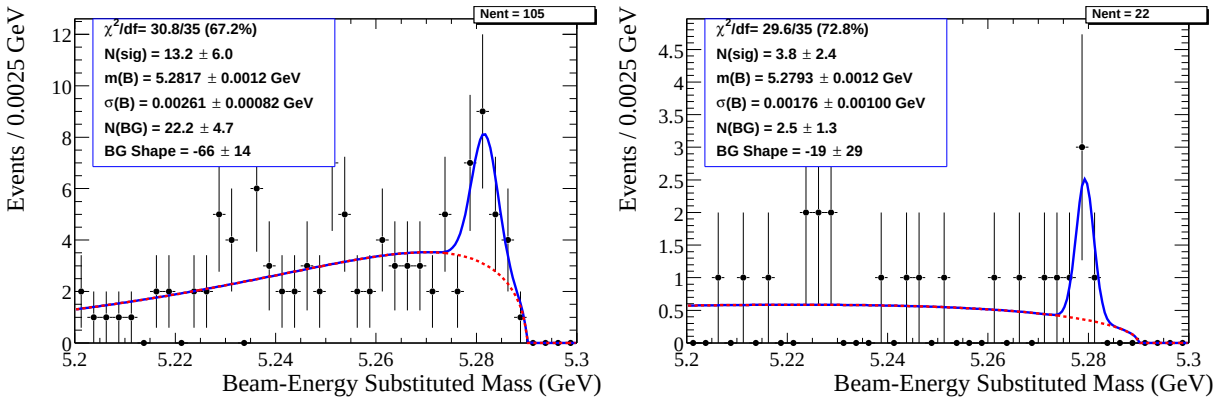

Figure 33: Argus + Gaussian fit to extract the Gaussian peaking background in the χ_{c1} $K^{\pm}$ (left) and χ_{c1} K^0_S (right) decay modes for the SP3 inclusive Monte-Carlo sample of 245000 J/ψ from B decays and for $J/\psi \to l^+l^-$ decays (no normalization factor is applied).

B Fit output

References

[1] J.H. Christenson *et al.*, Phys. Rev. Lett. **13**, 138 (1964);
NA31 Collaboration, G.D. Barr *et al.*, Phys. Lett. **317**, 233 (1993);
E731 Collaboration, L.K. Gibbons *et al.*, Phys. Rev. Lett. **70**, 1203 (1993).

[2] ZhETF Pis'ma 5 : 32-35 (1967) ; Traduction JETP Lett. 5 : 24-27 (1967).

[3] N. Cabibbo, Phys. Rev. Lett. **10**, 531 (1963); M. Kobayashi and T. Maskawa, Prog. Th. Phys. **49**, 652 (1973).

[4] See, for instance, "Overall determinations of the CKM matrix", in [6] section 14 and references therein.

[5] For an introduction to *CP* violation, see, for instance, "A *CP* violation primer", in [6] section 1 and references therein.

[6] P. H. Harrison and H. R. Quinn, eds., "The *BABAR* physics book", SLAC-R-504 (1998).

[7] M.B. Gavela *et al.*, Mod. Phys. Lett. **A9**, 795 (1994) and Nucl. Phys. **B340**, 382 (1994); P. Huet and E. Sather, Phys. Rev. **D51**, 379 (1995).

[8] C. Jarlskog, in *CP Violation*, C. Jarlskog ed., World Scientific, Singapore (1988).

[9] UA1 Collaboration, C. Albajar *et al.*, Phys. Lett. **B186** (1987) 247.

[10] ARGUS Collaboration, H. Albrecht *et al.*, Phys. Lett. **B192** (1987) 245.

[11] *BABAR* Collaboration, B. Aubert *et al.*, "Angular analysis of B decays to $J/\psi K^0_S$ decays", in preparation.

[12] http://babar-hn.slac.stanford.edu:5090/HyperNews/get/sin2beta/198.html (R. N. Cahn).

[13] J. D. Richman, Heavy-Quark Physics and *CP* violation (Les Houches lectures) (1998).

[14] PDG 2000

[15] B.A.D. 125 (contact G. Raven) Measurement of B^0 mixing using fully reconstructed hadronic B^0 decays

[16] Defined as $A \sim \sqrt{1-(m_{ES}/m_0)^2} \times exp(\kappa(1-(m_{ES}/m_0)^2)$ for $m_{ES} < m_0$. The default value of m_0 is 5.291 GeV.

[17] B.A.D. 56 (contact D. Wright) Analysis of $B^0 \to J/\psi K^0_L$

[18] B.A.D. 119 (contact J. Beringer) B Tagging in BaBar: Status for the sin2beta Journal Publication

[19] B.A.D. 102 (contact F.Martinez Vidal) The BaBar Vertexing

[20] B.A.D. 130 (contact F.Martinez Vidal) Performances and control samples of the *BABAR* vertexing

[21] B.A.D. 206 (contact O. Long) Measurement of sin2β with the decay mode $B^0 \to J/\psi\, K^0_L$

[22] B.A.D. 151 (S. Plaszczynski, L. Roos, M.H. Schune) Measurement of the mistag fractions with counting methods

[23] J. Beringer, *Changes in tagging and deltaT for events used for Osaka results*, sin2beta HN 192, January 19, 2001

[24] J. Beringer, *Comparison with and Unblinding of the Osaka Subsample*, sin2beta meeting, January 22, 2001

[25] J. Beringer et al., *Cut Based Tagging*, BaBar Analysis Document 118, Version 1, (2000)

[26] F. Porter, Interval Estimation Using the Likelihood Function.

[27] BABAR Physics Book

[28] http://babar-hn.slac.stanford.edu:5090/HyperNews/get/physAnal/1023.html (A. Gritsan).

[29] B.A.D 153 (contact H. Lacker) Constraining the CKM Matrix

[30] B.A.D 92 (contact G. Eigen) Inputs for the Unitarity Triangle Fits

[31] B.A.D 115 (contact D. Lange) Supporting document for the Run 1 sin2β analysis

[32] B.A.D 113 (contact S. McMahon) Measurement of Branching Ratios of Charged and Neutral B Mesons into Exclusive Charmonium Final States & B.A.D 198 (contact E. Varnes) Measurement of branching fractions for exclusive B decays to charmonium final states

[33] R. Balest et al. (CLEO collaboration), Inclusive decays of B mesons to charmonium, Physical Review D Vol 52 2661 (1995)

[34] B.A.D 139 (contact C. Hearty) Measurement of Inclusive Production of Charmonium States in B Meson Decays